The Dissertation Committee for Jeonghwan Lee Certifies that this is the approved version of the following Dissertation:

Approaches in optimization and machine learning towards post-stroke gait

Committee:

James S. Sulzer, Supervisor

Richard R. Neptune

Ashish Deshpande

Nicholas P. Fey

Steven A. Kautz

Approaches in optimization and machine learning towards post-stroke gait

by

Jeonghwan Lee

Dissertation

Presented to the Faculty of the Graduate School of

The University of Texas at Austin

in Partial Fulfillment

of the Requirements

for the Degree of

Doctor of Philosophy

The University of Texas at Austin

August 2022

Dedication

This dissertation is dedicated to my respectful parents, beloved wife, and son who constantly supported and encouraged me to finish my long academic journey.

Acknowledgements

First and foremost, I would like to express my deepest gratitude to my advisor Dr. James Sulzer for his continuous support throughout my Ph.D. study. Words cannot express my gratitude for his valuable mentorship, great brilliance, enthusiasm for research, constructive criticism, remarkable communication skills and countless jokes in 5 years at Rewire Lab. I could not have undertaken my academic journey without him.

I would like to thank Dr. Richard Neptune, Dr. Ashish Deshpande, Dr. Nicholas Fey, and Dr. Steven Kautz for serving on dissertation committees and providing new perspectives and insightful feedback on my work. I am also grateful to Dr. Hao-Yuan Hsiao for serving on my proposal committee. Their valuable comments and suggestions improved my research and widen the clinical viewpoints of my research.

I would like to extra thank collaborators including Dr. Robert Lee, Dr. Bryant Seamon, Dr. Hao Su and, Dr. Jarrod Lewis-Peacock for supporting clinical and engineering resources for my studies. I would like to thank Dr. Youngmok Yun for allowing me to keep improving my engineering skills in robotics through the Summer internship opportunities.

I had the pleasure of working with Rewire Lab folks from 2017 to 2022. I owe many thanks to Dr. Sung Yul Shin for taking me under his wing and having numerous random discussions during fresh-air break. Dr. Chungmin Han and Kyoungsoon Kim, I would have gotten no where with my research if you guys are not around me all the time. Dr. Tunc Akbas, I would be remiss in not mentioning my work is inspired by your former achievements. Sunil Prajapati, thank you for being my first graduate school friend, sitting on next to me as a 3rd floor crew, taking classes together, and improving my sarcastic communication in English. Justin Kilmarx, I would feel lonely if you had not constantly reacted to my guff. Mark Chiarello and Michael Normand, you guys' extraordinary talents

motivated me constantly, and thank you for patiently working with me. I cannot thank my other colleagues enough for my time here, including Dr. Ethan Oblak, Ana de Oliveira, Kevin Warburton, Allison Berman, Keith Macon, Lailu Li, Laura van Poppel, Franz Bachler, Seun Fashina and folks in ReNeu Robotics Lab.

Lastly, I would like to sincerely thank my beloved wife and son, Woojoo Jung and Louis Lee, my parents and older brother, and all my family-in-law for their continuous support and immense confidence. Throughout my educational journey, without their support, I would not be where I am today.

Abstract

Approaches in optimization and machine learning towards post-stroke gait

Jeonghwan Lee, Ph.D.

The University of Texas at Austin, 2022

Supervisor: Dr. James S. Sulzer

Gait disorders are common in stroke survivors. Engineering approaches to resolving such disorders have reached critical hurdles. One hurdle is that the devices remain in reach of only resource-rich institutions, although robot-assisted gait therapy has become more accepted in the clinical world. Another hurdle is a lack of consideration of neurological impairments in gait dysfunction for robot-assisted therapy. Lastly, the heterogeneous characteristics of disorders make it difficult to communicate between clinicians and compare between patients. This dissertation work takes steps towards each of these issues in rehabilitation engineering. In my first aim, I optimize and characterize linkage mechanism designs for an affordable gait trainer adjusting to a variety of gait patterns. In the second aim, I take a novel regression approach initiating an investigation of the kinematic predictors for quadriceps hyperreflexia to take into account such critical impairment in the development of assistive technology. In the third aim, I identify characteristics of common and specific gait dysfunction, known as Stiff-Knee gait, using

cluster analysis. This dissertation has helped bridge gaps between advanced technology and clinical practice through novel engineering approaches. The ultimate goal of this study is to provide a foundation for developing affordable but robust rehabilitation solutions toward complete recovery.

Table of Contents

List of Tables

List of Figures

Chapter 1: Introduction

Stroke is the largest cause of long-term disability affecting 795,000 people each year in the United States [1]. Gait disorders are common clinical problems in stroke survivors. More than 80% of stroke survivors have varying degrees of gait abnormalities [2], [3], and about 25% have a residual impairment that requires full physical assistance, despite rehabilitation efforts [4]. Consequently, many stroke survivors suffer from gait impairment that causes difficulties in performing activities of daily living, and recovering gait ability is one of the main goals of neurological patients undergoing rehabilitation treatment [5]. More people are in need of stroke rehabilitation every year, and the cost of continuous care is still high and projected to substantially increase in the next decade [1]. Numerous efforts bridging between state-of-the-art engineering techniques and clinical environments have been made to increase rehabilitation efficacy, resolve gait disorders, and eventually elicit a reduction of the patients' physical and financial burdens. Robot-assisted therapy, for instance, has become more accepted in the clinical world for its ability to automate, quantify, and tailor therapy [6]. However, such advanced engineering approaches have reached critical hurdles.

One hurdle is that the dexterous robotic devices remain in reach of only resource-rich institutions. Robot-assisted gait training has gained popularity as a potential solution to increase patient throughput with intensive, repetitive, and task-specific motor activities [7], [8]. It has been expected to substantially reduce the burden on clinicians, quantify training and increase the number of patients treated compared to conventional gait therapy

[9]. While robotic gait trainers reduce the physical burden on therapists and allow greater patient output [6], there was no clear evidence showing how such robotic trainers reduce the cost of therapy. For versatile assistance, these robotic gait trainers are often composed of multi-joint actuation systems to actively control knee, hip (and pelvic) motion during walking [10], resulting in skyrocketing device costs. Such a high capital cost makes them inaccessible to the vast majority of in/outpatient clinics and could negate the ostensible financial labor-saving benefit of robotic training. As one of the solutions, novel design approaches have been proposed based on a single degree-of-freedom (1-DOF) linkage mechanism not only maximizing the cost reduction but also maintaining a key feature of motorized gait trainer, individualized assistance [11]–[13]. However, an optimal solution among various 1-DOF mechanism configurations was still unclear.

Another hurdle is a lack of consideration of neurological impairments in gait dysfunction for robot-assisted therapy. The lower extremity wearable robotic exoskeleton has emerged due to its clear benefit in metabolic cost and muscle weakness for healthy individuals [14], [15]. With technological advances, exoskeletons are becoming lighter but powerful, and intelligent resulting in maximal efficacy of walking assistance [16]. Most exoskeletons, however, were specialized to address muscle weakness, leaving other neuromuscular impairments, such as spasticity [17], unaddressed. Neglecting clinically important impairments could produce counterproductive rehabilitation output. For instance, earlier studies with the lightweight powered knee orthosis [18] targeted post-stroke Stiff-Knee gait (SKG) swing-phase knee flexion assistance originally expected to restore gait functionality with a reduction in compensatory motions [19]. Exoskeletal

assistance restored sagittal-plane gait functionality but also resulted in quadriceps hyperreflexia [20], which could hinder rehabilitation efficacy. This implies that the necessity to take neurological impaired conditions into account in targeted therapy using rehabilitation robots. However, there has been a lack of investigation into what biomechanical factors should be considered to effectively integrate clinical impaired conditions into robotic techniques.

Lastly, the heterogeneous characteristics of disorders make it difficult to communicate between clinicians and compare between patients. The degree of gait deviation following a stroke can vary widely and relates to the severity of lower extremity motor impairment [21]. Accurate characterization of abnormal gait in stroke survivors is essential to guide proper interventions and develop a predictive model for rehabilitation outcomes. Numerous approaches have been proposed to identify and characterize common gait disorders following stroke (i.e., drop foot [22], SKG [23], knee hyperextension [24], etc.). Despite a long history of post-stroke gait characterization, there has been a lack of consensus on the specification and quantitative characteristics of SKG.

My dissertation work takes steps towards each of these issues in rehabilitation engineering. In my first aim, I optimize and characterize linkage mechanism designs for an affordable gait trainer adjusting to a variety of gait patterns. In the second aim, I take a novel regression approach initiating an investigation of the kinematic predictors for quadriceps hyperreflexia to take into account such critical impairment in the development of assistive technology. In the third aim, I identify characteristics of common and specific

gait dysfunction, known as Stiff-Knee gait, using cluster analysis. Here I describe the overview of specific goals through the following aims:

Aim 1. Kinematic comparison of single degree-of-freedom robotic gait trainers (Chapter 2)

There is a clear benefit to mechanized gait trainers, but their high cost prevents use in clinics and homes. Single degree-of-freedom mechanized gait trainers employing linkage mechanisms can imitate the gait trajectory of the human user at a potentially lower cost. My goal is to evaluate recently introduced four-, six- and eight-bar designs from the standpoint of kinematics, that is, the ability to follow a natural gait pattern, in addition to mechanical advantage. Based on the gait database of 113 healthy individuals, I synthesized mechanisms allowing two link length adjustments and compared trajectory and path accuracy of the ankle across mechanisms. I used cross-validation to obtain data-independent accuracy. I systematically investigated kinematic accuracy trends in walking varying by height and speed. I used gait trajectories from a large human database and predicted additional trajectories to represent the effects of varying heights and speeds. I found that trajectory error was significantly lower in the eight-bar mechanism (3.77 ± 0.17 cm, mean ± SD) than the four- (6.84 ± 0.37 cm) and six-bar (7.15 ± 0.48 cm) configurations ($p<0.001$). However, I did not observe differences in time-independent path error between configurations, or in mechanical advantage ($p>0.05$). I conclude that the eight-bar configuration is best when the mechanism is tied to a constant velocity actuator, whereas the four-bar mechanism performs as well if the actuator is well-controlled. Further research is needed to parse the relative benefits of these designs.

Aim 2: Kinematic predictors of quadriceps spasticity: Machine learning approaches and evaluation (Chapter 3)

Wearable assistive technology for the lower extremities has shown great promise towards improving gait function in people with neuromuscular injuries. But critical neurological impaired conditions, such as spasticity, have been often neglected in the development of assistive strategies, as a result, it could induce secondary complications. In this aim, I explore a clinically accessible biomechanical predictor set that can accurately predict RF reaction after knee flexion assistance in pre-swing by a powered orthosis. I examined a total of 14 gait parameters based on gait kinematic, kinetic, and simulated muscle-tendon states from 8 post-stroke individuals with Stiff-Knee gait (SKG) wearing a knee exoskeleton robot. Two independent variable selection approaches were performed using machine learning regression techniques: Generalized Linear Mixed Models using Least Absolute Shrinkage and Selection Operator (glmmLASSO) and Bayesian Additive Regression Trees (BART). Both methods discovered that four kinematic variables relevant to knee and hip joint motions were sufficient to effectively predict RF hyperreflexia in people with post-stroke SKG wearing an exoskeleton robot. These results suggest that effective monitoring and control of these accessible knee and hip kinematics may be more productive at regulating hyperreflexia than the more complex acquisition of muscle fiber stretch velocity.

Aim 3: Cluster analysis to characterize post-stroke Stiff-Knee gait (Chapter 4)

Stiff-Knee gait (SKG) is a common abnormal gait pattern following stroke, characterized by diminished knee flexion during the swing phase of the gait cycle. Despite

a long history of its characterization, there have not been rigorous quantitative or consistent definitions of post-stroke SKG. The purpose of this aim is to determine a more accurate specification of SKG as well as potential phenotypes of post-stroke SKG based on gait data from a cohort of 50 post-stroke individuals with varying walking impairments and 15 healthy controls. I quantified the best single specification out of 8 different SKG-associated parameters by univariate cluster analysis. The relative pre-swing knee flexion angle, which is a gait speed independent parameter, provides the most accurate and robust diagnosis and can be obtained with relative ease. Throughout time-series multivariate cluster analysis using compensatory motions, I found two gait subtypes, both of which could be considered SKG, expressing differing three-dimensional kinematics, muscle coordination patterns, and levels of impairment. One type exhibited stance phase co-activation of quadriceps and hamstrings together with very low swing knee flexion, high pre-swing pelvic obliquity, and more severe metrics of gait impairment. The other type was characterized by stance phase over-activation of quadriceps, low swing knee flexion, combined pelvic obliquity and hip abduction, and more moderate metrics of gait impairment compared to the first group. Awareness of these two phenotypes will help better prescribe specific treatments and homogenize study populations for post-stroke SKG interventions.

Chapter 2: Kinematic comparison of single degree-of-freedom robotic gait trainers[1]

2.1. INTRODUCTION

Gait impairments, including reduced gait speed and stride length, abnormal gait kinematics and kinetics, and asymmetry step length, are common among those with neurological insults such as stroke or spinal cord injury [25], [26]. Weakness [27], spasticity [28], and discoordination [29], [30] have been thought to be the leading causes of pathological gaits. It is critical to have as much training as possible within the first months following injury [25], [31], yet patients often transfer to lower-intensity outpatient therapy programs within weeks due to healthcare coverage restrictions [32]. Robot-assisted gait training has been proposed as a potential solution to increase patient throughput with intensive, repetitive, and task-oriented motor activities [7], [8]. These trainers, such as the Lokomat (commercially available from Hocoma AG, Volketswil, Switzerland) [33], are often composed of four actuators (or more) to actively control knee, hip (and pelvic) motion during walking [10]. However, the high capital cost of these trainers makes them inaccessible to the vast majority of in/outpatient clinics. While robotic gait training exhibits similar or better clinical benefits compared to conventional therapy [34], [35], the high capital cost could negate the ostensible financial labor-saving benefit of robotic training.

[1]Portions of this chapter has previously been published in the following article – J. Lee, L. Li, S. Y. Shin, A. Deshpande, and J. Sulzer, "Kinematic comparison of single degree-of-freedom robotic gait trainers," Mechanism and Machine Theory, vol. 159, p. 104258, 2021. The author carried out the literature review of the existing robotic gait trainers, and simulated the algorithm and benchmarked the different mechanisms.

Cost reduction could be achieved through clever design features. Since most commercialized robotic trainers use a single fixed trajectory focused on sagittal plane gait motion, a multiple degrees-of-freedom (DOFs) robotic gait trainer may not be necessary. Therefore, simpler designs with 1 DOF linkage mechanisms have been introduced. The Gait Trainer (GT I) is an early example of robotic locomotor training using a single motor [36], [37], now in its commercialized iteration (GT II). Based on a double crank and rocker gear system, the GT I/GT II is an elliptical trainer that drives end effector (foot) position, with some evidence of clinical success in stroke survivors [38]. Yet the elliptical designs do not produce accurate gait trajectories nor provide cutaneous stimulation of ground contact experienced during walking, potentially critical components to gait recovery [39].

In addition to ground contact, our main goals for a 1 DOF gait trainer were accurate reproduction of a human-like gait pattern and the ability to adapt to individuals. Advanced mechanism synthesis methodology can be used to achieve these goals. Approximate synthesis using numerical methods has been applied to a linkage mechanism design based on actual human gait data. Ji et al. optimized four-bar with normative ankle trajectory by solving a nonlinear least-square problem [40], and Kora et al. optimized it by a trust region-reflective algorithm [41]. Tsuge et al. applied a homotopy directed optimization for Stephenson III six-bar and ten-bar synthesis based on a single subject's ankle trajectory [42]–[44]. Shao employed a genetic algorithm to

design a cam-linkage mechanism based on Stephenson III six-bar with ankle trajectory from normative gait data [45]. Our own group recently introduced an eight-bar design based on a gait database of 113 healthy individuals [46]. The optimization problem for linkage synthesis was solved by the interior point method. We found that with a crank at a constant speed, an eight-bar design was capable of accurately facilitating gait motion over a wide range of human gait patterns with an offline adjustment of only two link lengths. Subsequent work by other researchers has further investigated this design with a single participant's ankle trajectory by a model-independent method based on the optimal trajectory tracking control of a shadow robot [47], [48]. However, a follow-up question has not been addressed: are simpler designs such as four- or six-bar mechanisms capable of exhibiting comparable performance? Simpler designs might be preferable because of the potential for further cost-savings and ease of operation and maintenance. A preliminary analysis in our previous work suggested that an eight-bar design has greater trajectory accuracy than a four-bar design operating at constant crank velocity [46]. However, this initial analysis did not address differences in gait speed, height, or a device capable of changing the crank velocity. A controlled crank velocity would be more amenable to situations of variable-speed overground training, whereas a constant velocity would be more appropriate for typical constant-speed treadmill training scenarios.

The objective of this study was to investigate three different 1 DOF linkage mechanisms that have been previously proposed in gait trainers: a four-bar [41], a Stephenson III six-bar [43], and an eight-bar mechanism [46]. The primary question of

this study was to compare the kinematic accuracy of these mechanisms and determine their relative benefits. We based our analysis on a gait dataset of 113 healthy human individuals [49] and used regression models to synthesize predicted changes in gait with height and speed [50]. We extracted the end effector (i.e., ankle position) error, both the time-dependent trajectory error and the time-independent path error, corresponding to constant input velocity and variable input velocity operation, respectively. We employed cross-validation to eliminate data bias and systematically investigated kinematic accuracy variation affected by varying height and gait speed. In addition to end-effector kinematics, we computed the mechanical advantage of the mechanism to identify the efficiency in force transfer of each design. This work presents a novel basis for objective comparison and insight into 1 DOF gait trainer designs. These insights will help prescribe the most appropriate mechanism for economical and accessible robotic gait training aimed at moderately to severely neurologically impaired individuals.

2.2. DIMENSIONAL SYNTHESIS

This study focuses on three different mechanisms: four-, six-, and eight-bar configurations offered in previous work [41], [43], [46]. The canonical topologies of these designs are illustrated in **Figure 2.1**. The linkage design for the 1 DOF gait trainer should have the capability of gait pattern reproduction, and it should be easily customizable to individuals. The following section details the dimensional synthesis to human gait data to obtain a best-fit customizable linkage configuration.

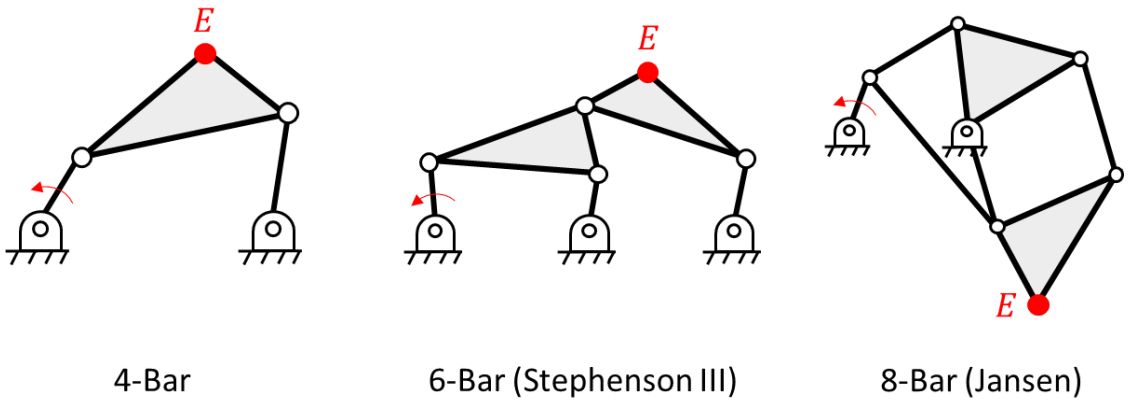

Figure 2.1: Linkage mechanism structural representation: four-bar, six-bar (Stephenson III), and eight-bar (Jansen) mechanisms. The designated end effector for gait pattern generation is denoted by E.

2.2.1. Prescribed Canonical Gait Patterns

Dimensional synthesis is an inverse problem that obtains the linkage dimensions required to achieve a prescribed output motion. To establish generality, we used multiple prescribed output motions (gait trajectories) representing the large variability of human gait [51]. Each gait trajectory was reflected as the time-dependent motion of the lateral malleolus. We reconstructed a total of nine canonical prescribed human gait trajectories from a database of 113 healthy individuals (50 male / 63 female, age 44.27 ± 14.93, height 164.82 ± 8.32 cm) walking at 3.0 km/h on a treadmill [49]. The nine prescribed gait trajectories consisted of the grand mean (*meta)*, largest, smallest, as well as six intermediate motions linearly interpolated from the former three (**Figure 2.2**) by the profile blending method [52] to more thoroughly span the manifold. The largest and smallest trajectories were an average of selected groups of 10 individuals with the largest

and smallest step lengths (upper and lower quantile of the database, respectively). We extracted the ankle trajectory relative to the hip in the sagittal plane divided into the single gait cycles based on heel strike events. All single gait cycle trajectories were normalized into 100-time frames. The reference gait trajectory, T_{ref}, is defined by $\{\mathbf{x}_{ref,i} \in \mathbb{R}^2 : \forall i \in \{1, \cdots, N\}\}$ where $\mathbf{x}_{ref,i}$ is a position vector of human ankle for the i-th time instance and N is the total number of time frames.

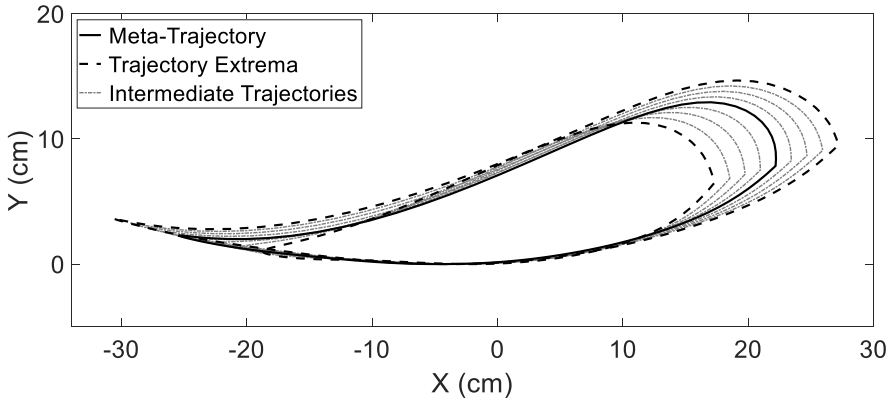

Figure 2.2: A total of nine reproduced reference natural human gait motions of the ankle joint (e.g., lateral malleolus) from the gait kinematic database. The mean of all subjects' gait motions is called the meta-trajectory (solid line). The largest and smallest gait trajectory (dashed lines) and interpolated gait trajectories (dotted lines) are in the Cartesian frame.

2.2.2. Optimization

The goal of optimization was to find the optimal linkage parameters that minimize the kinematic error with respect to human reference gait motion. Here, we established a

multi-objective function towards minimizing spatial and temporal motion differences between a machine and a human. Then, we introduced an iterative optimization scheme to determine the optimal adjustable link selection for customizing the device's trajectory to a wide range of gait patterns.

2.2.2.1. Objective Functions

The first objective function was mainly based on a prescribed reference gait trajectory, T_{ref}, determined in Section 2.2.1 and a trajectory of the mechanism end effector, T_E. The mechanism's output trajectory is defined as $\left\{\mathbf{x}_{E,i} \in \mathbb{R}^2 : \mathbf{x}_{E,i} = f\left(\theta_{c,i}, \boldsymbol{Z}\right), \forall i \in \{1, \cdots, N\} \; and \; \theta_{c,i} = \frac{2\pi}{N}(i-1) \in [0, 2\pi]\right\}$, where $\mathbf{x}_E$ is a position vector of the end effector computed by a well-known analytical kinematic approach, the vector loop method [53]. The analytical kinematics is simplified as the function of the input crank angle, θ_c, and a vector of linkage parameters, $\boldsymbol{Z} = [l_1, l_2, \cdots, l_a, \alpha, \emptyset_1, \cdots, \emptyset_b]$ where l is a link length, α is an angle of a ternary link if existing, $\emptyset$ is an angle of a ground link, for the mechanisms shown in **Figure 2.1**. Here, θ_c was equally distributed for one revolution by N samples, representing constant crank velocity. The objective function, J_1, is the root mean square (RMS) error between T_{ref} and T_E, formulated as

$$J_1(\boldsymbol{Z}) = \sqrt{\frac{1}{N}\sum_{i=1}^{N}\left\|\mathbf{x}_{ref,i} - \mathbf{x}_{E,i}(\boldsymbol{Z})\right\|^2}. \quad (1)$$

The objective function is based on a prescribed human-like trajectory [41], [46]. However, a geometrical shape in a motion could not be ideally matched by such a structural error function since it limits the search space [54]. In order to expand a search space and match a shape in a motion simultaneously, contour error between trajectories was used as the second objective. As shown in **Figure 2.3**, the contour error, c_e, is the shortest orthogonal distance between the desired human reference and the generated machine trajectory. The contour error provides a better shape indicator than the structural error due to its flexibility in timing. We deployed the local circular approximation [55] to estimate the contour error. The objective function, J_2, represents an overall contour error between trajectories formulated as

$$J_2(\boldsymbol{Z}) = \sqrt{\frac{1}{N}\sum_{i=1}^{N} c_{e,i}(\boldsymbol{Z})^2}. \tag{2}$$

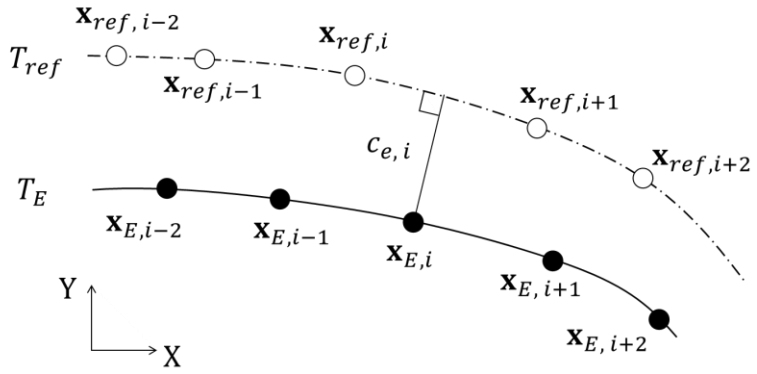

Figure 2.3: The contour error, c_e, which is the shortest orthogonal distance between the desired human reference and the generated machine trajectory.

We solved this two-objective problem by the ε-constraint method [56], which is applicable for the non-convex nonlinear problem. In the ε-constraint method, we minimize the objective function J_2 using J_1 as constraints, incorporating them in the constraint part of the model as shown below.

$$\begin{aligned} &\textbf{\textit{minimize}} && J_2(\boldsymbol{Z}) \\ &\textbf{\textit{s.t.}} && J_1(\boldsymbol{Z}) \le \epsilon_1 \\ & && J_1(\boldsymbol{Z}) \le J_2(\boldsymbol{Z}) \\ & && l_1 + l_2 - l_3 - l_4 \le 0 \\ & && FC_{max}(T_{ref}) = FC_{max}(T_E) \\ & && \boldsymbol{Z}_{LB} \le \boldsymbol{Z} \le \boldsymbol{Z}_{UB} \end{aligned} \tag{3}$$

The ε-constraint method can obtain different optima in the Pareto front by a systematic variation of the constraint bound, ϵ_1 [57]. The ε-constraint method needs attention in the selection of the bound since it should lie in the feasible objective space to acquire the proper solutions. Because we empirically identified the feasible objective space of J_1, we set ϵ_1 as 15 cm, which is between the minimum and maximum cost of J_1 across all mechanisms. This allows us to guarantee for a non-dominant solution weighted more on shape within our model. Additionally, since we know the cost of J_2 is always

larger than J_1, we limited the search space satisfying $J_1 \leq J_2$ for the efficiency in search. In order to guarantee the input crank rotates continuously, we set another inequality constraint using Grashof's condition [53] for the four-bar linkage loops in which the input crank is involved inside each mechanism ($l_1 l_2 l_3 l_4$ loop of the four- and the six-bar; $l_1 l_2 l_3 l_4$ and $l_1 l_7 l_8 l_4$ loops of the eight-bar in **Figure 2.5**). We also constrained a solution to have the same maximum foot clearance between trajectories. FC_{max} denotes the function of maximum foot clearance computing the difference between the maximum and minimum y-axis values of position vectors in a trajectory. This allows the solution to avoid an abnormal shape (e.g. flattened). Lastly, $\boldsymbol{Z}_{LB}$ and $\boldsymbol{Z}_{UB}$ are lower and upper bounds of a linkage parameter vector, respectively. Lower bounds for link length parameters were zero, which means searching only positive values, and there were no upper bounds. For angular parameters, there were no upper or lower bounds. Variable and fixed linkage configurations were differently organized depending on the purpose of optimization described in the following sections.

2.2.3. Customizing the Trajectory with Limited Adjustments

The individual link lengths of the mechanisms can be adjusted to fit a wide array of gait trajectories. However, it is time-consuming and impractical to adjust every link of a given mechanism, especially in a clinical setting. Based on our earlier research and input from our clinical partners, we determined an offline adjustment of two links as a practical limit for clinical use [46]. Thus, to be consistent across mechanisms, we limited our synthesis to have only two link adjustments of any link except for the input crank

length. The following procedure describes an iterative optimization scheme to determine the optimal two adjustable link combination.

The iterative optimization procedure was initiated from three different initial linkage parameter vectors attempting to scan the global minima. We performed pre-optimization to specify three initials by the following steps:

1) Specify the base initial linkage parameter vector, $\boldsymbol{Z}_{base} = [l_1, l_2, \cdots, l_a, \alpha, \emptyset_1, \cdots, \emptyset_b]$
2) Optimize $\boldsymbol{Z}_{base}$ for the meta-trajectory and two extrema trajectories (**Figure 2.2**), respectively, by varying all parameters.
3) Return the solutions as a set of initials $\{\boldsymbol{Z}_1, \boldsymbol{Z}_2, \boldsymbol{Z}_3\}$.

For $\boldsymbol{Z}_{base}$ in Step 1, we deployed the dimensions reported by the representative papers of each mechanism [41], [43], [46]. Based on three initials acquired in Step 3, we iteratively optimized the mechanism for a set of nine canonical trajectories (**Figure 2.2**) and scrutinized the best two-adjustable links combination as shown **Figure 2.4**.

Figure 2.5 and **Table A1** represent an optimized linkage configuration and parameters through the iterative optimization procedure. The blue labeled links are the adjustable links to produce an individual-specific gait trajectory. In practice, the one-time optimization using the same objective function in Section 2.2.2.1 must be performed to compute the lengths of the adjustable links for the new individual trajectory while maintaining the other link parameters fixed. The new individual trajectory will be the

predictive target gait trajectory. This can be acquired by the regression model [50] or stochastic prediction algorithm [49] based on patients' anthropometric and experimental data. The whole process was implemented in MATLAB R2019b (Mathworks Inc., Natick, MA) by using the *fmincon* function. We employed a sequential quadratic programming (SQP) method [58] as a nonlinear problem solver.

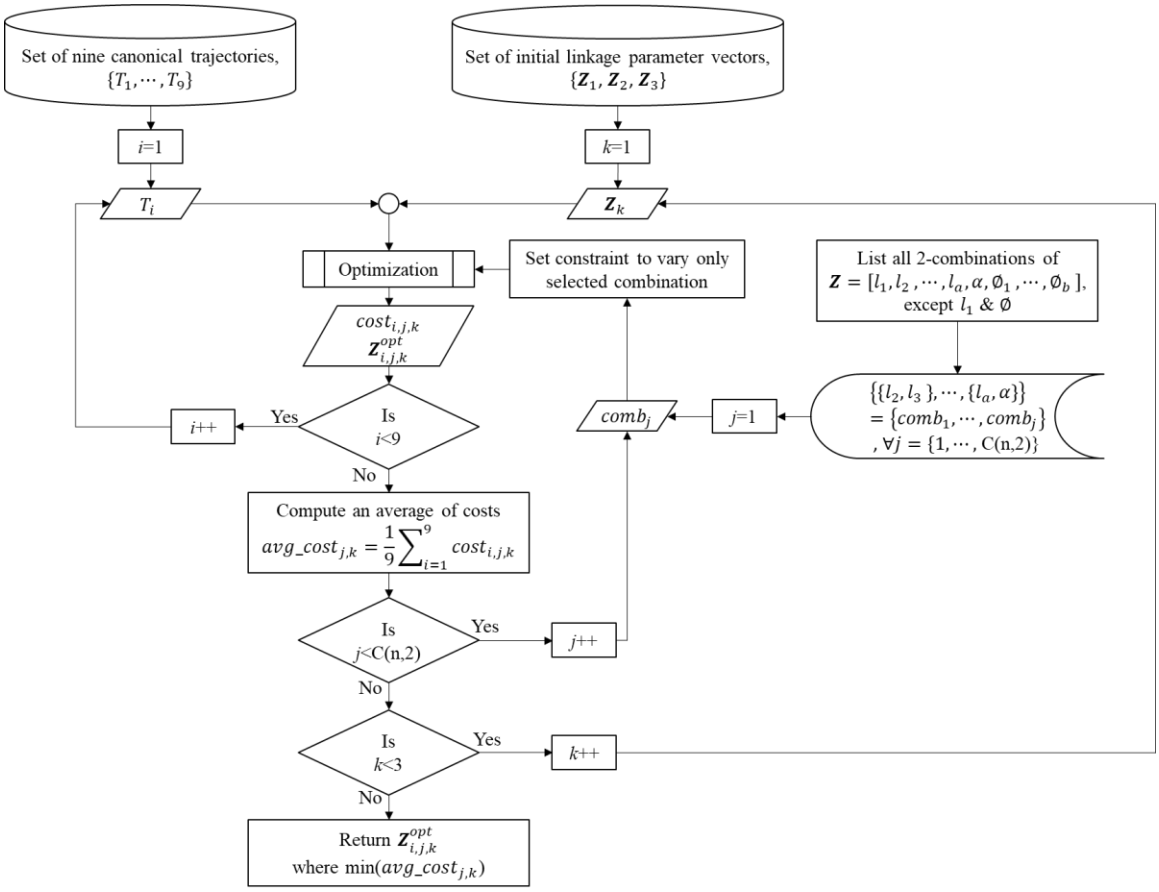

Figure 2.4: Flowchart for an iterative optimization procedure to determine the optimal linkage configuration, including two-adjustable link combinations.

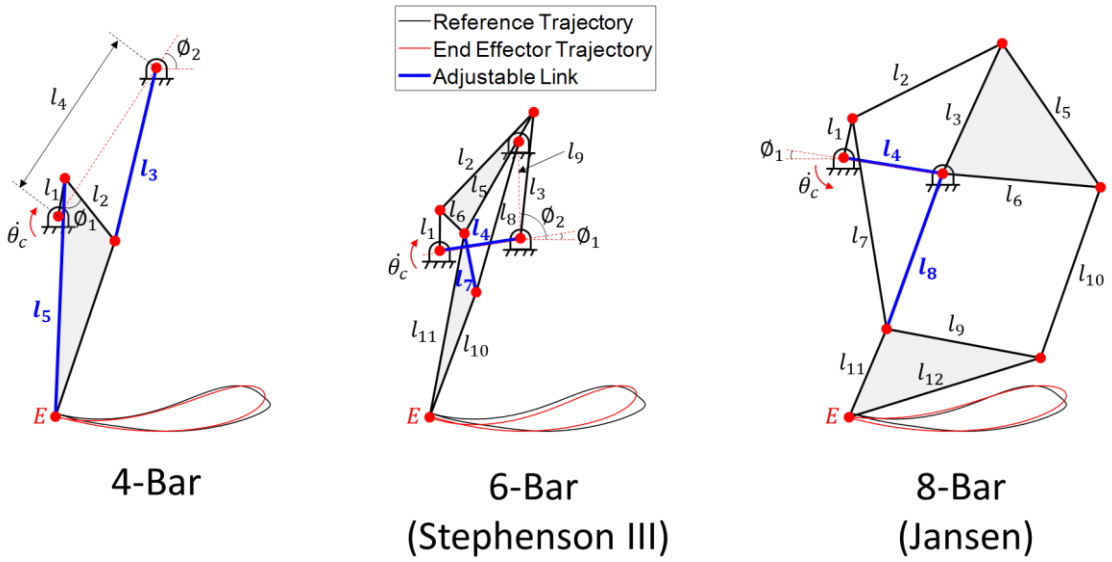

Figure 2.5: Optimized linkage configuration and optimization parameters. Blue colored links are adjustable links required to be changed offline to create individualized gait patterns. Other link parameters are fixed after synthesis.

2.3. EVALUATION

The primary aim of this study was to evaluate the output kinematics of a synthesized mechanism based on human gait motion and determine the optimal design among selected 1 DOF mechanisms. We conducted two evaluation processes. First, we compared mechanisms based on walking data of 113 healthy human individuals [49], followed by cross-validation to correct for biasing (Section 2.2.1). Second, we compared the effects of height and gait speed on kinematic accuracy between mechanisms via a set of 100 simulated gait trajectories.

2.3.1. Outcome Measures

The primary focus of this study was the kinematic accuracy of the end effector compared to the measured human ankle position during treadmill walking. We examined the kinematic accuracy both as a function of time (trajectory error via constant crank velocity) and independent of time (path error). We used the costs of each objective function (J_1 and J_2 in Section 2.2.2.1) as these outcome measures. J_1 represents the trajectory error which is the RMS distance between the end effector and ankle positions at given time points. J_2, the RMS contour error, indicates the path error which is a time-independent geometric shape difference. Simultaneously, we extracted the respective peak errors.

While we expected to see differences in kinematic error between configurations, we additionally wanted insight into the effort required to traverse these paths. Thus, we computed a mechanical advantage, M_A, of each mechanism. M_A is an applied force ratio between input and output, known as the force amplification. Given the conservation of energy, the ideal mechanical advantage can be rewritten by the relationship of the linear velocity as follows,

$$M_A = \frac{F_{out}}{F_{in}} = \frac{\tau_{out}}{r_{out}} \cdot \frac{r_{in}}{\tau_{in}} = \frac{\omega_{in}}{\omega_{out}} \cdot \frac{r_{in}}{r_{out}} = \frac{v_{in}}{v_{out}}, \quad (4)$$

where F is force, τ is torque, r is the moment arm, ω is the angular velocity of a rigid body, and v is the linear velocity. In this study, we specified the input velocity, v_{in}, as the linear velocity at the distal joint of input crank from the ground. To compute v_{in}, we

used the constant 2π rad/s for ω_{in} to match the given walking speed, and employed the optimized input crank length (l_1 in **Figure 2.5**) for r_{in}. The linear velocity, which is tangential to the trajectory of the end effector (E in **Figure 2.5**), was set as the output velocity, v_{out}. This can be calculated by the numerical derivative of the end-effector trajectory. We then extracted a portion of force amplification ($M_A > 1$) during one gait cycle as a secondary outcome measure to determine the efficiency in terms of force transfer.

2.3.2. Cross-validation

The canonical prescribed gait patterns in Section 2.2.1 could be biased if based on a small sample. In order to conduct an unbiased and generalized comparison, we employed cross-validation [59], [60] over the entire gait database. Under cross-validation, the available data are divided into *k* disjoint sets, called a fold. The *k* models are then trained, each on a different combination of $k - 1$ partitions, and tested on the remaining partition. The *k*-fold cross-validation estimate is the mean for each of the *k* models over the corresponding test partitions of the data. In this study, we used 10-fold cross-validation. We equally but randomly distributed the gait trajectories into folds from our database of 113 individuals at the stage of creating prescribed human trajectories in Section 2.2.1. After data distribution, each fold contained ten individual gait trajectories; therefore, the training set had 90 individuals' ($k - 1$ folds of total) and the test set had ten individuals' gait trajectories. As a result, every iteration in the cross-validation returned different sets of nine canonical trajectories and resulted in ten different optimal

configurations by the proposed dimensional synthesis. Then, we cross-validated results for the corresponding testing data. The flowchart of our 10-fold cross-validation procedure is represented in **Figure 2.6**.

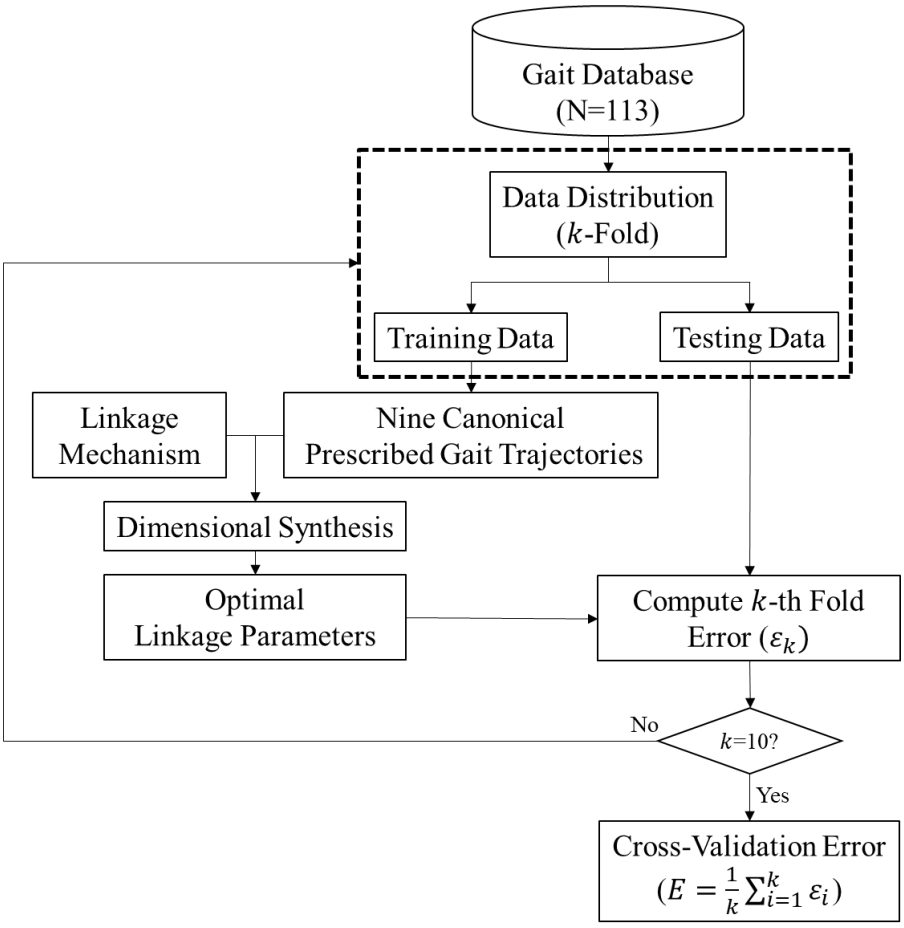

Figure 2.6: Evaluation flowchart for 10-fold cross-validation. Data distribution was conducted at the stage of reference trajectory generation. Cross-validation error is an average of all 10 folds of error.

2.3.3. Effects of Height and Gait Speed on Kinematic Accuracy

We evaluated the ability to match across a range of gait trajectories with varying heights and walking speeds. We generated an independent set of 100 gait trajectories based on previously determined algorithms of how gait trajectories change with height and speed [50]. This algorithm provided time-normalized joint trajectories (hip flex/extension, abd/adduction, knee flex/extension, and ankle dorsi/plantarflexion) with the input of arbitrary walking speed and an individual's height. We set our target range of the walking speed between 0.5 and 5 km/h with 0.5 intervals, and the height ranging from 152 to 188 cm with 4 cm intervals. We then extracted the joint trajectories of 10 discrete walking speeds for each of 10 discrete heights. The ankle trajectories in the sagittal plane were calculated by imposing the joint trajectories to the lower body kinematic model developed with lower limb lengths estimated by height [61]. As a linkage configuration to be tested, we employed the linkage solution from the 10-fold cross-validation (Section 2.3.2) that had shown the minimum error and variance for both trajectory and path errors among k folds. The selected linkage configuration, including two adjustable links, was optimized for the aforementioned 100 gait trajectories by optimizing only two adjustable links.

2.3.4. Statistics

We used a linear mixed model [62] for the statistical comparison of cross-validation errors across the mechanisms. The dependent variable was the trajectory or

path error, with a fixed variable of the type of mechanism and a random effect of fold coefficients. Tukey *post hoc* t-tests were used to compare pairwise conditions.

2.4. RESULTS

The generalized kinematic accuracy across 113 individuals and the relative performance between mechanisms were determined based on the cross-validation in Section 2.3.2. The differences in how the trajectory error between mechanisms changes over the gait cycle can be illustrated with the timecourse of the ankle position. **Figure 2.7** is based on an average of all tested individuals' ankle trajectories in the anterior-posterior (X) and superior-inferior (Y) directions (dashed black). The eight-bar trajectory in both directions (blue) matches very closely with the reference trajectory. However, the four-bar (red) and six-bar (green) show less agreement with the reference trajectory and more agreement with each other.

2.4.1. Effect of Configuration on Kinematic Accuracy

These effects carried into the larger comparison across all individuals. We found a significant difference in trajectory RMS error between mechanisms ($F(2, 288) = 354.07$, $p < 0.0001$). At the pairwise level, we observed a significant decrease in trajectory RMS error of the eight-bar compared to the four-bar (mean difference = 3.07 cm, $t(288) = 21.87$, $p < 0.0001$) and six-bar (mean difference = 3.38 cm, $t(288) = 24.07$, $p < 0.0001$). There was no statistically significant difference in trajectory RMS error of the four-bar compared to the six-bar configuration (mean difference = -0.31 cm, $t(288) = -2.20$, $p =$

0.09). We found the same relations with peak trajectory error ($F(2, 288) = 183.48$, $p < 0.0001$). The peak trajectory error in the eight-bar configuration was significantly less than in the four-bar (mean difference = 3.61 cm, $t(288) = 15.91$, $p < 0.0001$) and in the six-bar (mean difference = 3.90 cm, $t(288) = 17.20$, $p < 0.0001$) configurations. We did not observe significant difference in the peak trajectory error of the four-bar configuration compared to the six-bar configuration (mean difference = -0.29 cm, $t(288) = -1.29$, $p = 0.60$). Results are summarized in **Table 2.1**. As a basis for comparison, we extracted the within-subject variance of the ankle trajectory from our gait data at 5.02 cm. This is substantially more than the eight-bar trajectory error (3.76 cm), but less than the four- and six-bar trajectory error (6.84 and 7.15 cm, respectively).

We did not observe differences in path error among mechanism configurations. We compared path RMS error ($F(2, 288) = 0.58$, $p = 0.56$) as well as path peak error ($F(2, 288) = 1.29$, $p = 0.28$). All results are presented in **Table 2.1**. The within-subject variance of the ankle path was 3.83 cm, far above the path errors of the mechanism configurations of 0.63-0.67 cm.

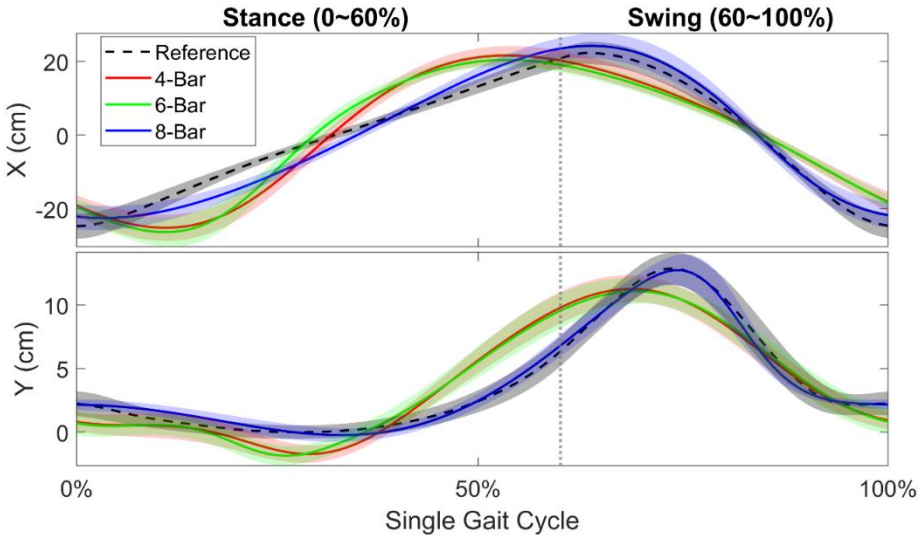

Figure 2.7: Average trajectory of all tested individuals by the cross-validation (dashed black) compared to four-bar (red), six-bar (green) and eight-bar (blue) configurations in anterior-posterior (X) and superior-inferior (Y) directions. The shaded area represents the standard deviation.

Table 2.1: Cross-validation errors: Mean and standard deviation of trajectory and path errors (RMS and peak error) for each mechanism configuration across cross-validation folds.

		4-bar	6-bar	8-bar
Trajectory Error (J_1)	RMS (cm)	6.84 ± 0.37	7.15 ± 0.48	3.76 ± 0.18
	Peak (cm)	11.42 ± 0.51	11.70 ± 0.71	7.80 ± 0.33
Path Error (J_2)	RMS (cm)	0.65 ± 0.12	0.67 ± 0.17	0.63 ± 0.09
	Peak (cm)	1.27 ± 0.18	1.28 ± 0.26	1.41 ± 0.17

2.4.2. Effects on Height and Gait Speed on Kinematic Accuracy

The effect of height and gait speed on kinematic accuracy provides additional insight. A comparison of trajectory and path RMS error are presented as heat maps and 3D surface plots in Figs. 8a and b, respectively. Peak errors are illustrated in **Figure A1**. A summary of the results is shown in **Table 2.2**. Across all gait patterns, the eight-bar mechanism had the lowest average trajectory RMS error (4.84 cm), with higher average trajectory error in the six-bar (9.38 cm) and four-bar (8.31 cm) mechanisms. We observed the same relations for peak trajectory error, albeit with higher magnitudes (**Table 2.2**). The eight-bar mechanism exhibited similar variance to the four-bar mechanism (0.99 and 0.79 cm, respectively) throughout the space, both lower than the six-bar mechanism (1.97 cm). The trajectory RMS and peak error of the four-bar mechanism performed best at small heights and low gait speeds and worst at large heights and high gait speeds (**Figure 2.8a**, left top). We observed the same relations with the six-bar mechanism but with greater variance (**Figure 2.8a**, left middle). The eight-bar mechanism exhibited its best trajectory RMS error performance at small heights and high gait speeds, and its worst performance at large height and low gait speeds (**Figure 2.8a**, left bottom).

Compared to trajectory error, there was a prominent decrease in path error across all mechanisms. All mechanisms similarly exhibited path errors below a centimeter. Specifically, the four-bar and the eight-bar mechanisms exhibited similar path RMS error and variance (0.74 ± 0.33 cm and 0.71 ± 0.26 cm, respectively), both lower than the six-bar mechanism (1.02 ± 0.43 cm, **Table 2.2**). Peak path errors mirrored these relations

(**Table 2.2**). The performance of the mechanisms can be directly compared in the overlaid 3D surface plots in **Figure 2.8b**.

Table 2.2: Mean and standard deviation of trajectory and path errors (RMS and peak error) for each mechanism configuration across varying heights and speeds.

		4-bar	6-bar	8-bar
Trajectory Error (J_1)	RMS (cm)	8.31 ± 0.79	9.38 ± 1.97	4.84 ± 0.99
	Peak (cm)	14.28 ± 1.57	16.68 ± 4.87	10.30 ± 2.02
Path Error (J_2)	RMS (cm)	0.74 ± 0.33	1.02 ± 0.43	0.71 ± 0.26
	Peak (cm)	1.51 ± 0.58	2.22 ± 1.04	1.33 ± 0.62

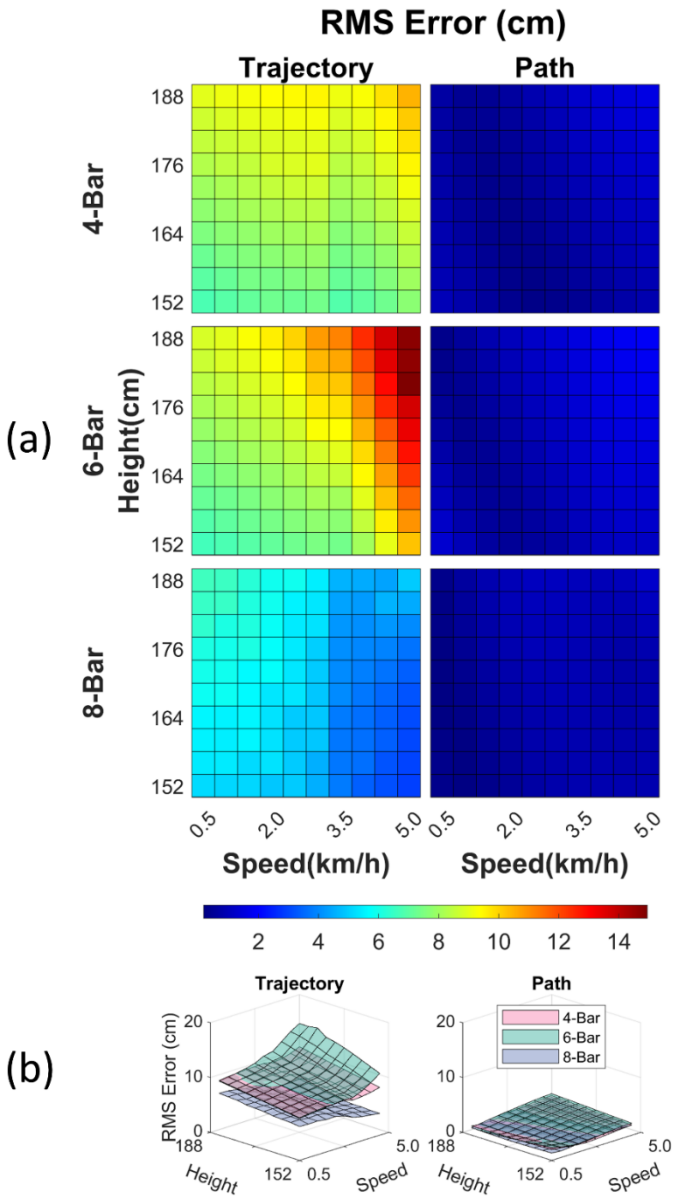

Figure 2.8: The heat map (a) and the surface plot (b) for the trajectory (left) and the path (right) RMS error across gait patterns varied by height and walking speed.

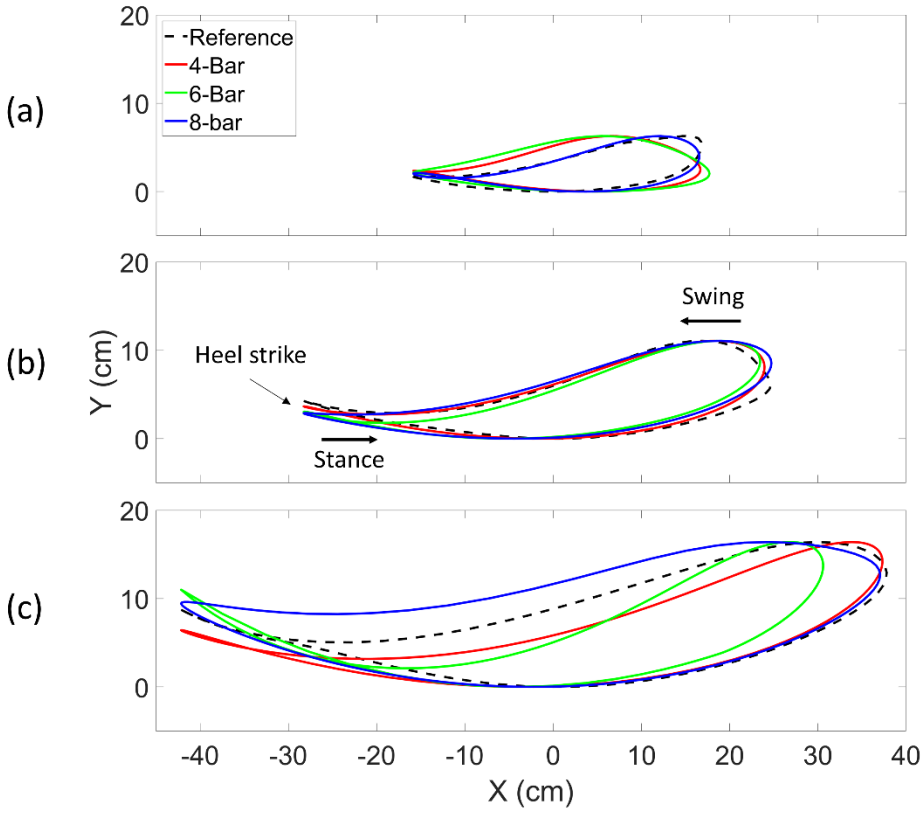

Figure 2.9: Paths of three representative cases (dashed black) compared to four-bar (red), six-bar (green) and eight-bar (blue) configurations in sagittal plane (X-Y): (a) the smallest case (0.5 km/h gait speed, 152 cm height), (b) the median case (2.5 km/h gait speed, 168 cm height), and (c) the largest case (5.0 km/h gait speed, 188 cm height).

Although all mechanisms showed an accurate path RMS error, there were notable outliers at extrema gait speeds. **Figure 2.9** illustrates synthesized paths in the sagittal plane (X-Y) from three representative cases based on gait motion size. The eight-bar path (blue) matched very closely with the reference path at the lowest gait speed of 0.5 km/h and the smallest body height of 152 cm (**Figure 2.9a**). However, the four-bar (red) and six-bar (green) show less agreement with the reference path and more agreement with

each other. Such an abnormal path in the four-bar and the six-bar mechanism was observed only at the lowest gait speed of 0.5 km/h, and it started being less severe as the body height was larger than 160 cm. At the highest gait speed of 5.0 km/h and the largest body height of 188 cm (**Figure 2.9c**), we observed a relatively larger distortion of the path in the six-bar mechanism than in the four-bar and the eight-bar mechanism. We often observed the same unnatural paths at higher gait speeds (> 3.0 km/h) and larger heights (> 172 cm) accompanying larger trajectory errors. On the other hand, the four-bar and the eight-bar configuration mostly showed a well-matched path with the reference having about the same step length and foot clearance at higher gait speed. However, both mechanisms exhibited larger path deviations during the swing phase compared to the synthesized path at the median range of gait speed.

2.4.3. Force Amplification

We did not observe a substantial difference between mechanism configurations in force amplification. **Figure 2.10a** shows the time course of mechanical advantage for the case at 2.5 km/h gait speed and 172 cm body height. In this case, approximately 25% of the gait cycle in each case resulted in a mechanical advantage above 1. Across varying speeds and heights, greater mechanical advantage (percentage of gait cycle with M_A>1) overall was observed at small heights and low gait speeds (**Figure 2.10b**). This contrasted with less mechanical advantage at large heights and high gait speeds. The smallest portions of the gait cycle showing force amplifications across configurations were 15% of the gait cycle in the four-bar, 21% in the six-bar, and 14% in the eight-bar

configurations. Across all gait patterns, the peak mechanical advantage was typically observed at the heel strike event (**Figure 2.10a**).

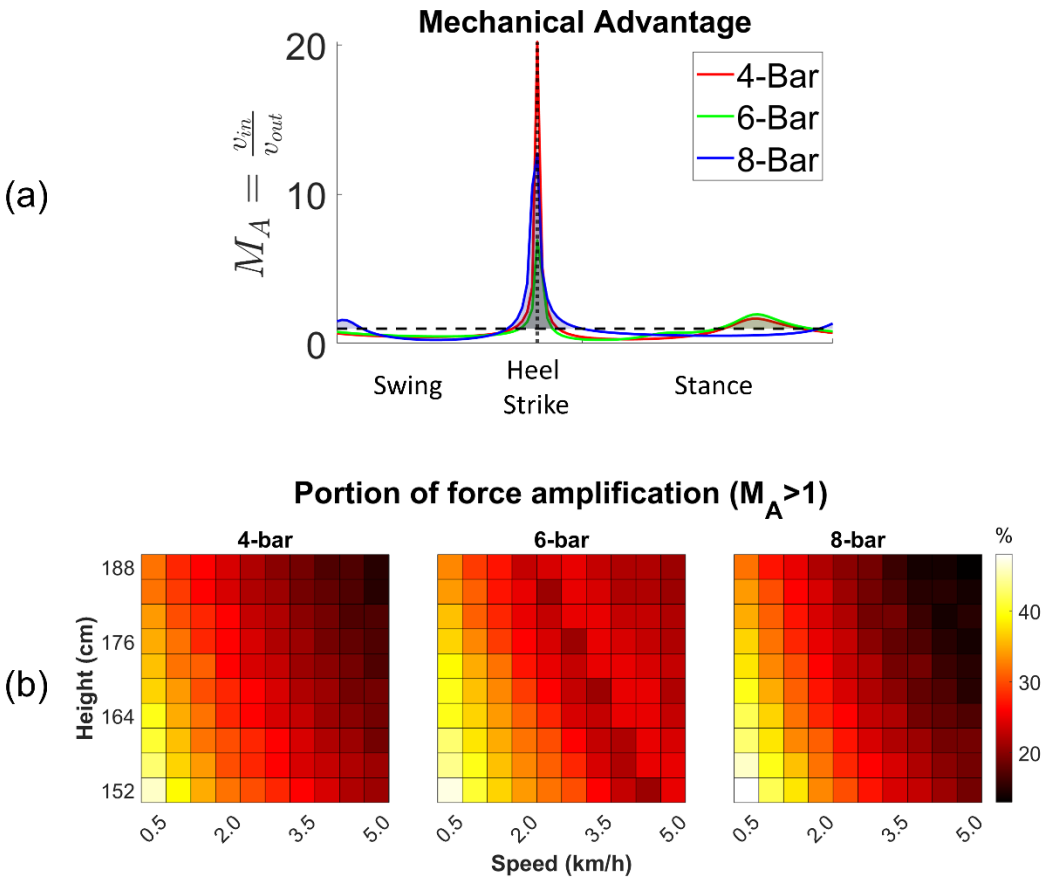

Figure 2.10: a) Time course of mechanical advantage for three mechanism configurations; b) Heat map for the portion of force amplification where $M_A > 1$ across gait patterns varied by height and walking speed. Peak mechanical advantage occurs at heel strike in all cases. The shaded area in an example mechanical advantage plot indicates where the input force starts to be amplified. Maximum mechanical advantage occurs at heel strike events.

2.5. DISCUSSION

In this work, we investigated the performance of three candidate mechanisms, four-, six- and eight-bar configurations, previously presented as solutions for electromechanical gait training [41], [43], [46]. We evaluated these mechanisms in terms of their kinematic accuracy in comparison to a large dataset of healthy individuals' gait trajectories using an optimization algorithm that adjusted two link lengths. We additionally reported kinematic error propagation of these mechanisms across different gait patterns based on varying height and walking speed. In the condition of a constant crank velocity, we observed that the eight-bar mechanism had less kinematic error than the four- and six-bar configurations between individuals or across heights and gait speeds. However, the time-independent path error between configurations was nearly identical. This work represents the first systematic comparison of single degree-of-freedom robotic gait trainer designs. These data provide a nuanced picture of which conditions are ideal for different mechanism configurations, resulting in a more effective situational design of mechanized gait trainers. These simplified gait trainers may be ideal as a more financially accessible electromechanical gait training option for clinics and at home.

The primary finding is that at constant crank velocity, the eight-bar mechanism has the lowest kinematic error of the three designs. Situations where constant crank velocity may be preferred include treadmill walking, especially if the machine itself is driven by the treadmill motor, similar to earlier versions of the LokoHelp [63].

Anchoring the input of the trainer to the treadmill negates the need for control, potentially reduces cost, and improves stability. The eight-bar was also the only configuration with an error under the within-subject gait trajectory variance, suggesting the clinical significance of the performance. The reduction in error relative to other mechanisms was invariant to different gait patterns derived from simulated changes in height and walking speed. The primacy of the eight-bar mechanism was expected since it has the greatest number of links, and thus has the greatest optimization flexibility for a desired gait pattern. This finding agrees with and extends our previous limited analysis comparing the eight-bar to a four-bar mechanism [46].

However, for cases where the mechanism is driven by its own motor independently, for example, in an overground walking configuration [41], [64], our results are not as clear. Based on the time-independent path error, we found the roughly equivalent performance of all three mechanism configurations. The errors were roughly equally low both compared to a large human gait dataset and gait patterns with simulated changes in height and gait speed. We expected to find that the eight-bar mechanism would perform better than the other two mechanisms. Instead, we observed that the kinematic tracking error of these mechanisms is governed by temporal instead of spatial considerations. We conclude that a greater number of links alone does not guarantee improved spatiotemporal behavior. Thus, based solely on kinematic error, given a well-controlled crank velocity, the four-bar mechanism [40], [41] is likely the best solution of the three configurations due to its simplicity.

One of the innovations of this work is that we compared the three mechanism configuration kinematics to a large human gait database [49] and simulated gait patterns with various height and walking speed [50] for a more comprehensive benchmark. Anthropometric parameters and walking speed modulate gait patterns [51], [65]. However, this large variance of gait patterns across individuals and walking speed have been disregarded in most gait trainer design studies using 1 DOF planar linkage mechanisms. Commonly a single gait trajectory from one subject or a normative gait trajectory was tested for proof-of-concept of mechanism synthesis [40]–[45]. This tremendously limits generalizability due to data bias and lack of information on other factors. The comparative examination in this study, utilizing low-bias cross-validation, provides a trustworthy, data-independent result. Also, extended analysis using simulated gait patterns provides insight regarding the effect of height and gait speed on kinematic accuracy.

The guiding philosophy behind the 1 DOF gait trainer is that inducing proprioceptive input as close as possible to natural gait will be most beneficial for recovery, and there is some evidence to support this hypothesis [66], [67]. Thus, training a natural gait motion along with inducing ground contact are crucial elements of the design. This study assumes that accurately assisting an ankle position in the sagittal plane could guarantee a natural proprioceptive input. However, it should be noted that a proper proprioceptive input would be further facilitated by controlling ankle orientation. The Lokomat and the gait trainers described here, with the exception of an additional cam

design for the six-bar mechanism [43], ignore ankle orientation. It is assumed that dorsiflexion is provided by elastic supports or through an ankle-foot orthosis. Future work should address whether the increased complexity of a controlled orientation of the ankle is justified.

This work is limited in its conclusions because it only compares three candidate mechanism configurations. There exist other possibilities, such as inversions of six-bar [64], [68] and eight-bar [69], [70] or more complex (e.g., ten-bar [44]) mechanisms that could have been considered for gait trainers, orthoses, and walking robots. It is possible that other six-bar and eight-bar configurations may perform more effectively compared to the examined Stephenson III six-bar and Jansen mechanism. We limited our scope to only Stephenson III and Jansen because they have been offered recently as candidate robotic gait trainers [43], [46]–[48]. We also did not examine designs with sliders or cams [43], [45], [71]. We avoided these design elements because they are not easily adjusted to fit an individual's gait trajectory. While we introduced the two-objective optimization for a comprehensive benchmark, researchers can differently configure the objective function based on J_1 and J_2 to obtain the linkage design appropriate for their specific operating scenario. Thus, while different solutions may be obtained by reducing cost functions to a single objective, we did not find any changes in the relationships between mechanisms in these conditions. There exist advanced methodologies that can draw an exact solution passing through precision points [72], [73]. Although we employed a numerical approach in order to modulate cost function to fit for the targeted

outcomes of comparison, such precise synthesis method should be considered to improve motion accuracy in future development. Another limitation is that the size of the mechanism and potential mechanical problems were not taken into consideration in this study. A compact device is preferable in a clinical environment and less problematic in practical application. For instance, the challenges faced with uncertainties arising from the manufacturing, assembly, sensors, control, and also numerical round-off errors would be severe in an eight-bar mechanism design. Future development should consider size and other practical issues with a novel approach taking any uncertainties into the mechanism synthesis [74]. Finally, our conclusions are limited to kinematic accuracy and mechanical advantage; considerations such as dynamics and controller performance are out of the scope of this work.

2.6. CONCLUSION

Recent research has offered numerous single DOF robotic gait trainer designs, but there is no systematic evidence comparing the performance of these designs. Our work focuses on the kinematic tracking error of three candidates, four-bar, six-bar, and eight-bar mechanism configurations. We observed that at constant crank velocity, such as controlled by a treadmill, the eight-bar mechanism has the best kinematic tracking, but all perform similarly if the crank velocity is well-controlled by an independent actuator. This work offers a quantitative approach to determining the relative performance between training mechanisms. This information will help determine cost-effective training solutions for rehabilitation clinics and possibly even home use.

Chapter 3: Kinematic predictors of quadriceps spasticity: Regression approaches and evaluation

3.1. INTRODUCTION

Gait disorders are common in stroke survivors. More than 80% of stroke survivors have varying degrees of gait abnormalities [2], [3], and about 25% have a residual impairment that requires full physical assistance, despite rehabilitation efforts [4]. Recent technological advances have introduced wearable robots as potential solutions to mitigate physical barriers for people with impaired mobility. There are various commercialized and research purpose lower-body exoskeletons showing promise in performance augmentation, mobility assistance, and gait therapy following neurological injuries [14], [75], [76]. Assistive strategies using exoskeletons incorporate force, torque, electromyography (EMG), and gait kinematics into the control loop [16], [76]. More recently, human-in-the-loop approaches have been introduced to maximize the benefit of the assistive device with feedback of metabolic energy measures in a real-time optimization [77], [78]. However, existing exoskeletons have only addressed weakness and ignored critical neuromuscular impairments, such as hyperreflexia, defined as a velocity-dependent exaggeration of stretch reflexes [79].

Stiff-Knee gait (SKG) is a common abnormal gait pattern following stroke, characterized by diminished knee flexion during the swing phase of the gait cycle. Sulzer et al. previously developed a lightweight, remotely actuated powered knee orthosis [18]

to assist post-stroke individuals with SKG. This robotic knee exoskeleton was expected to improve gait functionality with a reduction in compensatory motions. Hyperreflexia in the rectus femoris (RF), represented by higher than normal muscle activation in the pre-swing phase, primarily followed exoskeletal assistance, but occasionally without assistance as well [20]. Musculoskeletal modeling and simulation revealed that increased RF fiber stretch velocity preceded increases in RF muscle activation [20]. In a new cohort of individuals with SKG, Akbas et al. found that RF reflex excitability was highly associated with reduced swing phase knee flexion angle [80]. Taken together, this evidence indicates that robotic knee perturbations on post-stroke individuals with SKG could elicit counterproductive quadriceps hyperreflexia, a reaction likely spurred on by suprathreshold RF fiber stretch velocity. Thus, if excessive RF fiber stretch velocity could be avoided, it may be possible to enable the full benefits of exoskeletal assistance in those with post-stroke SKG. However, fiber stretch velocity is not easily measured or quantified in a real-time control system. Instead of muscle-tendon level mechanics, there is still a need for identifying clinically accessible controllable gait parameters to avoid hyperreflexia that could be elicited by exoskeletal assistance.

The objective of this study was to determine to what degree kinematic and kinetic features could substitute for RF fiber stretch velocity in predicting hyperreflexive RF muscle activation following exoskeletal assistance. To achieve this, I performed parametric and nonparametric multivariate regression analyses for variable selection on a knee exoskeleton gait data from 8 post-stroke participants with SKG [18]. I expected that

hip and knee flexion kinematics would predict RF hyperreflexia due to the biarticular characteristics of the RF. This work represents a novel statistical and machine learning regression approach to identify predictors of hyperreflexia. Obtaining clinically accessible predictors for hyperreflexia will lead to more effective assistive strategies that account for neural impairments.

3.2. METHODS

3.2.1. Experimental Data

I obtained previously collected data from 8 chronic, hemiparetic participants with post-stroke SKG who gave written informed consent using procedures approved by the local Institutional Review Board [19]. Inclusion criteria for the hemiparetic participants included their peak paretic knee flexion during swing was at least 15° less than their peak nonparetic knee flexion and the ability to walk for 20 min without rest at 0.55 m/s on a treadmill. A lightweight, powered knee orthosis was used to provide knee flexion torque perturbations during the pre-swing phase without affecting the remainder of the gait cycle [18]. Analog data, including GRF from the instrumented split-belt treadmill (Tecmachine, Andrez Boutheon, France) and applied torque by the powered orthosis, were acquired at 1 kHz. Motion capture data (Motion Analysis, Santa Rosa, CA) on the lower limbs was collected at 120 Hz. Electromyography (EMG) (Delsys Inc., Boston, MA) from the RF muscle was measured at 1 kHz.

The experimental protocol consisted of 3 treadmill walking stages. At the first stage, the torque calibration stage, each subject walked for approximately 60 seconds while receiving knee flexion torque assistance during pseudo-randomly chosen non-consecutive steps. Assistance ranged from 10 Nm to 40 Nm incrementing by 3 Nm and the maximum torque assistance amplitude was determined by the greatest peak knee flexion achieved during swing or 60º of swing phase knee flexion, whichever was lower torque for the participant. A baseline stage consisted of 60 s walking without assistance. Torque assistance was applied for the next 16 minutes at the level determined from the torque calibration stage. Through this assisted stage, four non-consecutive gait cycles were included with no assistance (catch trials). In this study, a total of 406 gait cycles were extracted from the torque calibration and torque assistance stages, representing both strides with and without exoskeletal assistance.

3.2.2. Musculoskeletal Modeling and Simulation

In order to determine muscle-tendon states (i.e., muscle fiber lengths and activations at each time instance), I employed musculoskeletal modeling and simulation through OpenSim 4.3 [81] using a method validated in previous work [20], [82]. To summarize, to account for a lower body marker set, I condensed upper body segments in the gait 2392 model of OpenSim to the pelvis segment so that it had 18 degrees of freedom and 90 muscle-tendon actuators. The modified model was scaled to match the anthropometry of each subject. Marker data were fed into the inverse kinematics tool, which generated joint kinematics with the least square fit of marker trajectories. A

residual reduction algorithm (RRA) adjusted the model to minimize dynamic inconsistencies between the experimental GRFs and body segment kinematics. Based on the adjusted model after RRA, computed muscle control (CMC) [83] estimated muscle-tendon states and excitation patterns that reproduced the motion while minimizing the sum of excitations squared. I took two external loads into account: assistive torques and unmeasured loads by a handrail. The assistive torques at the knee joint were modeled as equal and opposite external torques applied to the shank and the thigh segment. Force caused by holding a handrail, Fh, was modeled as Fh=i=1nmiai-Fgr, where mi and ai are the mass and acceleration of the *i*-th segment, respectively, Fgr is the ground reaction force vector, and n is a total number of segments. This estimated force was fed into the RRA to account for unmeasured loads by a handrail. All 3-dimensional residual forces and moments after compensation met the validity threshold (5 N of root mean squared residual forces and 30 Nm of root mean squared residual moment) [20] provided by the OpenSim guidelines [84]**.**

3.2.3. Dependent Variable

The dependent variable for the regression analysis was RF activity. The raw RF EMG signals were filtered with a fourth-order band-pass Butterworth filter with cutoff frequencies of 20–400 Hz to remove artifacts, demeaned, rectified, and low-pass filtered with a 4th order Butterworth filter at 10 Hz. To reduce inter-individual variability, I used the mean of the EMG envelope in the trial as the normalization reference [85]. The processed signals were divided into gait cycles based on a paretic limb heel-strike event

using vertical GRFs and then normalized into 100-time frames. A reflex response would occur within 120ms after stimulus onset through mono- or polysynaptic mechanisms [86]. This time interval has been employed to detect quadriceps stretch reflexes following mechanical knee perturbations during gait [87]. Similarly, I used a 120ms time window following stimulus onset to quantify quadriceps reflex responses. I defined the initiation of reflex as the timing of the peak pre-swing muscle fiber stretch velocity estimated from the musculoskeletal simulation. I then numerically integrated the 120ms RF EMG envelope following stimulus onset to obtain integrated EMG (iEMG) measures representing an involuntary response. We defined the voluntary component of RF iEMG occurring within 120 – 300ms following the stimulus onset. **Figure 3.1** visualizes RF iEMG for a voluntary and involuntary response.

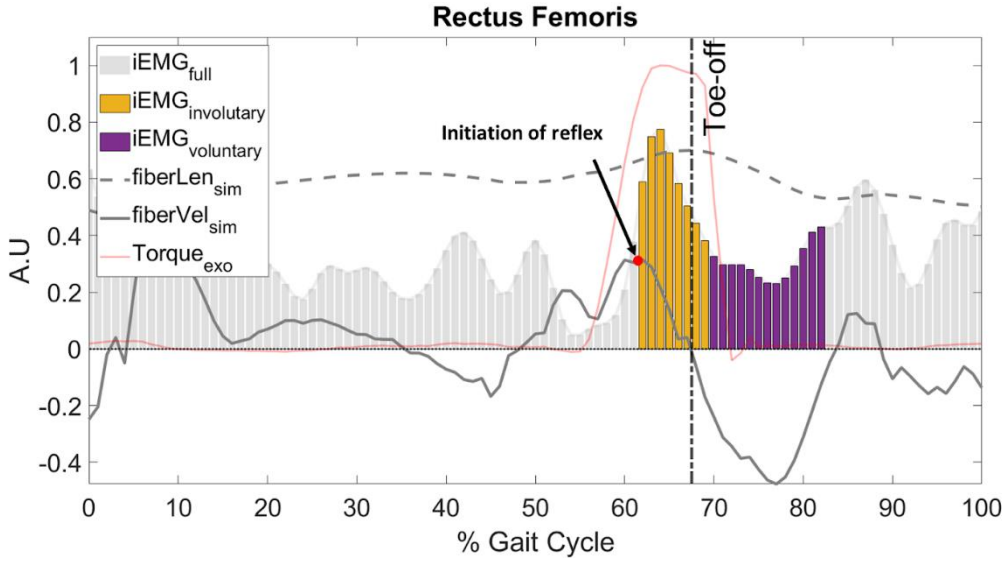

Figure 3.1: Visualization of the rectus femoris EMG signals, knee flexion torque assistance, and simulated muscle-tendon states. Gray-colored dashed and solid lines indicate simulated RF fiber length and velocity, respectively. Red solid line represents the external knee torque assistance profile by the powered knee exoskeleton device. Vertical bars show iEMG of RF muscle. The involuntary response is captured ranging from the peak simulated RF fiber velocity (initiation of reflex) and after 120ms (yellow). The voluntary response is defined by 120 – 300ms of time windows following peak RF fiber velocity (purple).

3.2.4. Independent Variables

A total of 14 predictors were extracted from each gait cycle based on muscle-tendon states as well as gait kinematic and kinetic data. One muscle-tendon relevant variable was selected from the musculoskeletal simulation: the peak pre-swing RF fiber stretch velocity. Three variables from hip and knee joint kinematics in the pre-swing phase (i.e., peak hip flexion and knee flexion velocity, and relative peak knee flexion velocity to peak hip flexion) were chosen due to the biarticular physiology of the RF and its associations with post-stroke SKG [88]. Correspondingly, I used 3 body kinematic

variables from the thigh and shank segments (i.e., peak thigh and shank angular velocity, and relative peak shank angular velocity to peak thigh) in the pre-swing phase. Rotation toward flexion was defined as a positive sign. Additionally, I used the pelvic segment acceleration in the anteroposterior plane as a proxy for body acceleration [89]. The remaining six variables were pulled out from propulsive/brake impulse and ground reaction forces. Specifically, I computed the paretic limb's propulsive, braking, and net impulse during the pre-swing phase, defined by the positive and the negative time integral of the anterior/posterior GRF curve, and the sum of the propulsive impulse plus the braking impulse, respectively [90]. GRF signals were processed to obtain the peak anterior/posterior GRF in the pre-swing phase, peak medial/lateral GRF in the stance phase, and peak vertical GRF in the stance phase. **Table 3.1** describes abbreviations of independent variables in this study.

Table 3.1: List of parameters.

Description	Abbreviation	Category
Peak rectus femoris fiber stretch velocity in pre-swing [20]	RectusFemoris_Vel	Muscle-tendon mechanics
Peak hip flexion velocity in pre-swing	HipFlex_Vel	Joint kinematics
Peak knee flexion velocity in pre-swing [91]	KneeFlex_Vel	Joint kinematics
Relative peak knee flexion velocity with respect to peak hip flexion	relKneeHip_Vel	Joint kinematics
Peak pelvic segment anterior/posterior acceleration in pre-swing [89]	Pelvic_AntPost_Acc	Body kinematics
Peak thigh segment angular velocity in pre-swing	Thigh_Vel	Body kinematics
Peak shank segment angular velocity in pre-swing	Shank_Vel	Body kinematics
Relative peak shank angular velocity with respect to thigh	relShankThigh_Vel	Body kinematics
Paretic propulsive impulse in pre-swing [90]	Propulsive_Impulse	Impulse
Paretic braking impulse in pre-swing [90]	Braking_Impulse	Impulse
Paretic net impulse in pre-swing [90]	Net_Impulse	Impulse
Peak anterior/posterior ground reaction force in pre-swing	AntPost_GRF	GRF
Peak mediolateral GRF in stance	MedLat_st_GRF	GRF
Peak vertical GRF in stance	Vert_st_GRF	GRF

3.2.5. Variable Selection using Regression Analysis

For a regression analysis, I considered two different machine learning regressors: Generalized Linear Mixed Models using Least Absolute Shrinkage and Selection Operator (glmmLASSO) and Bayesian Additive Regression Trees (BART). These two methods are parametric and nonparametric statistical approaches, respectively. The parametric approaches allow one to make generalizations from a sample to a population, provide intuitive and interpretable statistical inference, have greater statistical power, and work well with significantly less data than nonparametric methods. However, linear mixed models require assumptions of linearity and normal distribution, which may not be true in actual data. On the other hand, nonparametric methods do not need stringent assumptions about the nature of the population distribution. They are generally robust to outliers and tend to be more accurate as they seek to best fit the data points while they are usually not as efficient as parametric approaches due to a large number of observations and training requirements to accurately estimate the unknown function. In this study, I aimed to achieve a more comprehensive variable selection through both parametric and nonparametric regression methods.

3.2.5.1. Generalized Linear Mixed Models using LASSO

The least absolute shrinkage and selection operator (LASSO) method is a penalized regression technique that uses an L1-norm penalty on the regression coefficients [92]. It is often used for multidimensional variable selection because its nature of regularization removes variables with little influence on a dependent variable.

In linear regression, the best fit is usually determined by minimizing a cost function, such as the residual sum of squares (RSS), given by

$$RSS(\beta) = \sum_{i=1}^{n}(y_i - \beta_0 - \sum_{j=1}^{p}\beta_j x_{ij})^2, \quad (1)$$

where jare the regression coefficients associated with each feature. The LASSO method puts a constraint on the sum of the absolute values of the model parameters (L1-norm) in order to apply a regularization process shrinking the coefficients of the regression variables towards zero. The mathematical formulation of the penalized residual sum of squares (PRSS) with L1-norm penalty is given by

$$PRSS = RSS + \lambda \sum_{j=1}^{p}\beta_j^2, \quad (2)$$

where λ is a control parameter for coefficient shrinkage. By the addition of regularization, the LASSO regression produces a sparse and interpretable linear model with important variables automatically selected. LASSO-type regressors have established efficacy in variable selection from irrepresentable conditions (i.e., settings with high multicollinearity) [93], [94]. Statisticians also proposed L1-penalty approaches with the generalized linear mixed models for correlated and clustered responses [95], [96]. In this study, I applied generalized linear mixed models using LASSO (glmmLASSO) for a variable selection using the *glmmLasso* package in R statistical software [96]. I set a random intercept model with subjects as random effects and all predictors as fixed effects.

I then built repeated 5-fold cross-validation to avoid a bias in the evaluation regression model. In data splitting, stratified sampling was applied based on subjects to obtain a sample population that best represents the entire population. In every cross-validation loop, the parameter λ was tuned by grid search using Bayesian Information Criteria (BIC). To quantify the importance of each predictor variable in regression, I ranked variables based on the selection proportions defined by frequencies of each selected variable in trained LASSO models from repeated cross-validation. The selection proportions have a score ranging from 0 (always shrunk, unimportant feature) to 1 (never shrunk, essential feature) by averaging variable selection frequencies so that I could infer individual feature importance in the regression model. The same ranking method was used in a previous regression study for post-stroke clinical outcome [97]. In this study, I repeated 50 cross-validation repetitions to obtain variable selection proportions from the LASSO regression analysis. Variables above the threshold were determined as critical parameters for prediction. The threshold was 0.95 meaning 95% of the chance for selection across repeated cross-validation.

3.2.5.2. Bayesian Additive Regression Trees

Bayesian Additive Regression Trees (BART) is a nonparametric, ensemble method of regression tree models, introduced by Chipman et al [98]. It recently has gained popularity due to its improved prediction performance over other machine learning techniques (i.e., random forests, gradient boosting model, neural networks) in various study settings [98]–[100]. An ensemble method stands for a technique that

combines the predictions from multiple learning algorithms (weak learners) to improve predictive accuracy. BART combines the advantages of the Bayesian model, incorporating past information about a parameter and forming a prior distribution for future analysis, and ensemble methods.

A regression tree estimates the relationship between predictors and responses by recursive partitioning of the predictor space based on the importance of each predictor to the response. Suppose I have a continuous response *y* and *p*-dimensional vector of predictors $x = (x_1,\cdots,x_p)$. The basic BART model is a sum of regression trees defined as

$$y = \sum_{j=1}^{m} g(x; T_j, M_j) + \varepsilon, \quad \text{where } \varepsilon \sim N(0, \sigma^2) \tag{3}$$

where T_j is *j*-th binary regression tree, M_j is a set of its associated terminal node parameters (known as leaves), ε is a residual with a variance of σ^2, and *m* is the total number of trees in the model. The challenge with this additive regression trees model is avoiding overfitting. To prevent overfitting, BART relies on the prior distribution, posterior sampling, and averaging rather than loss minimization.

Prior distributions of parameters are required to form the Bayesian model. In the BART model, this prior distribution regularizes the size and fit of each tree to keep its effects from being overly influential. Prior independence is assumed between regression trees, node parameters, and the residual standard deviation. The form of the prior can be written as

$$p((T_1, M_1),\cdots,(T_m, M_m), \sigma) = \left[\prod_j \left\{\prod_i p(\mu_{ij}|T_j)\right\} p(T_j)\right] p(\sigma) \tag{4}$$

where $\mu_{ij} \in M_j$. The prior distribution of trees $p(T_j)$ is governed by its depth d whose probability is given by $\alpha(1+d)^{-\beta}$ with $\alpha \in (0,1)$ and $\beta \in [0,\infty)$. The parameter α controls how likely a node would split, while the parameter regularizes the number of terminal nodes. The prior distribution of $\mu_{ij}|T_j$ follows the conjugated normal distribution. To further avoid overfitting, the node parameters μ_{ij} are calibrated yielding $\mu_{ij} \sim N(0, \sigma_\mu^2)$, where $\sigma_\mu = 0.5/(k\sqrt{m})$. Recall that m is the number of trees and k is a controllable parameter that has the effect of shrinking the tree parameters μ_{ij} toward zero. The prior on usually follows the inverse Chi-square [98] or inverse Gamma distribution [101]. The degrees of freedom for this distribution can be specified to represent the probability that the model residual standard deviation is less than the estimated one from a linear regression fit to the data. These regularization priors keep individual tree components small to prevent overfitting.

BART uses Markov chain Monte Carlo (MCMC) algorithms to obtain a posterior distribution of the set of trees, terminal node parameters, and residual standard deviation. An MCMC algorithm can be constructed based on Gibbs sampling with some Metropolis-Hastings steps and Bayesian backfitting [102]. To sample the tree structures to be used for prediction, the sampler algorithm conventionally proposes a new tree by randomly choosing one of the following four moves: grow (node birth), prune (node death), change (changing splitting rule), and swap (swapping internal decision rule). More efficient MCMC algorithms for BART have been introduced and implemented in the R statistical software [101], [103], [104].

To evaluate the relative importance of each predictor variable from BART, Chipman et al. proposed the variable inclusion proportion corresponding to the proportion of times each variable is selected for splitting nodes across MCMC iterations in the sum-of-trees model [98]. Intuitively, variables with higher inclusion proportions are the more important variables in prediction. In this study, I implemented BART and extracted the variable inclusion proportions as a feature importance metric by using the *BART* package publicly available in R statistical software [105]. I performed a repeated 5-fold cross-validation with a total of 50 repetitions for unbiased regression outcomes. The stratified split dataset across repetitions was exactly the same as the one used for glmmLASSO for a lateral comparison. Variables above the threshold, denoted by 1/(total number of predictors), were determined as a crucial subset. This threshold stands for the probability of equal inclusion for all predictors in the model.

3.2.6. Model Selection

With key variables resulting from both parametric and nonparametric variable selection, I fit reduced models using a linear mixed and BART regression. For linear mixed model regression, I formulated a random intercept model with nested random effects in terms of subjects and exoskeletal assistance. Parametric and nonparametric models were compared to each other based on goodness-of-fit measures, such as adjusted R^2 and Root Mean Square Error (RMSE) acquired by 50 repetitions of 5-fold cross-validations. Based on the reduced fit model, I additionally performed a model selection through backward stepwise elimination. This stepwise regression eliminated insignificant

variables resulting in the final best fit model with minimum numbers of predictors. Additionally, the relationships between variables were examined by Spearman's rank correlation coefficient.

3.3. RESULTS

Figure 3.2 shows variable importance from the parametric (left) and the nonparametric approach (right) with the full model. Four parameters from kinematic and muscle-tendon state variables in the pre-swing phase remained (>95% of selection proportion) in the LASSO model across all 50 iterations: peak shank velocity, relative peak knee velocity with respect to hip, peak RF fiber stretch velocity, and peak knee flexion velocity. Using BART, six predictor variables from kinematic and muscle-tendon state variables in the pre-swing phase were determined as crucial variables. These were four common important variables between the parametric and nonparametric variable selection: the peak shank velocity, relative peak knee velocity with respect to the peak hip flexion, the peak RF fiber stretch velocity, and the peak knee flexion velocity. All parameters above the significance threshold using LASSO were also above the significance threshold using BART. Both variable selections resulted in low importance scores for all variables related to GRF and impulse.

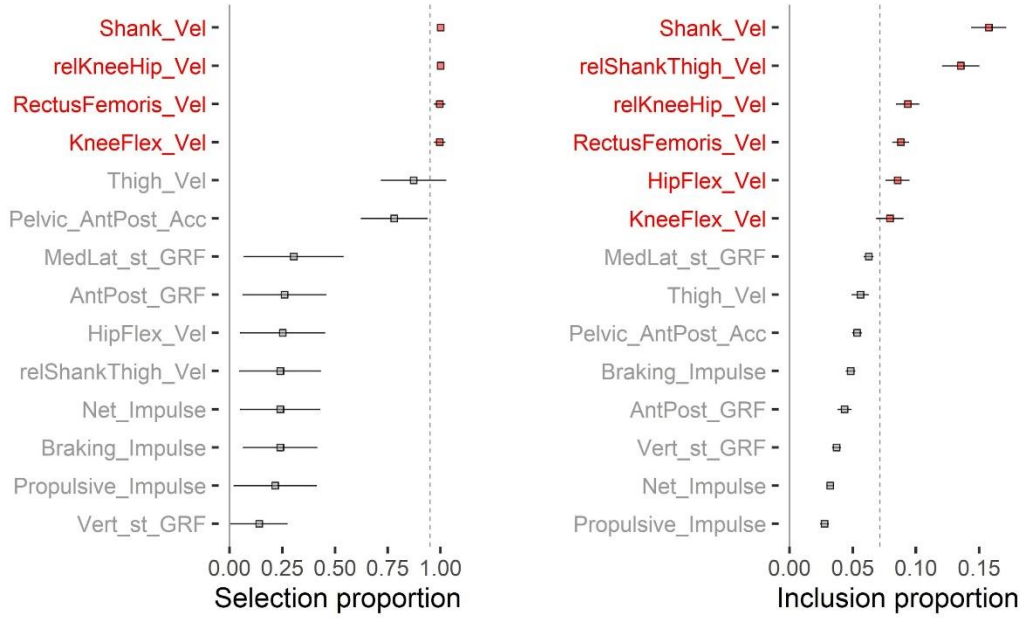

Figure 3.2: Variable selection results from glmmLASSO (left) and BART (right) for a total of 14 predictors. The square markers represent the average and the solid lines are the standard deviation of total 50 repetitions. The red-colored variables are essential variables showing above the threshold (vertical dashed line) denoted by 95% of selection proportions and 1/total number of variables for glmmLASSO and BART, respectively.

To ensure the model was both representative and not overly complex. I fitted a reduced model using all six significant predictors from **Figure 3.2**, and then evaluated the goodness-of-fit of models. I used the same random effects and the same hyperparameter setting as the variable selection. **Table 3.2** summarizes accuracy measures for full and reduced regression models from repeated 5-fold cross-validation. The reduced model showed slightly degraded goodness-of-fit (i.e., increased RMSE and decreased adjusted R^2) compared to the full model. Except for the parametric regression model's out-of-bag test, all accuracy measurements differed significantly between full and reduced models ($p < .001$).

Table 3.2: Summary of regression model accuracy from repeated 5-fold cross-validation.

		Linear Mixed Model		BART Model	
		Full model	**Reduced model**	**Full model**	**Reduced model**
No. Predictors		14	6	14	6
RMSE	**Train**	5.20 ± 0.01	5.39 ± 0.07	3.12 ± 0.08	3.86 ± 0.04
	Test	5.68 ± 0.06	5.64 ± 0.06	5.41 ± 0.11	5.52 ± 0.08
Adj. R^2	**Train**	0.47 ± 0.00	0.43 ± 0.00	0.83 ± 0.01	0.73 ± 0.01
	Test	0.40 ± 0.11	0.41 ± 0.01	0.46 ± 0.02	0.43 ± 0.02

Backward stepwise elimination additionally cut down the number of variables from the reduced model of six important predictors. The stepwise elimination on the parametric model was based on the Akaike information criterion (AIC). The adjusted R^2 was used for the nonparametric model's stepwise elimination. Stepwise regression using the parametric model, linear mixed model, determined the last four crucial variables including two joint kinematic and another two body kinematic variables: peak hip flexion velocity, relative peak knee velocity to peak hip flexion, peak shank velocity and the relative peak shank velocity to peak thigh velocity. **Table 3.3** represents the summary of the final regression model by a random intercept mixed model with nested random effects with respect to subject and assistance. Small marginal R^2 (0.074) but moderate conditional R^2 (0.505) accounted for the most variance of this model. The adjusted R^2 of this final model was 0.533. Backward elimination based on the nonparametric model,

BART, revealed the same last four critical predictors. **Figure 3.3** illustrates the goodness-of-fit changes through backward elimination using BART. Once the model consisted of less than four predictors, its adjusted R^2 started decreasing significantly meaning that variables in the gray shaded area of **Figure 3.3** were the minimum crucial predictor set. The adjusted R^2 of BART model with four variables was 0.638.

Table 3.3: Summary of final model from stepwise backward regression.

Marginal R^2 / Conditional R^2: 0.074 / 0.505 **Adjusted R^2:** 0.533		**Dependent Variable**	
Category	**Predictors**	**Slope estimates**	**[95% CI]**
Joint kinematics	HipFlex_Vel [rad/s]	11.30 **	[2.61, 19.98]
	relKneeHip_Vel [rad/s]	11.59 *	[3.38, 19.71]
Body kinematics	Shank_Vel [rad/s]	-21.11 **	[-37.10, -5.12]
	relShankThigh_Vel [rad/s]	10.54 **	[1.96, 19.11]

**** p<0.05 ** p<0.01 *** p<0.001***

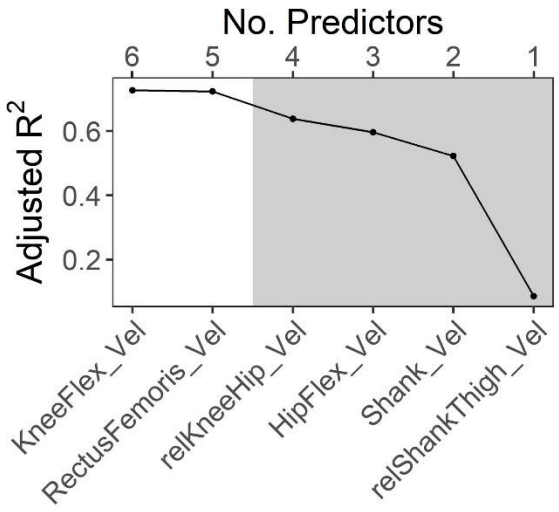

Figure 3.3: Goodness-of-fit changes by BART stepwise backward elimination. The variable names shown in the bottom axis are the predictors removed at each step. For example, "KneeFlex_Vel" was removed at the first step of elimination from a model with six variables. The gray shaded area indicated the steps that the adjusted R^2 was significantly affected by the elimination.

Table 3.4: Spearman's rank correlation coefficient between key kinematic predictors and pre-swing rectus femoris fiber stretch velocity.

Category	**Predictors**	**ρ**
Joint kinematics	HipFlex_Vel [rad/s]	0.59 ***
	relKneeHip_Vel [rad/s]	0.90 ***
Body kinematics	Shank_Vel [rad/s]	0.87 ***
	relShankThigh_Vel [rad/s]	-0.18 ***

**** p<0.05 ** p<0.01 *** p<0.001***

The relationships between selected kinematic predictors and muscle-tendon state, pre-swing rectus femoris fiber stretch velocity, were examined by Spearman's rank correlation coefficient. **Table 3.4** summarizes the coefficients.

3.4. DISCUSSION

Exoskeletal assistance and therapy has the potential to unload some of the effort from clinicians and caregivers but does not yet account for other neuromuscular impairments such as hyperreflexia [19], [80]. The aim of this study was to determine accessible biomechanical predictors of quadriceps hyperreflexia based on knee flexion perturbations of various torque magnitudes on those with post-stroke SKG. I used both parametric and non-parametric regression techniques to obtain two different perspectives of the key kinematic, kinetic and muscle-tendon predictors of rectus femoris hyperreflexia. I found four kinematic predictors obtained during pre-swing phase were shared between the regression techniques: peak hip flexion velocity, the relative peak knee to peak hip flexion velocity, peak shank angular velocity, and relative peak shank to peak thigh angular velocity. These parameters can be measured by two or three wearable sensors. The implication of these findings is that these parameters can be used to predict and control hyperreflexia during exoskeletal assistance. Further, these parameters may also offer insight into the mechanisms of quadriceps hyperreflexia.

Spasticity is often characterized as velocity-dependent hyperexcitability of the stretch reflex [106]. Since it was widely believed that the spindle proprioceptive receptors encode information for muscle length and velocity changes [107]–[109], spasticity

modeling has been based on muscle length and velocity feedback [110], [111]. Our group's previous musculoskeletal simulation analysis confirmed the strong association between simulated RF muscle fiber stretch velocity and simulated RF excitability [20]. In this study, both parametric and nonparametric regression techniques for variable selection resulted in the same finding that kinematic variables are predictive of an RF reflex. Indeed, there were strong correlations ($\rho \simeq 0.90$) between some of the selected predictors (relative peak knee flexion velocity to peak hip flexion velocity, peak shank angular velocity) and RF fiber stretch velocity (**Table 3.4**), as we expected. I did not expect that these parameters would be more predictive of a reflex than RF fiber stretch velocity, the physiological mechanism of a stretch reflex. The fiber stretch velocity was computed using generic Hill-type muscle models and mathematically driven cost functions [83], rather than direct measurement, a model validated in our previous work [20]. Yet, it remains possible that RF fiber stretch velocity could have played a stronger statistical role if the true value could have been obtained. Regardless of the level of significance between variables, it is notable that out of all 14 parameters, the ones found to be most predictive of a reflex were ones related to hip and knee kinematics as well as RF fiber stretch velocity. This finding is consistent with our hypothesis that more easily measurable kinematic variables can serve as a proxy for fiber stretch velocity in exoskeletal control.

My study has an important implication related to wearable robotics for rehabilitation. I discovered kinematic biomarkers that could effectively estimate

involuntary quadriceps reactions following exoskeletal assistance. This would justify the use of kinematic information in the wearable robotics control loop to address neurological impairment, instead of feedbacking direct measurement or estimation of muscle mechanics. This is significant from a practical perspective. Over the past decade, the exoskeleton community has moved towards personalized design and assistive strategies to allow natural and comfortable augmentation by incorporating human factors into the control loop [77], [78]. Even more, a real-time EMG-driven musculoskeletal modeling framework has been proposed [112] enabling the development of personalized assistive devices and rehabilitation strategies by real-time estimation of musculotendon mechanics. A soft exosuit for ankle motion assistance was integrated with onboard ultrasound imaging so that an individualized muscle-based assistance strategy was accomplished by directly measuring muscle dynamics [113], [114]. More recently, a wearable knee exoskeleton using real-time ultrasound-derived muscle state feedback was proposed [115]. Those state-of-the-art approaches have a great potential to take neurological impairment into the control strategy, however they remained limited to a few research institutes due to a dearth of engineering infrastructure. On the other hand, kinematic predictors from this study could be measured by only two or three portable motion sensors such as inertial measurement units. Enabling the use of ubiquitous sensor systems would allow exoskeleton engineers and rehabilitation researchers to design practical and effective devices.

This study suggested the potential necessity to consider multi-joint exoskeletal assistance (i.e., hip-knee) to improve the efficacy of assistive strategies in those after stroke. Multi-joint lower extremity exoskeleton robots had been introduced both for assistive and rehabilitative purposes [116], [117]. However, there is no clear evidence showing the benefit of multi-joint exoskeletons over single-joint versions, except for metabolic cost reduction [118], [119]. In this study, hip and relative kinematics following knee flexion assistance played a significant role as a biomarker for rectus femoris involuntary activity. This implies that the rectus femoris hyperactivation could be effectively controlled by optimizing multi-joint assistance [82].

It is possible that this work could lack a wide range of variables. Due to the exponential increase in the sampling volume, adding extra dimensionality is not always beneficial in regression analysis, specifically when there are sparse relevant predictors compared to the total number of predictors or the fundamental relationships are nonlinear (so called “curse of dimensionality”) [120]. To avoid these adverse effects, I limited the scope of parameter sources among previously assessed associations with post-stroke SKG. Additionally, I did not include joint kinetics that were not able to be directly measured, except for simulated muscle fiber stretch velocity. This omission was due to the practical difficulty in measuring real time joint kinetics. Therefore, in this work I aimed to balance comprehensiveness with overfitting.

This study has several limitations. Regression approaches based on observations from only 8 participants may affect generalization of the results. Despite the small sample

size, the repeated 5-fold cross-validation [121] took into account the randomness in sampling resulting in unbiased and trustworthy variable and model selection results. This study does not provide causal relationships between kinematic parameters and quadriceps hyperreflexia. However, it is notable that the predictors of RF hyperreflexia (i.e. related to knee-hip velocities) found in this work were all physiologically related to the biarticular span of the RF suggesting that this statistical approach may help reveal mechanisms of hyperreflexia. For instance, the relative peak angular velocity between the knee and hip was the most correlated variable with RF fiber stretch velocity ($\rho = 0.90$ in **Table 3.4**). Still, the relative peak angular velocity between the shank and thigh had a weak negative correlation ($\rho = -0.18$ in **Table 3.4**) to RF fiber stretch velocity. While thigh-shank segment and knee-hip joint velocities are not equivalent, the large difference in correlations is difficult to explain mechanistically and other approaches may be needed to investigate further. Lastly, my findings were based on two types of regression techniques among numerous statistical and machine learning approaches. Although there exists an advanced penalized regression approach improving the limitations of LASSO [122] (i.e., Elastic Net [123]), glmmLASSO in this study could result in a better model due to subjects' random-effects modeling. There were also popular tree-based machine learning algorithms, such as gradient boosting [124] and random forest methods [125]. It has been reported that BART has outperformed these other methods [98]. Therefore, the use of these two different regression methods was sufficient to get legitimate results.

3.5. CONCLUSIONS

Despite the rapid growth of wearable robot technology, there is still a lack of consideration regarding neuromuscular impairments such as hyperreflexia into device design. In this study, I introduced regression-based variable selection for predicting rectus femoris hyperreflexia following pre-swing knee flexion exoskeletal assistance. I found that four kinematic variables relevant to knee and hip joint motions were sufficient to effectively predict hyperreflexia in people with post-stroke SKG. These results suggest that effective monitoring and control of these accessible knee and hip kinematics may be more productive at regulating hyperreflexia than the more complex acquisition of muscle fiber stretch velocity. This work represents a novel statistical approach to identifying biomechanical associations with reflex function. This information could be used to further understand the mechanisms of hyperreflexia and its associated clinical interventions.

Chapter 4: Cluster analysis to characterize post-stroke Stiff-Knee gait

4.1. INTRODUCTION

Accurate diagnosis of impairment is a key to treatment. With this in mind, there have been numerous efforts in the identification and characterization of post-stroke gait patterns [22]–[24], [126]–[130]. Examples of abnormal gait patterns following stroke include drop foot (inability to dorsiflex at the ankle) [22], Stiff-Knee gait (SKG, reduced swing-phase knee flexion angle) [23], and knee hyperextension (also known as *genu recurvatum*) [24]. However, the selection of key parameters has been subjective and primarily based on visual inspection [126], [127], [129]. Such a practice can lead to misdiagnosis and miscommunication between care providers.

An example of a poorly defined gait disability is SKG. Post-stroke SKG is unstable and energy inefficient [131], [132]. It commonly occurs in post-stroke gait, but there is no quantifiable data on prevalence, perhaps due to its vague definition. Historically, descriptions of a "stiff" knee have been used to illustrate knee kinematics in children with cerebral palsy since at least the late 1800's [133], although by 1958 the term "stiff-legged" was used to denote a common condition in hemiplegic adults [134]. Perry and Burnfield defined SKG with greater detail, including "inadequate" knee flexion angle in initial swing, but also including toe drag and poor hip flexion angle preventing limb advancement [135]. Sutherland et al. characterized SKG by circumduction and toe dragging [136]. De Quervain et al. described the SKG pattern as prolonged reduced (i.e.

20 ~ 30°) knee flexion coupled with decreased ankle dorsiflexion throughout the stance phase of gait [127]. Subsequent work in post-stroke SKG maintained the knee flexion requirement but ignored toe drag, ankle dorsiflexion, and hip flexion when defining the disability [23], [137], [138]. Initially, describing low knee flexion as "stiff" may have been intended to provide better visualization of what gait looked like to other scientists and clinicians. However, defining SKG as a diagnosis takes on critical clinical importance with the advent of surgical [139], [140] and pharmacological [141]–[143] interventions available. In other words, the lack of an accurate and consistent definition of SKG is a hurdle for developing effective interventions.

Contemporary definitions of SKG lack appropriate specificity. Defining SKG based on knee flexion angle does not specify how much knee flexion constitutes "inadequate" [135] or how to account for confounding factors on knee angle such as walking speed or height. Studies use arbitrary boundaries, such as a 40 ~ 45^{o} knee flexion range, or knee flexion below two (or three) standard deviations of a sample population, or based on a specific threshold [88], [144]–[147]. Other approaches have used a between-limb difference in knee range of motion during the swing phase [19], [29], which can account for changes in gait speed, but still lacks rationale to what angular difference is required. SKG has even been defined by combinations of peak knee flexion during the swing phase, knee range of motion during the early swing phase, total knee range of motion, and timing of peak knee flexion during the swing phase compared to healthy controls [88], [148]–[153].

Further exasperating the vague definition of SKG is an equally equivocal understanding of its causes. Researchers have identified quadriceps overactivity [80], [91], [149], [154]–[156], decreased iliopsoas activity [154], insufficient calf muscle strength [23], decreased hamstring strength [135], muscle co-contractions [157], [158], and reduced muscle coordination [159] to be associated with SKG. Decreased knee flexion angle, velocity [88], [151], [160], delayed timing [136], [161] and reduced push-off acceleration [144] were kinematic correlates of SKG. Kinetic parameters such as excessive knee extension moment [88], [151] and paretic propulsion [162] have been associated with SKG. These parameters are not necessarily mutually exclusive. It also may be possible that such heterogeneity is due to multiple subtypes of SKG or other conditions being confused with SKG. The goal of this work is to sift through these gait characteristics associated with SKG and quantitatively determine whether there are multiple phenotypes of the condition.

In clinical gait analysis, cluster analysis has been adopted to identify homogeneous subgroups of pathological gait patterns using various sets of gait parameters mostly based on joint kinematics [128], [130], [163]–[168], spatiotemporal characteristics [127], [128], [166], [169]–[172], and muscle activity [129], [173]. Cluster analysis is a statistical technique separating data into different clusters on the basis of their compactness or separation. It is unsupervised learning aiming to find natural partitions in the feature space of input data. De Quervain et al. identified four distinguishable patterns including a stiff-knee among gait deviations in the early recovery

phase following stroke by visual inspection of the sagittal-plane joint kinematics [127]. More quantitatively, Mulroy et al. performed non-hierarchical cluster analysis based on spatiotemporal and the sagittal-plane kinematic characteristics resulting in four different clusters [128]. However, there were no analogous clusters that exhibited the stiff-knee pattern described by De Quervain et al. Straudi et al. similarly used sagittal-plane kinematics to separate hemiplegic gait patterns into three clusters and found one that showed a "stiff-knee" pattern characterized by reduced knee flexion in both the stance and swing, decreased plantarflexion at the push-off, inappropriate hip flexion/extension in the stance, and increased pelvic internal rotation [174]. These inconsistent results could be due to an overreliance on sagittal plane kinematics and ignoring characteristic frontal plane compensatory motions such as hip abduction and pelvic obliquity [175].

The primary goal of this study was to determine a more accurate specification of SKG as well as possible multiple phenotypes. I analyzed gait data from a cohort of 50 post-stroke individuals with varying walking impairments and 15 healthy controls by cluster analysis together with more holistic biomechanical characteristics of SKG. I based clustering techniques to examine two independent goals. First, I used univariate clustering to determine the most acceptable single variable specification for the post-stroke SKG cohort identification. The second goal was to investigate the existence of post-stroke SKG phenotypes. I employed time-series kernel *k*-means clustering [176] with a global alignment kernel [177] based on compensatory strategies commonly associated with post-stroke SKG [175], but notably not knee flexion angle to avoid

biasing the results. I hypothesized that frontal plane compensatory motion differences between individuals with stroke would reveal different subgroups of SKG, which are associated with different motor control profiles. This work presents quantitative characterizations of post-stroke SKG using unsupervised machine learning techniques. The findings from this study will make SKG-associated gait characteristics clearer, help better prescribe specific treatments, and homogenize study populations for interventions.

4.2. METHODS

4.2.1. Data Source

Gait data were collected from 50 hemiparetic post-stroke individuals (31 left hemiparesis, 31 male, 57 ± 13.46 years) and 15 healthy controls (7 male, 54.47 ± 8.73 years). Participants provided informed written consent to the Institutional Review Board approved protocol. Participants walked on a split-belt instrumented treadmill (Bertec, Columbus, Ohio) at their self-selected speed. Prior to data collection, participants practiced treadmill walking to get comfortable with the experimental setup. Participants walked for at least 10 seconds to reach a steady-state walking pattern before each 30-second trial. Motion capture marker data were collected at 120 Hz using a 12-camera motion capture system (PhaseSpace, San Leandro, CA) with a modified Helen Hayes marker set using 65 active markers. EMG data were collected (Motion Labs, Cortlandt, NY) at 1000 Hz from bilateral electrodes placed on the medial gastrocnemius (GAS), soleus (SOL), tibialis anterior (TA), vastus medialis (VA), lateral hamstrings (LH),

medial hamstrings (MH), rectus femoris (RF), and gluteus medius (GM). EMG data were high-pass filtered at 40 Hz, demeaned, rectified and low-pass filtered at 4 Hz. For each muscle, the filtered signal was normalized to its mean value of EMG envelope during each trial to reduce inter-individual variability [85]. Ground reaction force (GRF) data were measured by an embedded force plate in a split-belt treadmill and low-pass filtered at 15Hz. Using the kinematics and dynamics solver within OpenSim 4.3 [81], joint kinematics, body kinematics, and joint kinetics were obtained. All synchronized time-series biomechanical gait data in section 4.2.1 were divided into strides by a paretic limb heel-strike event using vertical GRFs and expressed as a percentage of the cycle time. Five strides per subject were randomly selected from 30-second treadmill walking trials for further analysis.

To create a clinical diagnosis label, I reconstructed 3D animations with 4 different camera view angles from the motion captured data by using OpenSim software. An expert clinician reviewed these anonymized animated videos and diagnosed whether subjects exhibited post-stroke SKG.

4.2.2. Univariate Cluster Analysis

The goal of univariate cluster analysis was to determine the most acceptable single specification from characteristics commonly used for differentiating post-stroke SKG cohorts in previous studies. I applied one of the popular partitioning methods, *k*-means clustering [178], with a single input variable. I primarily considered disability-specific kinematic characteristics in the sagittal plane: peak knee flexion in the swing

phase, between-limb difference of the peak knee flexion in the swing phase, peak knee flexion velocity in the pre-swing phase, knee range of motion in the initial swing phase measured from toe-off to the first half of swing, and total knee range of motion during gait [19], [88], [137]. I additionally tested the peak knee extension during the stance phase with the assumption of the potential causal effect of hyperextension to SKG based on potential existence of stance-phase knee hyperextension [135], [179]. Among spatiotemporal characteristics of SKG, I assessed the timing of peak knee flexion during the swing phase from the evidence of delayed knee flexion [136]. Lastly, I examined the peak vertical lateral malleolus acceleration during the pre-swing phase proposed as a method to differentiate inadequate push-off associated with post-stroke SKG [144].

Figure 4.1 summarizes the 9 parameters used in this study. The correlations were examined by the Kendall rank correlation coefficient for filtering out poorly associated features to post-stroke SKG primarily represented by reduced knee flexion kinematics. Features considered as poor characteristics were excluded from further validity analysis.

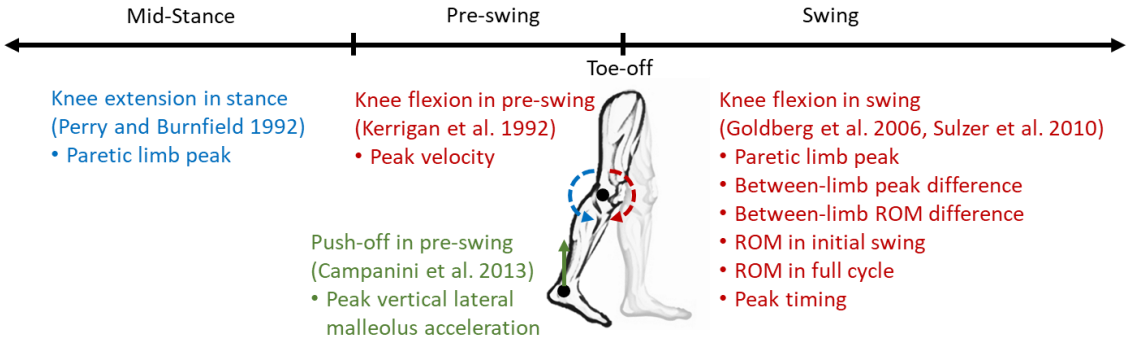

Figure 4.1: A total of 9 knee joint-relevant features for univariate clustering analysis.

The univariate *k*-means clustering was repeatedly performed according to each input variable. Here, I set the number of clusters to two, representing supposed SKG and non-SKG groups. Cluster validation went through using external information about the data, known as an external cluster validation [180]. External cluster validation uses a priori knowledge of dataset information, such as gold standard labels. Such clinical diagnosis enables evaluation of the goodness of clusters [181]. In this univariate cluster analysis, I aimed to quantitatively verify the binary clusters resulting from individual variables used for clustering. Given clinical diagnosis labels, I computed external measures to determine the optimal univariate input feature resulting in the best clusters. These included F1 score [181], Purity [181], Adjusted Rand Index [182], Adjusted Mutual Information [183], and V-measure [184]. F1 score is a measure of accuracy which is defined as a harmonic mean of precision and recall. Purity measures the ratio of the objects from the majority class. Adjusted Rand Index is a pair-counting measure, which is based on counting the pairs of objects in the data set on which two different partitions agree or disagree. Adjusted Mutual Information measures the information that two clusters share. The V-measure is defined as the harmonic mean of homogeneity and completeness of the clustering, which are measures of how much each cluster contains elements of a few different classes and how much putting all elements of each class in single clusters, respectively. Higher values mean better quality of clusters for all measures.

4.2.3. Multivariate Cluster Analysis

Multivariate cluster analysis aimed to establish quantifiable and holistic characteristics of post-stroke SKG. Post-stroke SKG has often been characterized by frontal-plane compensatory strategies (i.e., pelvic hiking and hip circumduction) as an effort to achieve foot clearance [136], [185]. Recent research suggests that it is possible hip abduction may not be a compensation, but rather part of a larger coordination pattern [19], [29]. As such, SKG may not be best explained solely by its most visible component in the knee, but rather by multiple parameters. Early analysis for pathological gait described the initial swing characteristics of SKG accompanying inadequate hip flexion, toe dragging, and reduced dorsiflexion [127], [135], [136]. Its consequential compensatory movements were suggested as follows: circumduction (paretic hip abduction during the swing); vaulting (non-paretic ankle plantarflexion and/or hip abduction in the stance phase); upward pelvic hiking (paretic pelvic obliquity and/or hip abduction in the swing phase) and pelvic lag (paretic pelvic external rotation in swing phase) [136], [138], [175]. In this multivariate clustering, I based my analysis on these parameters, specifically supposed frontal-plane compensatory strategies following stroke. As multivariate clustering inputs, I used paretic pelvic obliquity, paretic hip abduction, and non-paretic hip abduction, all major components of hip circumduction and upward pelvic hiking following stroke. The underlying philosophy of the multivariate clustering was to define SKG based on motions associated with SKG, but not using disability-specific characteristics, such as knee flexion to avoid a bias towards this parameter.

The caveat of using abstracted variables to analyze time-course gait data is a potential loss of crucial information. Specifically, a fragmentary feature of a time-series could lead to an inappropriate grouping in a clustering algorithm. To avoid this risk, I employed dedicated methods that can address the high correlation between consecutive samples in a time series. I implemented a time-series kernel *k*-means algorithm [176]. One drawback of the standard *k*-means algorithm is that it only assumes linearly separable clusters. The kernel *k*-means is an extension of the standard *k*-means algorithm using a kernel function for a distance/similarity computation to overcome this limitation. The kernelized function non-linearly maps the data into a high dimensional feature space resulting in non-linearly separated clusters in input space. To deal with kernel *k*-means in a time-series manner, it worked with a global alignment kernel [177] casting the widely-used family of Dynamic Time Warping similarity into positive definite kernels for time-series. This method could generate phase-dependent clusters, which can account for holistic pattern changes in time-series signals. In this work, I used a publicly available Python package, *tslearn 0.5.2* [186], to implement the aforementioned time-series kernel k-means clustering with multivariate inputs.

The number of clusters to be tested from the sample population was determined using inertia and silhouette scores. The inertia score is a measure of cohesion defined by the sum of squared distance of samples to their closest cluster center. The silhouette score is calculated using the mean intra-cluster distance and the mean nearest-cluster distance taking both cohesion and separation into account [187]. A relatively low inertia and high

silhouette score indicate good quality clustering. Through the elbow method [188] with these two measures, I determined the number of clusters that are supposed to be in the sample population.

Output clusters were then analyzed with respect to known correlates with post-stroke SKG including joint kinematics and kinematics in the sagittal plane, common compensatory motions (i.e., hip circumduction, pelvic obliquity, and non-paretic ankle vaulting) [135], [185], body kinematics, muscle activity, gait speed, propulsive asymmetry and number of motor modules, obtained by nonnegative matrix factorization [159]. I examined the sub-classes by matching individuals who belong to the clinical diagnosis of post-SKG to get an insight into the existence of phenotypes of SKG.

4.2.4. Statistics

Outcome measures are primarily continuous time-course signals. I employed statistical parametric mapping (SPM) analysis to examine differences between clusters of one-dimensional time-series data. SPM was originally developed for statistical inference of multidimensional neuroimaging based on random field theory [189] and its generalized version for one-dimensional time-course signals, such as biomechanics and physiological signals, has recently gained popularity [190]. SPM can perform linear statistical testing (i.e., t-test, ANOVA, etc.) for time-series signals. Because SPM does not require assumptions and abstraction of signals dependent on the spatiotemporal foci of signals, it provides apparent and intuitive statistical results described in the original sampling space [191]. In this study, I performed SPM one-way ANOVA to compare

clustered post-stroke gait patterns. As a part of post hoc analysis, I applied a pairwise two-tailed t-test with Bonferroni correction using SPM. To examine relationships and interactions of outcome measures (e.g., gait speed, propulsive asymmetry, number of motor modules) according to clusters, I used a linear mixed model and a pairwise t-test with Bonferroni correction of post hoc analysis. SPM one-way ANOVA and its post hoc analyses were completed by an open source SPM1D package (http://www.spm1d.org/, version of 0.4.8) using Python version of 3.8.10 [190]. A linear mixed model and multiple comparisons were done by statsmodels package (version of 0.13.2) in Python.

4.3. RESULTS

4.3.1. Clinical Diagnosis Labels

Twenty-four post-stroke individuals out of 50 were diagnosed with SKG by an expert clinician. The detailed diagnosis chart and participant's demographics are attached in **Table B1.**

4.3.2. Univariate Clusters

I observed correlations between many of the features describing SKG. **Figure 4.2** shows Kendall rank correlation coefficient across input variables and gait speed used in univariate k-means clustering. Most features showed significant correlations with gait speed, knee flexion angle, and velocity which are commonly considered as the main associations of post-stroke SKG. However, the swing-phase temporal characteristic of

knee flexion, the peak timing, was not significantly correlated with walking speed (τ = -0.18, p = .075), knee flexion in swing (τ = 0.03, p = .763), and knee flexion velocity in pre-swing (τ = -0.05, p = .581). While the stance-phase peak knee extension showed a significant negative correlation with the pre-swing phase knee flexion velocity (τ = -0.36, p < .001), it was not significantly correlated to walking speed (τ = -0.06, p = .539) and knee flexion in swing (τ = -0.03, p = .744). These two variables were excluded from further clustering analysis due to the poor correlations to the most common post-stroke SKG characteristics.

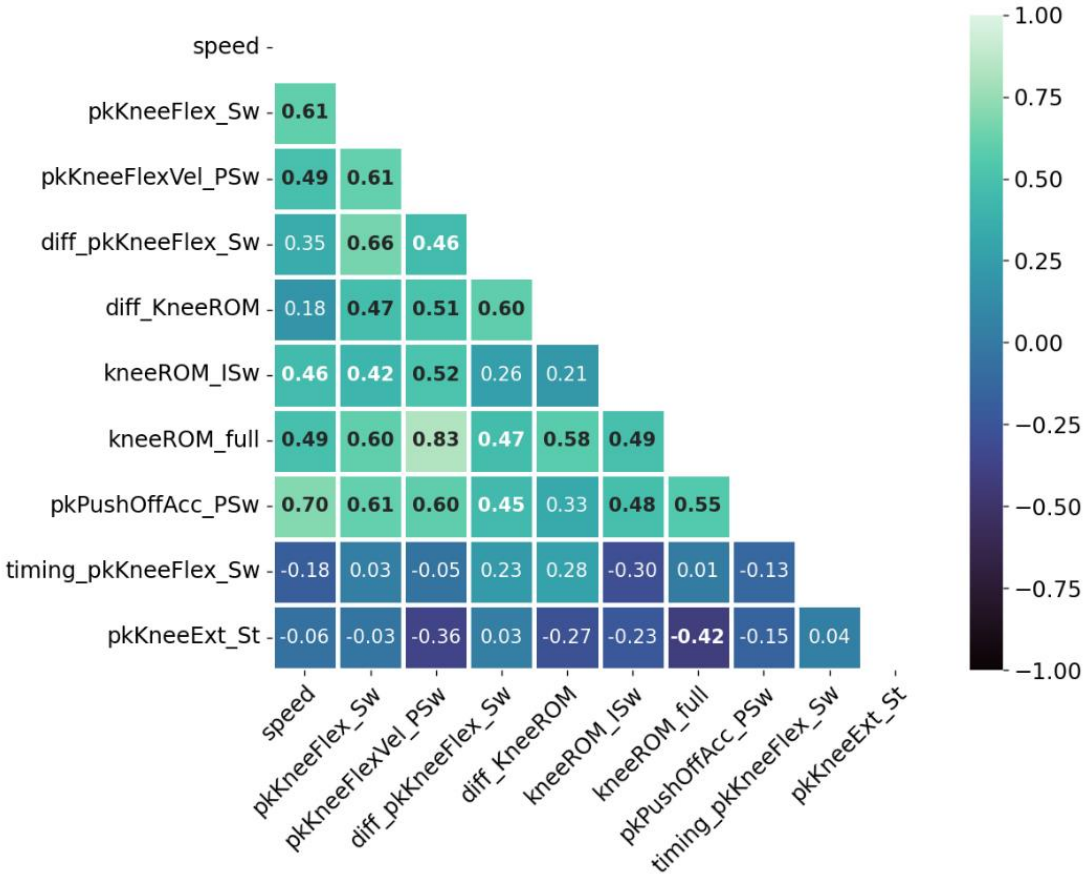

Figure 4.2: Kendall rank correlation coefficient across input variables and gait speed. Coefficients above 0.4, indicating strong relationships, are bold font. Labels stand for the following: *pkKneeFlex_Sw* (peak knee flexion in swing); *diff_pkKneeFlex_Sw* (between-limb difference peak knee flexion between limbs in swing); *diff_KneeROM* (between-limb difference knee flexion range of motion); *pkKneeFlexVel_PSw* (peak knee flexion velocity in pre-swing); *kneeROM_ISw* (knee range of motion in initial swing); *kneeROM_full* (knee range of motion in full cycle); *pkPushOffAcc_PSw* (peak push off acceleration in pre-swing); *timing_pkKneeFlex_Sw* (timing of peak knee flexion in swing); *pkKneeExt_St* (peak knee extension in stance)

The validity scores indicate which parameters were the best indicators of SKG. **Table 4.1** shows external validity measures for each univariate clustering output. Among selected 7 clustering input variables, the between-limb difference in peak knee flexion

resulted in the best external validity scores across all different types of measures. The boundary for clusters was 15.4°. Its sensitivity, defined by True Positive over True Positive plus False Negative, was 90.9%. Specificity, denoted by True Negative over False Positive plus True Negative, was 78.6%. The peak swing-phase knee flexion angle resulted in similarly good quality of clusters with 87.5% of sensitivity and 80.8% of specificity. The boundary angle was 44.28°. **Figure 4.3** is a binary heatmap of cluster labels from the *k*-means algorithm using each of these two variables. Cluster with a lower swing peak knee flexion angle was labeled as SKG. These univariate clustering labels were compared to clinical diagnosis labels. Although external validity measures described a decent quality of clusters, each variable resulted in 8 different labels out of 50 (16% in total) with respect to the clinical diagnosis, respectively.

Table 4.1: External validity measures for each univariate clustering output. Bold font values denote peak of outcome measure. All external validity measures were computed based on clinical diagnosis labels.

Feature	F1 score	Purity	Adjusted Rand Index	Adjusted Mutual Information	V-measure
pkKneeFlex_Sw	**0.8400**	**0.8400**	**0.4512**	**0.3616**	**0.3711**
pkKneeFlexVel_Psw	0.6809	0.7000	0.1426	0.1046	0.1180
diff_pkKneeFlex_Sw	**0.8462**	**0.8400**	**0.4514**	**0.3786**	**0.3879**
diff_KneeROM	0.8000	0.8200	0.3976	0.3167	0.3270
kneeROM_ISw	0.5926	0.5600	-0.0053	-0.0026	0.0126
kneeROM_full	0.7200	0.7200	0.1769	0.1336	0.1465
pkPushOffAcc_Psw	0.6792	0.6600	0.0842	0.0677	0.0818

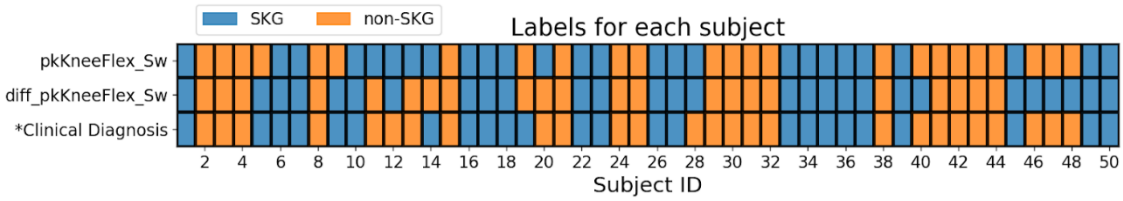

Figure 4.3: Binary heatmap of clustered labels from *k*-means clustering using each variable. 13 individuals out of 50 (26% in total) did not have common labels.

4.3.3. Multivariate Clusters

The goal of multivariate cluster analysis was to characterize post-stroke SKG with a different perspective compared to the conventional characteristics of reduced knee flexion during the swing phase. Instead of using variables related to knee flexion as input variables which would bias the results towards different levels of knee flexion, instead I focused on frontal plane kinematics, the supposed effects of SKG (i.e., pelvic obliquity, paretic, and non-paretic hip abduction). **Figure 4** represents inertial and silhouette measures across a varying number of clusters to determine an optimal number of multivariate clusters. Three was the best cluster number since the inertia measure showed a relatively low decrease rate to the next number while the silhouette score was the highest. As a result, a total of 50 post-stroke individuals were separated into three clusters denoted as A (13), B (23), and C (14).

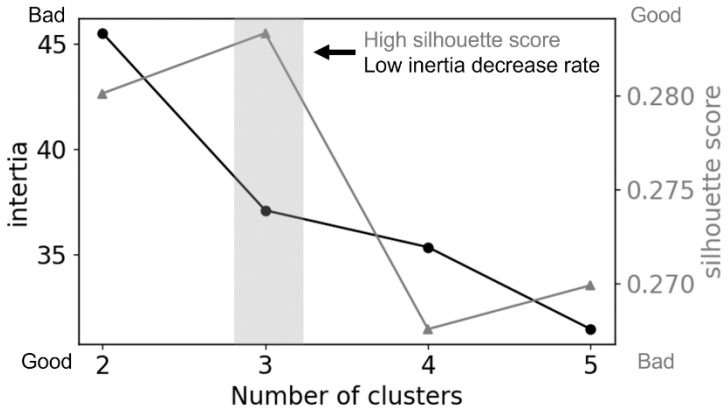

Figure 4.4: Inertia and silhouette score changes for varying numbers of clusters. Lower inertia and high silhouette score indicate better quality of clusters.

Once obtaining the clusters, I compared the results to the clinical diagnosis (**Table A1**). There were 24 individuals diagnosed with post-stroke SKG. These individuals were primarily distributed into Clusters A (10/13) and B (11/23), but also 3 in Cluster C out of 14 total.

Time-series clustering based on frontal plane compensations resulted in walking speed, knee flexion, and propulsive asymmetry dependent clusters. By the random intercept and slope model using a linear mixed model, I found that there were significant differences in self-selected walking speed ($\beta = 0.16$, $t = 7.14$, $p < .001$), the peak swing-phase knee flexion angle ($\beta = 11.64$, $t = 8.73$, $p < .001$), and the propulsive asymmetry ($\beta = -7.34$, $t = -4.76$, $p < .001$) for the three clusters and healthy controls. **Figure 4.5** visualizes post hoc pairwise t-test results with Bonferroni correction. In general, outcomes showed increasing trends from people in Cluster A to B, and then between C and healthy controls.

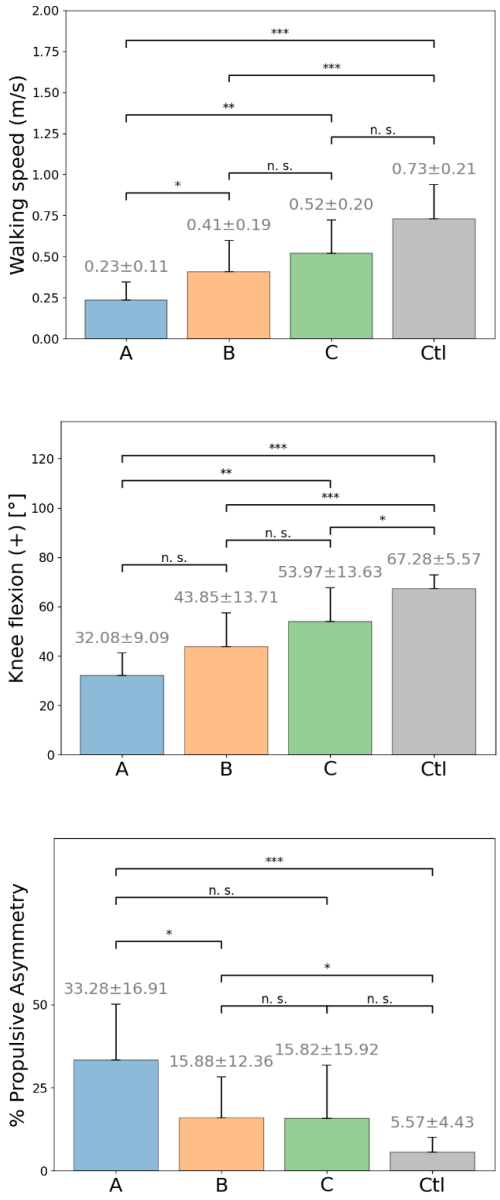

Figure 4.5: Differences in gait speed, knee flexion angle and propulsion asymmetry across groups. Post hoc multiple comparisons for the self-selected walking speed (top), the peak knee flexion in the swing (middle), and the propulsive asymmetry (bottom) across clusters by pairwise t-test with Bonferroni correction. Note *** ($p < 0.001$), ** ($0.001 < p < 0.01$), * ($0.01 < p < 0.05$), and n.s. (not significant).

Commonly known compensatory motions following stroke, such as hip hiking, hip circumduction, and contralateral ankle vaulting were examined based on four kinematic profiles (i.e., paretic pelvic obliquity, paretic hip abduction, non-paretic hip abduction, and non-paretic ankle plantarflexion) by using SPM one-way ANOVA and post hoc multiple comparisons (**Figure 4.6**). I observed statistically discernible patterns of pelvic motions in individuals from Cluster A and B (47 - 100% gait cycle, $F^* = 5.271$, $p < .001$). Note that F^* denotes a critical threshold for SPM one-way ANOVA, equivalent to F-statistic. Specifically, people in Cluster A had 6.85° more pelvic obliquity than Cluster B and 9.03° more than in healthy controls. Cluster A initiated hip hiking in the pre-swing phase but Cluster B in the swing phase. Cluster A had 7.20° less hip abduction than healthy controls ($p < .001$). There were differences in the non-paretic hip abduction (38 - 94% of gait cycle, $F^* = 5.372$, $p < .001$). Individuals in Cluster A exhibited 7.53° greater non-paretic hip abduction compared to Cluster B and 9.19° more than healthy controls. No significant differences in non-paretic ankle motion were found ($F^* = 5.951$, $p > .05$). A summary of statistical comparisons between all groups is shown in **Table 4.2**.

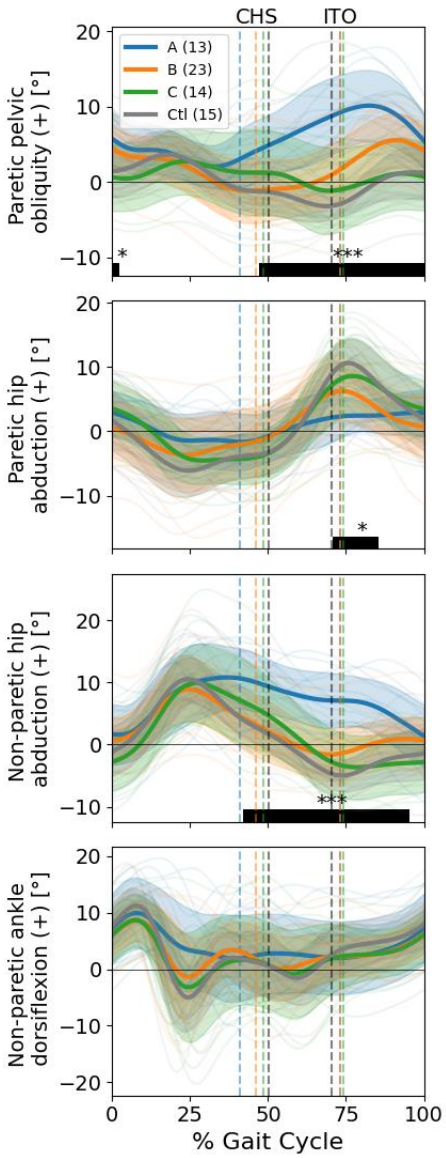

Figure 4.6: SPM One-way ANOVA on multivariate clustering for compensatory motions. Solid black bars at the bottom show the statistically significant portion of the gait cycle as determined by SPM. Note *** ($p < .001$), ** ($.001 < p < .01$), and * ($.01 < p < .05$). Thick solid and shaded areas are average and standard deviations of each group, respectively. Thin solid lines in backgrounds represent individual data. Left and right vertical dashed lines indicate contralateral heel strike (CHS) and ipsilateral toe-off (ITO) events, respectively. Note that the gait cycle is based on the paretic limb's heel strike (0%).

Sagittal plane joint kinematics and kinetics differed between clusters. **Figure 4.7** illustrates SPM one-way ANOVA results on the sagittal-plane joint kinematics (left) and kinetics (right). I observed differences in pre-swing hip flexion angle (52 - 72% gait cycle, $F^* = 4.988$, $p = .033$), mid-stance hip moment (23 - 40% gait cycle, $F^* = 6.685$, $p < .001$), and pre-swing hip kinetics (49 - 61% gait cycle, $F^* = 6.685$, $p < .001$). Individuals in Cluster A had 18.13° less hip extension than Cluster B and 21.60° less than healthy controls in pre-swing. Cluster A had reduced hip extension moment, 29.15 Nm/kg less than Cluster B and 24.15 Nm/kg less than controls. People in Cluster A had 30.50° less knee flexion than controls, and Cluster B had 22.12° less than controls, but no significant difference between each other ($p > .05$). I observed differences in knee flexion moment (50 - 60% gait cycle, $F^* = 6.903$, $p < .01$), with people in Cluster B 23.31 Nm/kg less than healthy controls. Ankle plantar flexion moment (44 - 64% gait cycle, $F^* = 7.206$, $p < .001$) showed differences, with individuals in Cluster A walking with 49.18 Nm/kg lower plantar flexion moment compared to healthy controls, and those in Cluster B with 39.28 Nm/kg less than controls. No significant differences between people in Cluster C were found compared to people in Cluster B or healthy controls. Comparisons are summarized in **Table 4.2**.

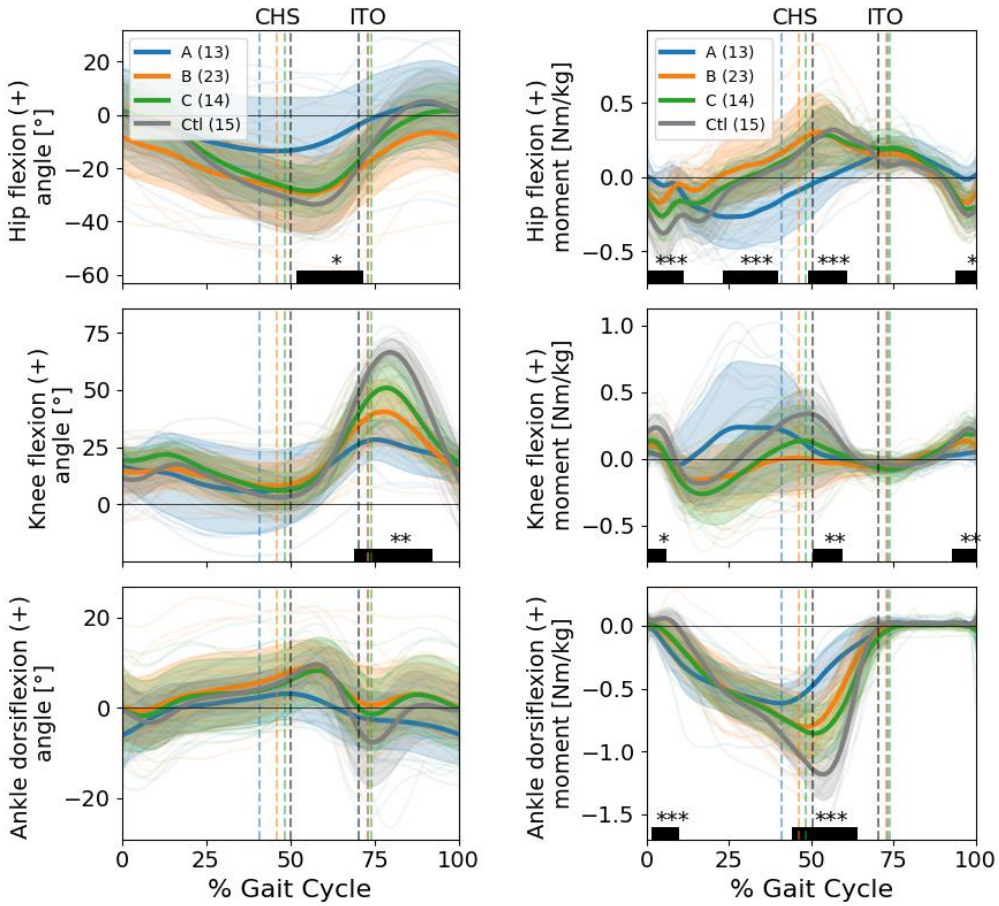

Figure 4.7: Kinematic and kinetic comparisons between groups. The left column represents sagittal plane kinematics, and the right column represents sagittal plane kinetics. Statistics derived from SPM One-way ANOVA.

I observed differences in the body center of mass acceleration, known to be correlated with paretic propulsion [90] (**Figure 4.8**). Specifically, differences were found in pre-swing (45 - 55% of gait cycle, F* = 7.180, $p < .001$) and initial swing phase (68 - 80% of gait cycle, F* = 7.180, $p < .001$). All three clusters had lower magnitude acceleration than healthy controls, the largest difference at Cluster A was 0.89 m/s^2, Cluster B at 0.74 m/s^2, and Cluster C at 0.50 m/s^2.

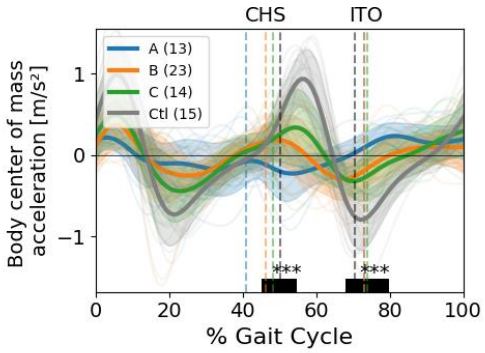

Figure 4.8: SPM One-way ANOVA on multivariate clustering for body center of mass acceleration.

There were also differences observed in muscle activity. Two muscles showed differences between clusters, the vastus medialis (VM) and lateral hamstrings (LH). Both VM (25 - 39% of gait cycle, F* = 6.728, $p < .001$) and LH (11 - 39% of gait cycle, F* = 6.755, $p < .001$) activity differed during mid-stance (**Figure 4.10**). Individuals in Cluster A had greater LH EMG activity than those in Cluster B (0.58, arbitrary units), Cluster C (0.66) and healthy controls (0.91). In VM activity, those in Cluster A had greater mid-stance activity than healthy controls (0.78), and those in Cluster B also had greater activity (0.55), but no differences between the clusters were found. Other muscles were activated differently from healthy controls but there was no difference between the clusters. All pairwise comparisons including mean differences, duration of the gait cycle, and p-values are summarized in **Table 4.2.**

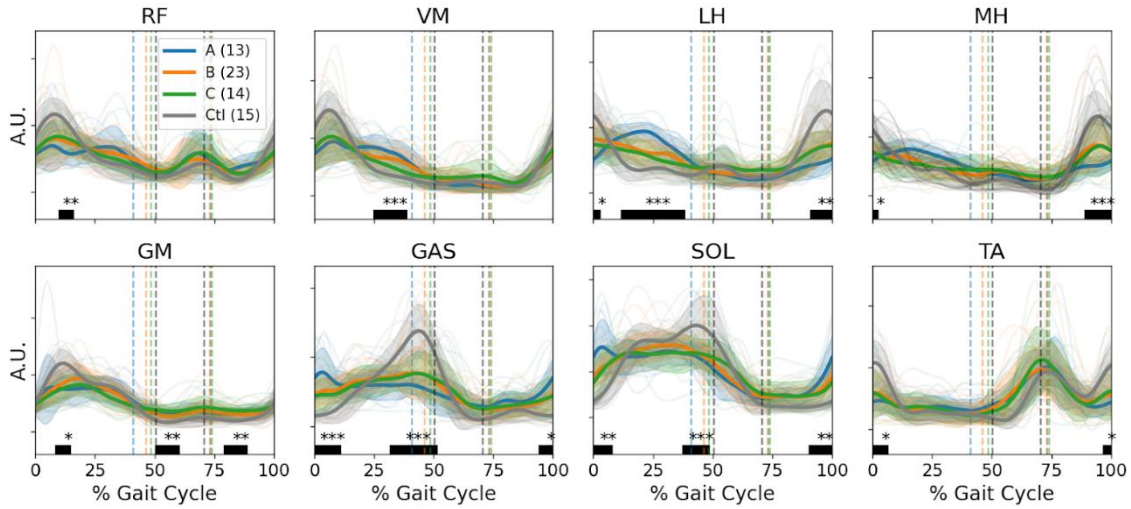

Figure 4.9: SPM One-way ANOVA on multivariate clustering for muscle EMG signals. Abbreviations are Rectus Femoris (RF), Vastus Medialis (VA), Lateral Hamstrings (LH), Medial Hamstrings (MH), Gluteus Medius (GM), Medial Gastrocnemius (GAS), Soleus (SOL), and Tibialis Anterior (TA).

The distribution of motor modules for a paretic limb across clusters is illustrated in **Figure 4.10**. I observed distinct motor module differences between Cluster A and B. Cluster A mostly consisted of people with low complexity (2 modules, 5 out of 13) and moderate complexity motor modules (3 modules, 7 out of 13). On the other hand, Cluster B was primarily composed of moderate (3 modules, 16 out of 23) and some of high complexity individuals (4 modules, 5 out of 23). Similarly, Cluster C was composed of moderate (3 modules, 6 out of 14) and high complexity modules (4 modules, 6 out of 14). Within clinically SKG-diagnosed individuals (24 out of 50), all SKG individuals were with low and moderate complexity motor modules, except one participant with high complexity modules in Cluster B. Of the cases of low complexity motor modules, most

were diagnosed with SKG (7 out of 9 participants with two modules), and of those, most were in Cluster A (4 participants).

I examined the relationship between the level of the paretic limb's motor module complexity and propulsive asymmetry, and their interaction with respect to clusters. By linear mixed model, I found that the motor module complexity in all post-stroke participants was significantly associated with propulsive asymmetry ($\beta = -9.75$, $t = -2.79$, $p < .01$). However, this relationship was insignificant within SKG participants ($p = .157$). I also observed a significant change in the number of motor modules according to clusters ($\beta = 0.13$, $t = 2.32$, $p = .02$), but did not observe significance within SKG participants ($p = .289$). I did not observe a significant interaction between motor modules and propulsive asymmetry regarding clusters in all post-stroke samples ($p = .734$) as well as in SKG ($p = .423$).

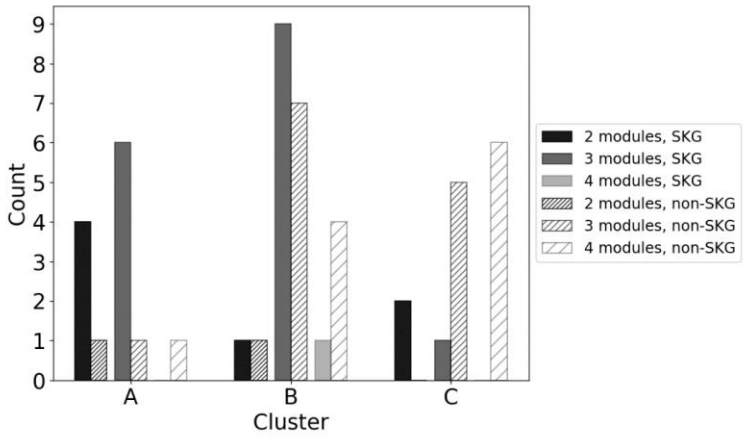

Figure 4.10: Number of motor modules per individual for each cluster. Participants are separated by clinical diagnosis.

I performed additional post hoc analyses to determine whether the subset of individuals diagnosed with SKG within each cluster show different relationships with all of the biomechanical parameters described above. **Figures B1 – B5** and **Table B2** visualize these differences.

Table 4.2: Summary of post hoc multiple comparisons for outcome measures by SPM two-tailed t-tests with Bonferroni correction. Positive values in flexion direction. Statistical significance denoted by * ($p<0.05$), ** ($p<0.01$), *** ($p<0.001$).

			A - B	A - C	A - Ctl	B - C	B - Ctl	C - Ctl
Frontal Plane Kinematics	**Paretic Pelvic Obliquity Angle [°]**	Δmean [95% CI]	6.85 [3.78, 9.92] ***	9.11 [5.20, 13.02] **	9.03 [6.30, 11.76] ***	-	4.68 [2.74, 6.62] **	-
		% cycle	46 - 85	62 - 96	44 - 97	-	70 - 95	-
	Paretic Hip Abd / Add Angle [°]	Δmean [95% CI]	-	-	-7.20 [-9.71, -4.69] *	-	-	-
		% cycle	-	-	68 - 84	-	-	-
	Non-paretic Hip Abd / Add Angle [°]	Δmean [95% CI]	7.53 [4.72, 10.35] ***	9.16 [5.52, 12.81] **	9.19 [6.70, 11.69] ***	-	-	-
		% cycle	41 - 87	60 - 92	39 - 91	-	-	-
Sagittal Plane Kinematics	**Paretic Hip Flex / Ext Angle [°]**	Δmean [95% CI]	18.13 [6.78, 29.49] *	-	21.60 [10.06, 33.14] *	-	-	-
		% cycle	60 – 68	-	55 - 69	-	-	-
	Paretic Knee Flex / Ext Angle [°]	Δmean [95% CI]	-	-21.33 [-30.63, -12.03] *	-30.50 [-36.56, -24.45] ***	-	-22.12 [-28.20, -16.04] ***	-
		% cycle	-	73 - 85	67 - 91	-	71 - 92	-
	Paretic Ankle Dorsi / Plantar Flex Angle [°]	Δmean [95% CI]	-	-	-	-	-	-
		% cycle	-	-	-	-	-	-
	Paratic Hip Flex / Ext	Δmean [95% CI]	-28.72 [-43.16, -14.28] *** -29.15 [-43.13, -15.16] ***	-	-24.15 [-34.31, -14.00] ***	-	-	-

Sagittal Plane Kinetics	**Moment [Nm/kg]**	% cycle	21 - 40 43 - 58	-	53 - 63	-	-	-
	Paretic Knee Flex / Ext Moment [Nm/kg]	Δmean [95% CI]	-	-	-	-	-23.31 [-32.40, -14.22] ***	-
		% cycle	-	-	-	-	48 - 60	-
	Paretic Ankle Dorsi / Plantar Flex Moment [Nm/kg]	Δmean [95% CI]	-	42.57 [23.10, 62.04] **	49.18 [35.93, 62.43] ***	-	39.28 [25.47, 53.10] ***	-
		% cycle	-	52 - 58	43 - 63	-	52 - 63	-
Body Kinematics	**Body COM Acceleration [m/s^2]**	Δmean [95% CI]	-	0.31 [0.16, 0.45] *	-0.89 [-1.08, -0.70] *** 0.64 [0.50, 0.78] ***	-	-0.74 [-0.94, -0.54] *** 0.45 [0.31, 0.59] ***	0.50 [0.26, 0.74] *
		% cycle	-	69 - 72	49 - 62 68 - 88	-	51 - 63 69 - 88	72 - 75
Muscle Activity	**Paretic Vastus Medialis EMG [A.U.]**	Δmean [95% CI]	-	-	0.78 [0.50, 1.05] ***	-	0.55 [0.33, 0.76] ***	-
		% cycle	-	-	24 - 38	-	27 - 38	-
	Paretic Lateral Hamstrings EMG [A.U.]	Δmean [95% CI]	0.58 [0.36, 0.81] ***	0.66 [0.41, 0.92] ***	0.91 [0.72, 1.10] ***	-	0.60 [0.37, 0.83] *** 0.45 [0.24, 0.66] ***	0.55 [0.27, 0.82] *
		% cycle	17 - 27	16 - 31	12 - 40	-	12 - 24 30 - 38	18 - 19

4.4. DISCUSSION

Despite SKG being one of the most common gait impairments following stroke, there is still no precise characterization of the disability. One proximate issue is the lack of a single parameter that most closely defines SKG. I found that out of 8 different parameters, the relative pre-swing knee flexion angle provides the most accurate and robust diagnosis and can be obtained with relative ease. However, multivariate clustering analysis indicated that SKG is more nuanced than previously thought. Using the variation in compensatory motions between individuals, I found two gait subtypes, both of which could be considered SKG, expressing differing three-dimensional kinematics, muscle coordination patterns, and levels of impairment. Cluster A exhibited the highest level of impairment with low gait speed and high propulsion asymmetry. People in this cluster walked with greater pelvic obliquity (hip hiking), stance-phase co-contraction of the muscles around the knee, and very low knee flexion angle. Cluster B, on the other hand, exhibited greater gait speed and better propulsion asymmetry than Cluster A. People in this group walked with large hip hiking and hip abduction motions in swing, excessive quadriceps activation during stance, and reduced swing knee flexion angle compared to healthy controls. Those in Cluster C had reduced propulsion and hamstrings activity compared to healthy controls, but knee flexion and all other parameters were closest to healthy controls of the clusters. The vast majority of clinically diagnosed individuals with SKG were distributed between Clusters A and B, suggesting two gait patterns that could

be classified as phenotypes of SKG. These results suggest the need for more specific diagnoses in post-stroke SKG and may lead to more effective, targeted interventions.

The inclusion criteria for post-stroke SKG in clinical studies have been surprisingly inconsistent, even though post-stroke gait including SKG has been characterized many times in recent years [126], [135]. Lack of consensus in definitions could be responsible for mixed results in clinical trials and such adverse effects were reported in studies targeting the mild stroke population [192]. This work represents a quantitative attempt to compare these differing definitions of SKG. My approach used univariate clustering and correlation analysis to show that the relative swing-phase knee flexion angle between the legs was the most accurate and robust single specification. However, peak knee flexion angle was also highly rated. Commonly, peak knee flexion of the affected side was expected to be the best specification of post-stroke SKG, but there was a counterintuitive result from my univariate analysis. It is important to note that swing-phase peak knee flexion of the affected limb was speed-dependent ($\tau = 0.61$ in **Figure 2**). Additionally, its speed-dependent increase was observed according to within-subject walking speed changes [193]. This implies that some post-stroke individuals with reduced knee flexion around the boundary angle between SKG and non-SKG were likely misdiagnosed once they walked faster and vice versa. Therefore, a less sensitive parameter to gait speed, like relative knee flexion angle between limbs, must be a more robust single specification of post-stroke SKG.

This study described a novel approach in multivariate clustering analysis for post-stroke gait. Clustering analysis in post-stroke gait has primarily relied on sagittal plane factors [127], [128], [174]. Frontal plane kinematics were often neglected as input parameters for clustering, despite being commonly associated with SKG [126]. Additionally, prior investigations depended on discrete measures of biomechanical factors (i.e., mean or peak) which resulted in data loss and potential bias in feature selection. To our knowledge, few studies have attempted to categorize post-stroke gait based on a full complement of biomechanical factors [194], [195]. The time series-based clustering algorithm of this study, kernel k-means [176], using a global alignment kernel [177], could account for the non-linear structure of biomechanical signal differences and produce phase dependent clusters. Thus, the results in this study offer a more holistic perspective through unbiased clustering by using a comprehensive set of biomechanical signals.

There is precedence for the gait pattern found in Cluster A. Earlier work has classified post-stroke gait based on muscle activation patterns. For instance, based on lower extremity EMG profiles, Knutsson and Richards found three types of disturbed motor control in post-stroke gait: Type I (premature activation of the calf muscles in early and mid stance), Type II (no or weak activity in two or more muscles), and Type III (coactivation of major muscle groups) [129]. Shiavi et al. further classified Type III gait into two subgroups: one with quadriceps and hamstring coactivation during stance (Type III-S) and the other during the transition periods (Type III-T) [196]. Inappropriate stance-

phase hamstrings activation of the affected side, observed in Cluster A, was similar to Type III-S. It has been suggested that Type III-S gait must compensate for a diminished ankle plantarflexor moment with stance phase hip extensor moment or forward postural lean [126]. Indeed, our data is consistent with this hypothesis, showing excessive hip extensor moment during stance in Cluster A (**Table 4.2**). Additionally, early pre-swing initiation of pelvic obliquity is often used to improve balance [126]. This early hip hiking characterizes Cluster A. Cluster A was primarily composed of those diagnosed with SKG (10/13). They were the most impaired, as evidenced by lowest gait speed, knee flexion, muscle modules, and propulsion asymmetry (**Figure 5** and **A5**).

Based on the pattern found in Cluster A, a useful intervention for this type of post-stroke gait may be techniques focused on restoring gait by targeting propulsion as well as co-contraction of the quadriceps and hamstrings during stance. Indeed, propulsion-focused technologies targeting the different aspects of propulsion impairment have emerged and shown significant efficacy in the restoration of gait [162]. These include task-specific training [197], functional electrical stimulation (FES) with fast treadmill walking [198], propulsion-augmenting exosuits [199], [200], body COM assistance/resistance for propulsion retraining [201], and propulsion biofeedback [202]. It had been also reported that abnormal muscle coactivation could be modulated by myoelectric computer interface [203], [204] or weight shift practice [205]. Their efficacy for reduction of the upper arm and ankle muscle co-activation in chronic stroke survivors were successfully presented, respectively. These earlier successes at different muscles

indicate that tailored strategies to stance-phase quadriceps and hamstring coactivation may be beneficial by those types of rehabilitation technologies.

While I observed similarities in kinematic and muscle activation profiles from Cluster A and Type III-S, identifying the "other" SKG group, Cluster B, is not as straightforward. Cluster B individuals use both hip abduction and hip hiking. They have reduced knee flexion, slow walking speed, reduced body acceleration and moderately high propulsion asymmetry, indicating moderate levels of gait impairment. There is also excessive quadriceps activation during stance, but not co-contraction like in Cluster A. The hip abduction observed in this group fits with some textbook definitions of SKG. However, only 11/23 individuals in this cluster were diagnosed with SKG. Separating those with clinically diagnosed SKG and reanalyzing the data (**Figures A1 - A4**) shows that the characteristics described above remain the same. This suggests that Cluster B could fit under an SKG umbrella, but it may also be possible that a more precise definition for this gait pattern than a term developed about 150 years ago to quickly describe a feature of gait may be necessary. Our previous work observed hip abduction in a small cohort diagnosed with SKG and applied robotic knee flexion perturbations during walking [19]. We found that assistance increased hip abduction instead of the hypothesized drop of the supposed compensatory motion. Our later analysis revealed that the robotic assistance likely evoked a spastic quadriceps response, and this response was coupled with hip abductor activation [29]. In a new group of post-stroke SKG individuals, we found that quadriceps reflex excitability was highly correlated to knee

flexion kinematics [80]. Another study matched the knee flexion angle observed in the SKG cohort found in [19] using a knee brace on healthy individuals [29]. We found that despite similar levels of knee flexion between those post-stroke and healthy individuals, only post-stroke individuals exhibited excessive hip abduction, suggesting a neural basis for this ostensible compensation. While far from conclusive, together this suggests that those in Cluster B may benefit the most from interventions that reduce quadriceps spasticity [206].

It is possible that Clusters A and B differ in kinematics because they represent groups of two different gait speeds. In fact, Stanhope et al, found that greater circumduction occurs at greater gait speeds in post-stroke walking [185]. Circumduction has been generally recognized as a compensatory movement for reduced swing-phase knee flexion [135]. I did observe increasing trends of swing-phase hip abduction across clusters, but did not observe excessive motion compared to healthy controls. There are several feasible reasons. First, this was possible due to the slow walking speed samples in this study. Earlier studies showed an association between self-selected walking speed and compensatory strategies. Stanhope et al. found that hip hiking was inversely correlated with walking speed but hip circumduction was not [185]. In their study, excessive peak paretic hip abduction angle existed at only a fast walking speed (> 0.8m/s). Kim and Eng reported that hip circumduction in swing was more often observed in the fast walking group (mean of 0.86 m/s) [207]. The walking speed of post-stroke samples in my study was 0.39 ± 0.21 m/s (**Table B1**), such that excessive hip abduction was not likely

observed. Second, hip abduction angle may be an inappropriate quantification measure of hip circumduction. Paretic hip abduction angle in post-stroke gait investigations often remained below the level of health although there were significantly increased pelvic obliquity angles [208], [209]. In an early study of post-stroke characterization, Kerrigan et al. quantitatively defined hip circumduction using frontal plane affected thigh angle in midswing, rather than hip abduction angle to avoid the potential overlapping of the meaning of hip hiking and circumduction [175]. For the same reason, Perry's description of circumduction included hiking [135] and it was often measured by the distance of the maximal lateral displacement of the paretic limb from the line of progression [131], [210]. There may be noticeable circumduction patterns with different quantifiable measurements. Nevertheless, I found significantly differing hip abduction profiles across clusters.

One of the limitations of this study involves the clinical diagnosis of post-stroke SKG. The clinical diagnosis in this study was based on a single expert's opinion from previously collected data, i.e., not an in-person diagnosis. It is possible that if we obtained more clinical opinions our diagnoses could have been somewhat different, but this did not affect our classification algorithm. Another limitation is the exploratory nature of this study regarding heterogeneous post-stroke impairment. Machine learning techniques mathematically differentiate clusters based on only the inclusion of multiple variables, whereby there was limited explanatory capability regarding the heterogeneity of post-stroke impairment. Indeed, I observed 2 post-stroke individuals with low motor

complexity and high propulsion asymmetry in Cluster C, which was a counterintuitive clustering (**Figure 10**) given the frontal plane kinematics were consistent with others in Cluster C. Thus, the results after machine learning must be viewed with caution. In this study, however, such outliers were rare and did not affect any overall trends of clusters.

4.5. CONCLUSION

The primary goal of this study was to determine a better specification and potential phenotypes of post-stroke SKG. I quantified the best single specification of post-stroke SKG by univariate cluster analysis. Through time-series multivariate cluster analysis, I also discovered two gait patterns that could be considered phenotypes of SKG. One type exhibited stance phase co-activation of quadriceps and hamstrings as well as high pre-swing pelvic obliquity. The other type was characterized by stance phase over-activation of quadriceps and combined pelvic obliquity and hip abduction. The former group exhibited greater propulsion asymmetry, lower body acceleration, lower swing knee flexion and lower gait speed, i.e., more severe gait impairment, than the latter group. Awareness of these two phenotypes will help better prescribe specific treatments and homogenize study populations for post-stroke SKG interventions.

Chapter 5: Conclusions and Future Work

In this dissertation, I have sought solutions to remove obstacles to the proliferation of technological advances in post-stroke gait rehabilitation through optimal design, statistical, and machine learning techniques. Individual aims provided insight into an affordable robotic gait trainer design, integration of neurological impairment into assistive devices, and gait phenotypes of post-stroke SKG for a better, tailored, and timed treatment.

My first two aims made several contributions to the field of rehabilitation robotics. In Chapter 2, I systematically evaluated and characterized three popular mechanisms (4-, 6-, and 8-bar) using numerical optimization techniques. This aim provided the intuition of optimal solutions for the development of low-cost gait trainers balanced between accurate tracking of large variable human lower-limb kinematic patterns and simplicity. Future work in this area could use this information to develop a low-cost gait trainer, for example, one driven by only the motor of the treadmill. This seamless integration with the treadmill can drastically minimize device costs compared to a multi-joint robotic gait trainer. One challenge would be the lack of force control capability. Commercially available treadmills were usually composed of a simple PWM speed controller. In terms of human-machine interaction directly related to user safety, force control is superior to speed control. However, such a deficit would be complemented by the smart design of the human-machine interface. For instance,

implementing elastic components or compliant mechanisms into linkage structure could physically produce elastic force fields similar to a virtual tunnel proposed by multi-joint gait training systems [211], [212]. I expect that such a mechanical structure would overcome the limitations of lack of control flexibility. Another drawback could be the restriction to the sagittal plane, but 3D motion is possible with a cam setup. Future development of this device, therefore, should involve other novel mechanical designs adding functionality. But it should remain cost-effective and modular to be easily maintained. The advantage of a device like this would be an easy-to-convert common treadmill into a gait rehabilitation device. The implication is that people of limited means would have access to the same concepts of robotic gait training that are only available to resource-rich areas, and possibly even greater access if brought into the home.

In Chapter 3, I attempted to determine the accessible kinematic biomarkers for tracking quadriceps hyperreflexia after exoskeletal knee flexion assistance by a systematic variable selection approach based on statistical and machine learning regression analysis. I found that the kinematic gait factors related to knee and hip joint motions can effectively predict quadriceps hyperreflexia in people with post-stroke SKG. This means that more easily measurable kinematic variables can serve as a proxy for fiber stretch velocity that needs to be measured directly by special equipment or simulated by computationally expensive musculoskeletal simulation. The immediate impact of this research would be towards a controller, such as human-in-the-loop optimization, that uses kinematics in feedback control of a knee exoskeleton. It would most likely apply to a

situation where a predictive model is continuously updated based on the current kinematic state, e.g., Model adaptive control. Future research would be interesting to investigate how Botox-reduced quadriceps combined with open loop knee flexion exoskeletal assistance compares to neurally intelligent assistance.

The finding from Chapter 3 is not limited to exoskeletal applications. Further applications could be biofeedback gait rehabilitation. Many biofeedback applications tend to limit the scope to static or lab-based activities due to the immobility of measuring instruments for biomechanical signals (i.e., GRF, EMG, etc.). Kinematic parameters, however, can be free from this spatial limitation by incorporating mobile wearable sensors, such as inertial measurement units. In the future, I could apply the same variable selection method for dynamic activities (i.e., stair climbing) to discover kinematic predictors. It would be interesting to investigate the feasibility of kinematics-based biofeedback to reduce spasticity under the various dynamic activities.

My third aim made contributions to general post-stroke clinical study. In Chapter 4, I quantitatively characterized post-stroke SKG by unsupervised machine learning techniques. I found that a reduced between-limb knee flexion angle difference in swing phase was a robust single specification of SKG. I also discovered two distinct SKG subtypes. One type exhibited stance phase co-activation of quadriceps and hamstrings as well as high pre-swing pelvic obliquity. The other type was characterized by stance phase over-activation of quadriceps and combined pelvic obliquity and hip abduction. The former group exhibited greater propulsion asymmetry, lower body acceleration, lower

swing knee flexion and lower gait speed, i.e., more severe gait impairment, than the latter group. The delineation of two subtypes of SKG could greatly impact clinically efficacy of interventions. The idea behind this investigation was to take a gait deviation diagnosed based on its most prominent visual characteristic (i.e., knee flexion) and determine whether there are multiple ways of arriving at the same deviation. This strategy could be applied more widely. In the future, I could apply this same method to other gait deviations such as steppage, scissors, spastic, and waddling gait caused by other types of neurological impairment.

Taken together, this dissertation bridged the gap between advanced technology and clinical practice through novel engineering approaches. The ultimate goal of this study is to provide a foundation for developing affordable but robust rehabilitation solutions toward complete recovery.

Appendix A: Supplemental Materials for Chapter 2

Table A1: **Linkage parameters used for analyses. Figure 3** indicates all notations of each mechanism.

	4-bar	**6-bar**	**8-bar**
$\boldsymbol{l_1}$ $(\boldsymbol{cm})$	10.40	10.90	10.70
$\boldsymbol{l_2}$ $(\boldsymbol{cm})$	21.60	36.50	45.40
$\boldsymbol{l_3}$ $(\boldsymbol{cm})$	43.00 ~ 49.90	34.10	38.60
$\boldsymbol{l_4}$ $(\boldsymbol{cm})$	47.90	19.70 ~ 38.70	20.70 ~ 43.30
$\boldsymbol{l_5}$ $(\boldsymbol{cm})$	37.90 ~ 85.00	37.60	46.40
$\boldsymbol{l_6}$ $(\boldsymbol{cm})$	-	9.10	42.70
$\boldsymbol{l_7}$ $(\boldsymbol{cm})$	-	15.10 ~ 25.00	57.70
$\boldsymbol{l_8}$ $(\boldsymbol{cm})$	-	42.10	30.30 ~ 50.00
$\boldsymbol{l_9}$ $(\boldsymbol{cm})$	-	26.00	42.10
$\boldsymbol{l_{10}}$ $(\boldsymbol{cm})$	-	35.90	48.70
$\boldsymbol{l_{11}}$ $(\boldsymbol{cm})$	-	50.30	26.00
$\boldsymbol{l_{12}}$ $(\boldsymbol{cm})$	-	-	54.40
$\boldsymbol{\emptyset_1}$ (°)	40.90	8.70	9.10
$\boldsymbol{\emptyset_2}$ (°)	56.50	89.10	-

Figure A1: Heat map (a) and the surface plot (b) for the trajectory and the path peak error across heights and walking speed.

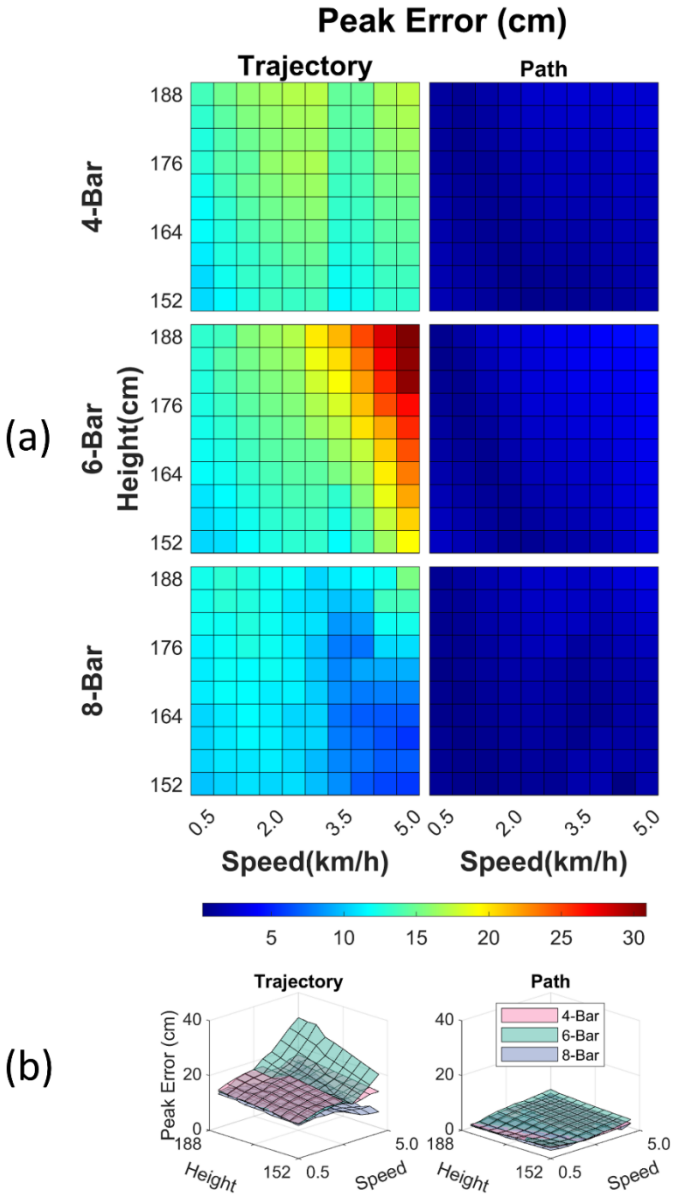

Appendix B: Supplemental Materials for Chapter 4

Table B1: Subject information, clinical diagnosis of SKG labels, and multivariate clustering labels.

ID	Age	Gender	Walking Speed (m/s)	SKG Label (TRUE / FALSE)	Multivariate Clustering Label
S01	75	M	0.44	T	B
S02	72	M	0.70	F	C
S03	67	F	0.55	F	C
S04	54	F	0.90	F	B
S05	58	F	0.55	F	B
S06	48	M	0.75	T	C
S07	59	M	0.30	T	B
S08	60	M	0.60	F	B
S09	68	M	0.75	T	B
S10	43	M	0.20	T	A
S11	71	F	0.15	F	B
S12	71	F	0.10	F	B
S13	49	M	0.15	T	A
S14	69	F	0.20	F	C
S15	51	M	0.55	F	C
S16	40	M	0.10	T	A
S17	61	M	0.15	F	C
S18	72	M	0.15	T	A
S19	28	F	0.50	T	B
S20	70	F	0.15	F	A
S21	68	M	0.55	F	B
S22	47	M	0.40	T	A

S23	**58**	**M**	**0.15**	**T**	**A**
S24	**53**	**F**	**0.35**	**F**	**C**
S25	**66**	**F**	**0.50**	**F**	**B**
S26	**58**	**F**	**0.10**	**F**	**B**
S27	**26**	**F**	**0.30**	**T**	**A**
S28	**82**	**M**	**0.30**	**F**	**C**
S29	**49**	**M**	**0.40**	**T**	**C**
S30	**35**	**F**	**0.50**	**F**	**B**
S31	**76**	**F**	**0.40**	**F**	**B**
S32	**59**	**M**	**0.70**	**F**	**C**
S33	**25**	**F**	**0.15**	**F**	**A**
S34	**33**	**M**	**0.20**	**T**	**A**
S35	**49**	**M**	**0.45**	**T**	**B**
S36	**70**	**M**	**0.30**	**F**	**B**
S37	**70**	**M**	**0.30**	**T**	**B**
S38	**56**	**F**	**0.55**	**F**	**C**
S39	**55**	**F**	**0.30**	**F**	**B**
S40	**60**	**M**	**0.45**	**F**	**A**
S41	**64**	**M**	**0.30**	**F**	**B**
S42	**42**	**F**	**0.80**	**F**	**C**
S43	**62**	**M**	**0.65**	**F**	**C**
S44	**41**	**F**	**0.20**	**F**	**B**
S45	**66**	**M**	**0.40**	**T**	**A**
S46	**50**	**M**	**0.50**	**T**	**B**
S47	**63**	**M**	**0.40**	**F**	**B**
S48	**58**	**M**	**0.65**	**F**	**C**
S49	**62**	**M**	**0.25**	**F**	**B**
S50	**50**	**M**	**0.25**	**T**	**A**
C01	**74**	**M**	**0.70**	**-**	**Control**

C02	**50**	**F**	**0.75**	**-**	**Control**
C03	**53**	**F**	**1.10**	**-**	**Control**
C04	**46**	**F**	**0.50**	**-**	**Control**
C05	**51**	**F**	**0.70**	**-**	**Control**
C06	**52**	**F**	**1.00**	**-**	**Control**
C07	**65**	**F**	**0.80**	**-**	**Control**
C08	**58**	**F**	**0.80**	**-**	**Control**
C09	**64**	**F**	**0.50**	**-**	**Control**
C10	**48**	**M**	**0.40**	**-**	**Control**
C11	**59**	**M**	**0.50**	**-**	**Control**
C12	**59**	**M**	**0.55**	**-**	**Control**
C13	**47**	**M**	**0.75**	**-**	**Control**
C14	**51**	**M**	**0.80**	**-**	**Control**
C15	**40**	**M**	**1.10**	**-**	**Control**

Table B2: Summary of post hoc multiple comparisons for outcome measures by SPM two-tailed t-tests with Bonferroni correction.

			A - B	A - C	A - Ctl	B - C	B - Ctl	C - Ctl
Frontal Plane Kinematics	**Paretic Pelvic Obliquity Angle [°]**	Δmean [95% CI]	-	-	9.03 [6.79, 12.98] ***	-	6.75 [4.66, 8.84] **	-
		% cycle	-	-	43 - 98	-	61 - 100	-
	Paretic Hip Abd / Add Angle [°]	Δmean [95% CI]	-	-	-7.71 [-10.48, -4.95] *	-	-6.35 [-9.62, -3.08] *	-
		% cycle	-	-	69 - 84	-	75 - 84	-
	Non-paretic Hip Abd / Add Angle [°]	Δmean [95% CI]	-	-	9.97 [7.10, 12.83] ***	-	5.90 [3.05, 8.75] *	-
		% cycle	-	-	39 - 91	-	67 - 85	-
Sagittal Plane Kinematics	**Paretic Hip Flex / Ext Angle [°]**	Δmean [95% CI]	-23.12 [-34.14, -12.10] *	-	-21.88 [-30.21, -13.54] **	-	-	-
		% cycle	54 - 55	-	54 - 64	-	-	-
	Paretic Knee Flex / Ext Angle [°]	Δmean [95% CI]	-	-	-	-	-24.68 [-35.29, -14.06] ***	-
		% cycle	-	-	-	-	51 - 61	-
	Paretic Ankle Dorsi / Plantar Flex Angle [°]	Δmean [95% CI]	-	-	54.71 [39.90, 69.53] ***	-	49.09 [35.24, 62.94] ***	-
		% cycle	-	-	44 - 64	-	50 - 64	-
Sagittal Plane Kinetics	**Paratic Hip Flex / Ext Moment [Nm/kg]**	Δmean [95% CI]	-23.12 [-34.14, -12.10] *	-	-21.88 [-30.21, -13.54] **	-	-	-
		% cycle	54 - 55	-	54 - 64	-	-	-

	Paretic Knee Flex / Ext Moment [Nm/kg]	Δmean [95% CI]	-	-	-	-	-24.68 [-35.29, -14.06] ***	-
		% cycle	-	-	-	-	51 - 61	-
	Paretic Ankle Dorsi / Plantar Flex Moment [Nm/kg]	Δmean [95% CI]	-	-	54.71 [39.90, 69.53] ***	-	49.09 [35.24, 62.94] ***	-
		% cycle	-	-	44 - 64	-	50 - 64	-
Body Kinematics	**Body COM Acceleration [m/s^2]**	Δmean [95% CI]	-	-	-0.89 [-1.09, -0.70] *** 0.70 [0.55, 0.85] ***	-	-0.91 [-1.13, -0.68] *** 0.56 [0.40, 0.73] ***	-
		% cycle	-	-	48 - 61 68 - 88	-	51 - 63 71 - 87	-
Muscle Activity	**Paretic Vastus Medialis EMG [A.U.]**	Δmean [95% CI]	-	-	0.74 [0.41, 1.07] ***	-	0.59 [0.29, 0.88] **	-
		% cycle	-	-	26 - 37	-	29 - 35	-
	Paretic Lateral Hamstrings EMG [A.U.]	Δmean [95% CI]	0.77 [0.43, 1.11] *	-	0.99 [0.79, 1.19] ***	-	0.65 [0.35, 0.95] *	-
		% cycle	20 - 25	-	12 - 39	-	14 - 18	-

Figure B1: Post hoc multiple comparisons on SKG diagnosed individuals within multivariate clustering for the self-selected walking speed (top), the peak knee flexion in the swing (middle), and the propulsive asymmetry (bottom) across clusters by pairwise t-test with Bonferroni correction. Note *** ($p < 0.001$), ** ($0.001 < p < 0.01$), * ($0.01 < p < 0.05$), and n.s. (not significant).

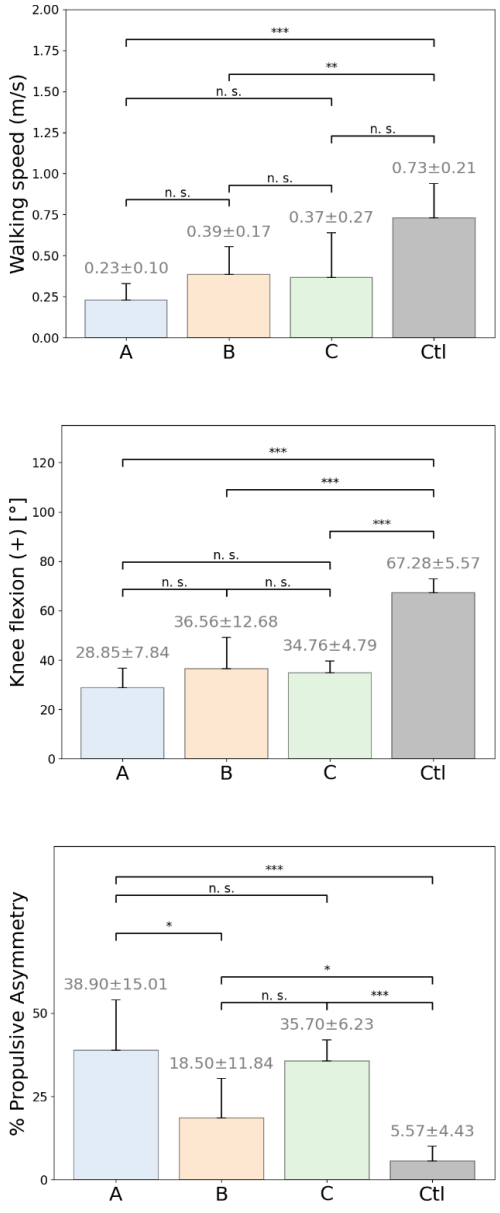

Figure B2: SPM One-way ANOVA on SKG diagnosed individuals within multivariate clustering for compensatory motions.

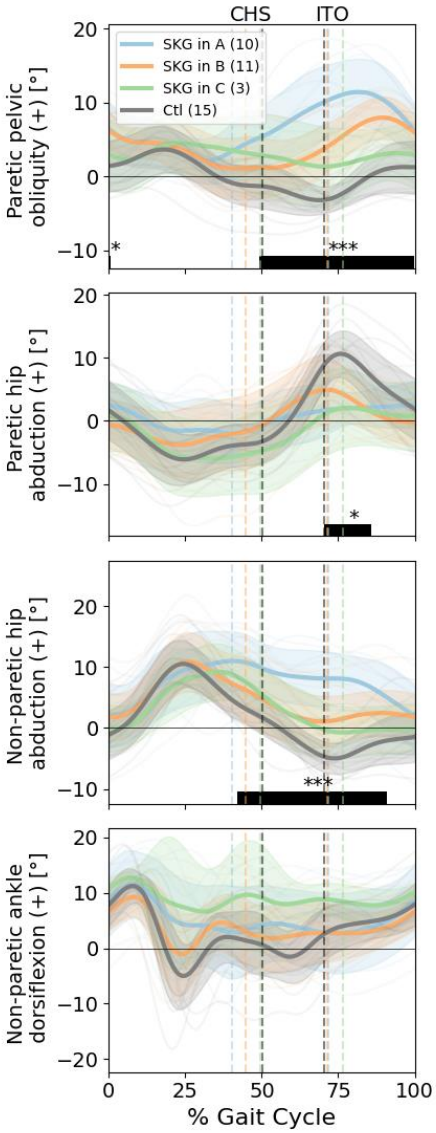

Figure B3: SPM One-way ANOVA on SKG diagnosed individuals within multivariate clustering for the sagittal plane joint kinematics (left) and kinetics (right).

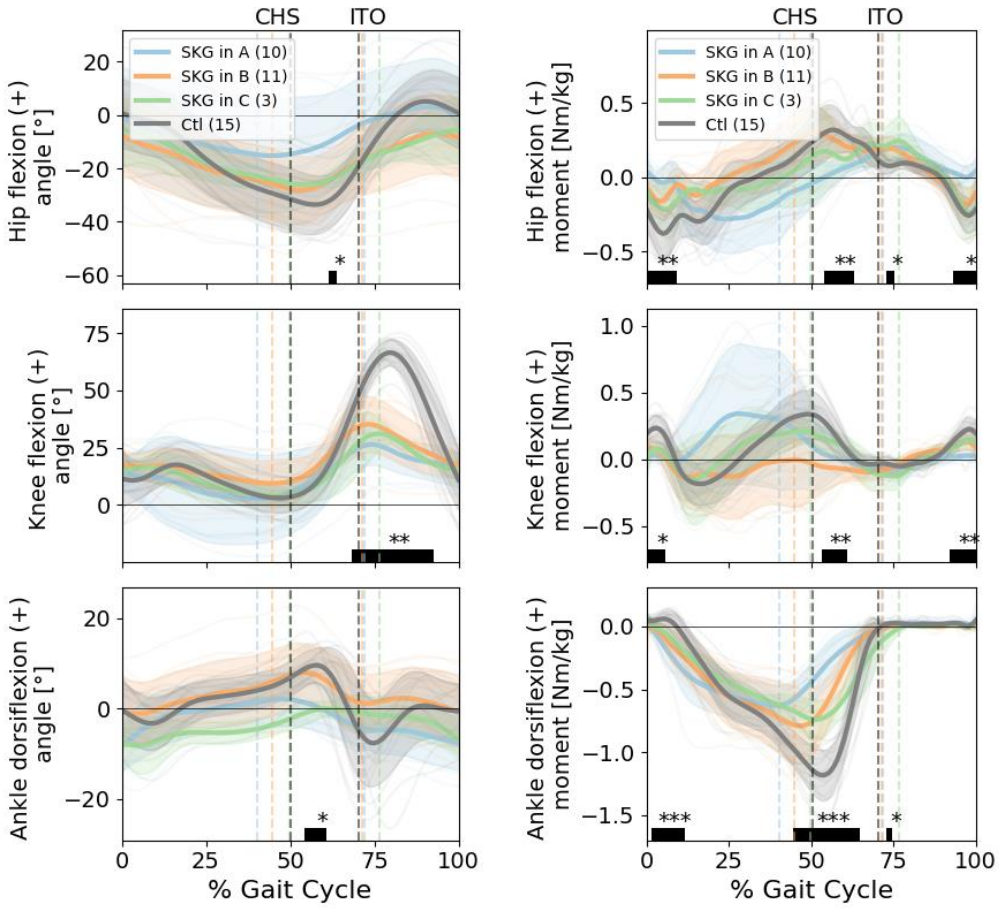

Figure B4: SPM One-way ANOVA on SKG diagnosed individuals within multivariate clustering for body center of mass acceleration.

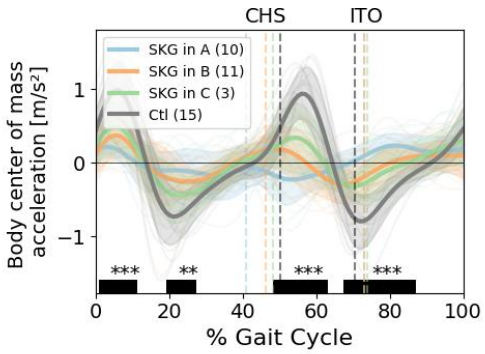

Figure B5: SPM One-way ANOVA on SKG diagnosed individuals within multivariate clustering for muscle EMG signals. Abbreviations are Rectus Femoris (RF), Vastus Medialis (VA), Lateral Hamstrings (LH), Medial Hamstrings (MH), Gluteus Medius (GM), Medial Gastrocnemius (GAS), Soleus (SOL), and Tibialis Anterior (TA).

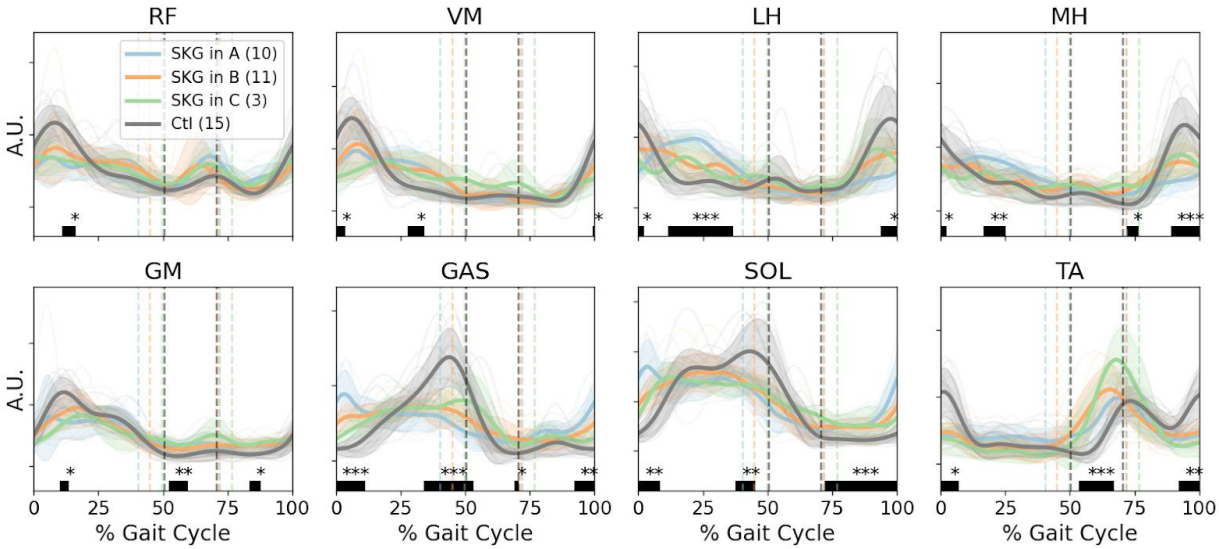

Vita

Jeonghwan Lee received the degree of Bachelor of Science in Mechanical Engineering from Hanyang University, South Korea, in 2013. From 2014 to 2016, he was a research assistant at the University of Texas Health Science Center at Houston. Then, he received the degree of Master of Science in Mechanical Engineering from Seoul National University, South Korea, in 2017. In Fall 2017, he entered the Mechanical Engineering graduate program at The University of Texas at Austin. From 2017 to 2022, he was employed as a graduate research assistant in Rewire Lab, and has contributed to post-stroke gait rehabilitation research.

Contact email: jlee85@utexas.edu

This dissertation was typed by the author.

References

[1] S. S. Virani *et al.*, "Heart disease and stroke statistics—2021 update: a report from the American Heart Association," *Circulation*, vol. 143, no. 8, pp. e254–e743, 2021.

[2] H. S. Jørgensen, H. Nakayama, H. O. Raaschou, and T. S. Olsen, "Recovery of walking function in stroke patients: The copenhagen stroke study," *Archives of Physical Medicine and Rehabilitation*, vol. 76, no. 1, pp. 27–32, Jan. 1995, doi: 10.1016/S0003-9993(95)80038-7.

[3] P. W. Duncan *et al.*, "Management of Adult Stroke Rehabilitation Care," *Stroke*, vol. 36, no. 9, pp. e100–e143, Sep. 2005, doi: 10.1161/01.STR.0000180861.54180.FF.

[4] H. T. Hendricks, J. van Limbeek, A. C. Geurts, and M. J. Zwarts, "Motor recovery after stroke: A systematic review of the literature," *Archives of Physical Medicine and Rehabilitation*, vol. 83, no. 11, pp. 1629–1637, Nov. 2002, doi: 10.1053/apmr.2002.35473.

[5] B. H. Dobkin, "Rehabilitation after Stroke," *New England Journal of Medicine*, vol. 352, no. 16, pp. 1677–1684, Apr. 2005, doi: 10.1056/NEJMcp043511.

[6] J. Mehrholz, S. Thomas, J. Kugler, M. Pohl, and B. Elsner, "Electromechanical-assisted training for walking after stroke," *Cochrane Database of Systematic Reviews*, no. 10, 2020, doi: 10.1002/14651858.CD006185.pub5.

[7] R. P. Van Peppen, G. Kwakkel, S. Wood-Dauphinee, H. J. Hendriks, P. J. Van der Wees, and J. Dekker, "The impact of physical therapy on functional outcomes after stroke: What's the evidence?," *Clinical Rehabilitation*, vol. 18, no. 8. pp. 833–862, Dec. 2004. doi: 10.1191/0269215504cr843oa.

[8] S. C. Cramer and J. D. Riley, "Neuroplasticity and brain repair after stroke," *Current Opinion in Neurology*, vol. 21, no. 1. pp. 76–82, Feb. 2008. doi: 10.1097/WCO.0b013e3282f36cb6.

[9] G. Colombo, M. Joerg, R. Schreier, and V. Dietz, "Treadmill training of paraplegic patients using a robotic orthosis," *Journal of rehabilitation research and development*, vol. 37, no. 6, pp. 693–700, 2000.

[10] R. Riener, "Technology of the robotic gait orthosis Lokomat," in *Neurorehabilitation Technology, Second Edition*, Springer International Publishing, 2016, pp. 395–407. doi: 10.1007/978-3-319-28603-7_19.

[11] K. Kora, J. Stinear, and A. McDaid, "Design, Analysis, and Optimization of an Acute Stroke Gait Rehabilitation Device," *Journal of Medical Devices*, vol. 11, no. 1, Dec. 2016, doi: 10.1115/1.4035127.

[12] B. Y. Tsuge and J. Michael McCarthy, "An Adjustable Single Degree-of-Freedom System to Guide Natural Walking Movement for Rehabilitation," *Journal of Medical Devices*, vol. 10, no. 4, Aug. 2016, doi: 10.1115/1.4033329.

[13] S. Y. Shin, A. D. Deshpande, and J. Sulzer, "Design of a Single Degree-of-Freedom, Adaptable Electromechanical Gait Trainer for People With Neurological

Injury," *Journal of Mechanisms and Robotics*, vol. 10, no. 4, May 2018, doi: 10.1115/1.4039973.
[14] A. Esquenazi, M. Talaty, and A. Jayaraman, "Powered Exoskeletons for Walking Assistance in Persons with Central Nervous System Injuries: A Narrative Review," *PM&R*, vol. 9, no. 1, pp. 46–62, Jan. 2017, doi: 10.1016/j.pmrj.2016.07.534.
[15] R. Gassert and V. Dietz, "Rehabilitation robots for the treatment of sensorimotor deficits: a neurophysiological perspective," *Journal of NeuroEngineering and Rehabilitation*, vol. 15, no. 1, p. 46, Jun. 2018, doi: 10.1186/s12984-018-0383-x.
[16] B. Kalita, J. Narayan, and S. K. Dwivedy, "Development of Active Lower Limb Robotic-Based Orthosis and Exoskeleton Devices: A Systematic Review," *Int J of Soc Robotics*, vol. 13, no. 4, pp. 775–793, Jul. 2021, doi: 10.1007/s12369-020-00662-9.
[17] R. G. Feldmann, "Spasticity: disordered motor control." Med. Publ., 1980.
[18] J. S. Sulzer, R. A. Roiz, M. A. Peshkin, and J. L. Patton, "A Highly Backdrivable, Lightweight Knee Actuator for Investigating Gait in Stroke," *IEEE Transactions on Robotics*, vol. 25, no. 3, pp. 539–548, Jun. 2009, doi: 10.1109/TRO.2009.2019788.
[19] J. S. Sulzer, K. E. Gordon, Y. Y. Dhaher, M. A. Peshkin, and J. L. Patton, "Preswing Knee Flexion Assistance Is Coupled With Hip Abduction in People With Stiff-Knee Gait After Stroke," *Stroke*, vol. 41, no. 8, pp. 1709–1714, Aug. 2010, doi: 10.1161/STROKEAHA.110.586917.
[20] T. Akbas, R. R. Neptune, and J. Sulzer, "Neuromusculoskeletal Simulation Reveals Abnormal Rectus Femoris-Gluteus Medius Coupling in Post-stroke Gait," *Frontiers in Neurology*, vol. 10, p. 301, 2019, doi: 10.3389/fneur.2019.00301.
[21] J. Perry, M. Garrett, J. K. Gronley, and S. J. Mulroy, "Classification of Walking Handicap in the Stroke Population," *Stroke*, vol. 26, no. 6, pp. 982–989, Jun. 1995, doi: 10.1161/01.STR.26.6.982.
[22] A. E. Chisholm, S. D. Perry, and W. E. McIlroy, "Correlations between ankle–foot impairments and dropped foot gait deviations among stroke survivors," *Clinical Biomechanics*, vol. 28, no. 9, pp. 1049–1054, Nov. 2013, doi: 10.1016/j.clinbiomech.2013.09.007.
[23] D. C. Kerrigan, J. Gronley, and J. Perry, "Stiff-legged gait in spastic paresis. A study of quadriceps and hamstrings muscle activity," *Am J Phys Med Rehabil*, vol. 70, no. 6, pp. 294–300, Dec. 1991.
[24] A. Cooper, G. A. Alghamdi, M. A. Alghamdi, A. Altowaijri, and S. Richardson, "The Relationship of Lower Limb Muscle Strength and Knee Joint Hyperextension during the Stance Phase of Gait in Hemiparetic Stroke Patients," *Physiotherapy Research International*, vol. 17, no. 3, pp. 150–156, 2012, doi: 10.1002/pri.528.
[25] H. S. Jørgensen, H. Nakayama, H. O. Raaschou, and T. S. Olsen, "Recovery of walking function in stroke patients: The copenhagen stroke study," *Archives of Physical Medicine and Rehabilitation*, vol. 76, no. 1, pp. 27–32, 1995, doi: 10.1016/S0003-9993(95)80038-7.

[26] M. Wyndaele and J. J. Wyndaele, “Incidence, prevalence and epidemiology of spinal cord injury: What learns a worldwide literature survey?,” *Spinal Cord*, vol. 44, no. 9. pp. 523–529, Sep. 13, 2006. doi: 10.1038/sj.sc.3101893.
[27] Sulzer James S., Gordon Keith E., Dhaher Yasin Y., Peshkin Michael A., and Patton James L., “Preswing Knee Flexion Assistance Is Coupled With Hip Abduction in People With Stiff-Knee Gait After Stroke,” *Stroke*, vol. 41, no. 8, pp. 1709–1714, Aug. 2010, doi: 10.1161/STROKEAHA.110.586917.
[28] T. Akbas *et al.*, “Rectus femoris hyperreflexia contributes to Stiff-Knee gait after stroke,” *Journal of NeuroEngineering and Rehabilitation*, vol. 17, no. 1, p. 117, Aug. 2020, doi: 10.1186/s12984-020-00724-z.
[29] T. Akbas, S. Prajapati, D. Ziemnicki, P. Tamma, S. Gross, and J. Sulzer, “Hip circumduction is not a compensation for reduced knee flexion angle during gait,” *Journal of Biomechanics*, vol. 87, pp. 150–156, Apr. 2019, doi: 10.1016/j.jbiomech.2019.02.026.
[30] T. Akbas, R. R. Neptune, and J. Sulzer, “Neuromusculoskeletal Simulation Reveals Abnormal Rectus Femoris-Gluteus Medius Coupling in Post-stroke Gait,” *Front. Neurol.*, vol. 10, 2019, doi: 10.3389/fneur.2019.00301.
[31] G. Kwakkel, B. Kollen, and J. Twisk, “Impact of time on improvement of outcome after stroke,” *Stroke*, vol. 37, no. 9, pp. 2348–2353, Sep. 2006, doi: 10.1161/01.STR.0000238594.91938.1e.
[32] M. Camicia, H. Wang, M. Divita, J. Mix, and P. Niewczyk, “Length of Stay at Inpatient Rehabilitation Facility and Stroke Patient Outcomes,” *Rehabilitation Nursing*, vol. 41, no. 2, pp. 78–90, Mar. 2016, doi: 10.1002/rnj.218.
[33] G. Colombo, M. Joerg, R. Schreier, and V. Dietz, “Treadmill training of paraplegic patients using a robotic orthosis,” *Journal of Rehabilitation Research and Development*, vol. 37, no. 6, pp. 693–700, 2000.
[34] J. Mehrholz, S. Thomas, C. Werner, J. Kugler, M. Pohl, and B. Elsner, “Electromechanical-assisted training for walking after stroke,” *Cochrane Database of Systematic Reviews*, vol. 2017, no. 5. May 10, 2017. doi: 10.1002/14651858.CD006185.pub4.
[35] K. Y. Nam, H. J. Kim, B. S. Kwon, J. W. Park, H. J. Lee, and A. Yoo, “Robot-assisted gait training (Lokomat) improves walking function and activity in people with spinal cord injury: a systematic review,” *Journal of NeuroEngineering and Rehabilitation*, vol. 14, no. 1, p. 24, Dec. 2017, doi: 10.1186/s12984-017-0232-3.
[36] S. Hesse and D. Uhlenbrock, “A mechanized gait trainer for restoration of gait,” *Journal of Rehabilitation Research and Development*, vol. 37, no. 6, pp. 701–708, 2000.
[37] S. Hesse, C. Werner, D. Uhlenbrock, S. V. Frankenberg, A. Bardeleben, and B. Brandl-Hesse, “An Electromechanical Gait Trainer for Restoration of Gait in Hemiparetic Stroke Patients: Preliminary Results,” *Neurorehabilitation and Neural Repair*, vol. 15, no. 1, pp. 39–50, 2001, doi: 10.1177/154596830101500106.
[38] N. Smania, C. Geroin, N. Valè, and M. Gandolfi, “The End-Effector Device for Gait Rehabilitation,” in *Advanced Technologies for the Rehabilitation of Gait and*

Balance Disorders, G. Sandrini, V. Homberg, L. Saltuari, N. Smania, and A. Pedrocchi, Eds. Cham: Springer International Publishing, 2018, pp. 267–283. doi: 10.1007/978-3-319-72736-3_19.
[39] V. Dietz, "Proprioception and locomotor disorders," *Nature Reviews Neuroscience*, vol. 3, no. 10, pp. 781–790, 2002, doi: 10.1038/nrn939.
[40] Z. Ji and Y. Manna, "Synthesis of a pattern generation mechanism for gait rehabilitation," *Journal of Medical Devices, Transactions of the ASME*, vol. 2, no. 3, 2008, doi: 10.1115/1.2975964.
[41] K. Kora, J. Stinear, and A. McDaid, "Design, analysis, and optimization of an acute stroke gait rehabilitation device," *Journal of Medical Devices, Transactions of the ASME*, vol. 11, no. 1, 2017, doi: 10.1115/1.4035127.
[42] B. Y. Tsuge, M. M. Plecnik, and J. M. McCarthy, "Homotopy directed optimization to design a six-bar linkage for a lower limb with a natural ankle trajectory," *Journal of Mechanisms and Robotics*, vol. 8, no. 6, pp. 1–7, 2016, doi: 10.1115/1.4034141.
[43] B. Y. Tsuge and J. M. McCarthy, "An adjustable single degree-of-freedom system to guide natural walking movement for rehabilitation," *Journal of Medical Devices, Transactions of the ASME*, vol. 10, no. 4, 2016, doi: 10.1115/1.4033329.
[44] B. Y. Tsuge and J. M. McCarthy, "Synthesis of a 10-bar linkage to guide the gait cycle of the human leg," in *Proceedings of the ASME Design Engineering Technical Conference*, Aug. 2015, vol. 5B-2015. doi: 10.1115/DETC201547723.
[45] Y. Shao, Z. Xiang, H. Liu, and L. Li, "Conceptual design and dimensional synthesis of cam-linkage mechanisms for gait rehabilitation," *Mechanism and Machine Theory*, vol. 104, pp. 31–42, Oct. 2016, doi: 10.1016/j.mechmachtheory.2016.05.018.
[46] S. Yul Shin, A. D. Deshpande, and J. Sulzer, "Design of a Single Degree-of-Freedom, Adaptable Electromechanical Gait Trainer for People With Neurological Injury," *Journal of Mechanisms and Robotics*, vol. 10, no. 4, p. 044503, 2018, doi: 10.1115/1.4039973.
[47] M. R. Sabaapour, H. Lee, M. R. Afzal, A. Eizad, and J. Yoon, "Development of a Novel Gait Rehabilitation Device with Hip Interaction and a Single DOF Mechanism," in *2019 International Conference on Robotics and Automation (ICRA)*, May 2019, pp. 1492–1498. doi: 10.1109/ICRA.2019.8794269.
[48] M. R. Haghjoo, H. Lee, M. R. Afzal, A. Eizad, and J. Yoon, "Mech-Walker: A Novel Single-DOF Linkage Device with Movable-Frame for Gait Rehabilitation," *IEEE/ASME Transactions on Mechatronics*, pp. 1–1, 2020, doi: 10.1109/TMECH.2020.2993799.
[49] Y. Yun, H. C. Kim, S. Y. Shin, J. Lee, A. D. Deshpande, and C. Kim, "Statistical method for prediction of gait kinematics with Gaussian process regression," *Journal of Biomechanics*, vol. 47, no. 1, pp. 186–192, Jan. 2014, doi: 10.1016/j.jbiomech.2013.09.032.
[50] B. Koopman, E. H. F. van Asseldonk, and H. Van der Kooij, "Speed-dependent reference joint trajectory generation for robotic gait support," *Journal of*

Biomechanics, vol. 47, no. 6, pp. 1447–1458, 2014, doi: 10.1016/j.jbiomech.2014.01.037.
[51] D. A. Cunningham, P. A. Rechnitzer, M. E. Pearce, and A. P. Donner, "Determinants of self-selected walking pace across ages 19 to 66," *Journals of Gerontology*, vol. 37, no. 5, pp. 560–564, 1982, doi: 10.1093/geronj/37.5.560.
[52] S. Y. Shin and J. Sulzer, "An Online Transition of Speed-dependent Reference Joint Trajectories for Robotic Gait Training," in *2019 IEEE 16th International Conference on Rehabilitation Robotics (ICORR)*, Jun. 2019, pp. 983–987. doi: 10.1109/ICORR.2019.8779359.
[53] R. Norton, *Design of machinery: an introduction to the synthesis and analysis of mechanisms and machines*. New York: McGraw-Hill Education, 2004.
[54] I. Ullah and S. Kota, "Optimal Synthesis of Mechanisms for Path Generation Using Fourier Descriptors and Global Search Methods," *J. Mech. Des*, vol. 119, no. 4, pp. 504–510, Dec. 1997, doi: 10.1115/1.2826396.
[55] J. Yang and Z. Li, "A novel contour error estimation for position loop-based cross-coupled control," *IEEE/ASME transactions on mechatronics*, vol. 16, no. 4, pp. 643–655, 2010.
[56] Y. HAIMES, "On a bicriterion formulation of the problems of integrated system identification and system optimization," *IEEE Transactions on Systems, Man, and Cybernetics*, vol. 1, no. 3, pp. 296–297, 1971, doi: 10.1109/TSMC.1971.4308298.
[57] M. Laumanns, L. Thiele, and E. Zitzler, "An Adaptive Scheme to Generate the Pareto Front Based on the Epsilon-Constraint Method," in *Practical Approaches to Multi-Objective Optimization*, Dagstuhl, Germany, 2005, no. 04461. Accessed: Aug. 20, 2020. [Online]. Available: http://drops.dagstuhl.de/opus/volltexte/2005/246
[58] M. J. D. Powell, "Variable Metric Methods for Constrained Optimization," in *Mathematical Programming The State of the Art*, Springer Berlin Heidelberg, 1983, pp. 288–311. doi: 10.1007/978-3-642-68874-4_12.
[59] M. Stone, "Cross-Validatory Choice and Assessment of Statistical Predictions," *Journal of the Royal Statistical Society: Series B (Methodological)*, vol. 36, no. 2, pp. 111–133, Jan. 1974, doi: 10.1111/j.2517-6161.1974.tb00994.x.
[60] T. Hastie, R. Tibshirani, and J. Friedman, *The elements of statistical learning: data mining, inference, and prediction*. Springer Science & Business Media, 2009.
[61] D. A. Winter, *Biomechanics and Motor Control of Human Movement: Fourth Edition*. 2009. doi: 10.1002/9780470549148.
[62] C. E. McCulloch and J. M. Neuhaus, "Generalized Linear Mixed Models," in *Encyclopedia of Biostatistics*, American Cancer Society, 2005. doi: 10.1002/0470011815.b2a10021.
[63] S. Freivogel, J. Mehrholz, T. Husak-Sotomayor, and D. Schmalohr, "Gait training with the newly developed 'LokoHelp'-system is feasible for non-ambulatory patients after stroke, spinal cord and brain injury. A feasibility study," *Brain Injury*, vol. 22, no. 7–8, pp. 625–632, 2008, doi: 10.1080/02699050801941771.

[64] F. C. Wang, C. H. Yu, T. Y. Chou, and N. C. Chang, “Design and control of an active gait trainer,” in *IEEE International Symposium on Industrial Electronics*, 2009, pp. 1779–1784. doi: 10.1109/ISIE.2009.5213304.
[65] C. A. Fukuchi, R. K. Fukuchi, and M. Duarte, “Effects of walking speed on gait biomechanics in healthy participants: A systematic review and meta-analysis,” *Systematic Reviews*, vol. 8, no. 1. BioMed Central Ltd., Jun. 27, 2019. doi: 10.1186/s13643-019-1063-z.
[66] V. Dietz, G. Colombo, and L. Jensen, “Locomotor activity in spinal man,” *The Lancet*, vol. 344, no. 8932, pp. 1260–1263, Nov. 1994, doi: 10.1016/S0140-6736(94)90751-X.
[67] V. Dietz, “Proprioception and locomotor disorders,” *Nature Reviews Neuroscience*, vol. 3, no. 10, Art. no. 10, Oct. 2002, doi: 10.1038/nrn939.
[68] S. Ghosh, N. Robson, and J. M. McCarthy, “Kinematic Design and Evaluation of a Six-bar Knee-ankle-foot Orthosis,” *Journal of Engineering and Science in Medical Diagnostics and Therapy*, vol. 3, no. 2, Feb. 2020, doi: 10.1115/1.4046474.
[69] J. McKendry, B. Brown, E. R. Westervelt, and J. P. Schmiedeler, “Kinematic design and dynamic analysis of a planar biped robot mechanically coordinated by a single degree of freedom,” in *Proceedings - IEEE International Conference on Robotics and Automation*, 2007, pp. 1875–1880. doi: 10.1109/ROBOT.2007.363595.
[70] O. Al-Araidah, W. Batayneh, T. Darabseh, and S. M. BaniHani, “Conceptual design of a single DOF human-like eight-bar leg mechanism,” *Jordan Journal of Mechanical and Industrial Engineering*, vol. 5, no. 4, pp. 285–289, 2011.
[71] P. Zhao, L. Zhu, B. Zi, and X. Li, “Design of planar 1-DOF cam-linkages for lower-limb rehabilitation via kinematic-mapping motion synthesis framework,” *Journal of Mechanisms and Robotics*, vol. 11, no. 4, 2019, doi: 10.1115/1.4043459.
[72] S. Bai, Z. Li, and R. Li, “Exact synthesis and input–output analysis of 1-dof planar linkages for visiting 10 poses,” *Mechanism and Machine Theory*, vol. 143, p. 103625, Jan. 2020, doi: 10.1016/j.mechmachtheory.2019.103625.
[73] X. Li, S. Wei, Q. Liao, and Y. Zhang, “A novel analytical method for four-bar path generation synthesis based on Fourier series,” *Mechanism and Machine Theory*, vol. 144, p. 103671, Feb. 2020, doi: 10.1016/j.mechmachtheory.2019.103671.
[74] J. K. Pickard, J. A. Carretero, and J.-P. Merlet, “Appropriate synthesis of the four-bar linkage,” *Mechanism and Machine Theory*, vol. 153, p. 103965, Nov. 2020, doi: 10.1016/j.mechmachtheory.2020.103965.
[75] A. Kapsalyamov, P. K. Jamwal, S. Hussain, and M. H. Ghayesh, “State of the Art Lower Limb Robotic Exoskeletons for Elderly Assistance,” *IEEE Access*, vol. 7, pp. 95075–95086, 2019, doi: 10.1109/ACCESS.2019.2928010.
[76] A. J. Young and D. P. Ferris, “State of the Art and Future Directions for Lower Limb Robotic Exoskeletons,” *IEEE Transactions on Neural Systems and Rehabilitation Engineering*, vol. 25, no. 2, pp. 171–182, Feb. 2017, doi: 10.1109/TNSRE.2016.2521160.
[77] J. Zhang *et al.*, “Human-in-the-loop optimization of exoskeleton assistance during walking,” *Science*, Jun. 2017, doi: 10.1126/science.aal5054.

[78] Y. Ding, M. Kim, S. Kuindersma, and C. J. Walsh, “Human-in-the-loop optimization of hip assistance with a soft exosuit during walking,” *Science Robotics*, Feb. 2018, doi: 10.1126/scirobotics.aar5438.
[79] R. R. Young, “Spasticity: a review,” *Neurology*, vol. 44, no. 11 Suppl 9, pp. S12-20, Nov. 1994.
[80] T. Akbas *et al.*, “Rectus femoris hyperreflexia contributes to Stiff-Knee gait after stroke,” *Journal of NeuroEngineering and Rehabilitation*, vol. 17, no. 1, p. 117, Aug. 2020, doi: 10.1186/s12984-020-00724-z.
[81] S. L. Delp *et al.*, “OpenSim: Open-Source Software to Create and Analyze Dynamic Simulations of Movement,” *IEEE Transactions on Biomedical Engineering*, vol. 54, no. 11, pp. 1940–1950, Nov. 2007, doi: 10.1109/TBME.2007.901024.
[82] T. Akbas and J. Sulzer, “Musculoskeletal simulation framework for impairment-based exoskeletal assistance post-stroke,” in *2019 IEEE 16th International Conference on Rehabilitation Robotics (ICORR)*, Jun. 2019, pp. 1185–1190. doi: 10.1109/ICORR.2019.8779564.
[83] D. G. Thelen and F. C. Anderson, “Using computed muscle control to generate forward dynamic simulations of human walking from experimental data,” *Journal of Biomechanics*, vol. 39, no. 6, pp. 1107–1115, Jan. 2006, doi: 10.1016/j.jbiomech.2005.02.010.
[84] J. L. Hicks, T. K. Uchida, A. Seth, A. Rajagopal, and S. L. Delp, “Is My Model Good Enough? Best Practices for Verification and Validation of Musculoskeletal Models and Simulations of Movement,” *Journal of Biomechanical Engineering*, vol. 137, no. 2, Feb. 2015, doi: 10.1115/1.4029304.
[85] A. Burden, “How should we normalize electromyograms obtained from healthy participants? What we have learned from over 25years of research,” *Journal of Electromyography and Kinesiology*, vol. 20, no. 6, pp. 1023–1035, Dec. 2010, doi: 10.1016/j.jelekin.2010.07.004.
[86] E. Pierrot-Deseilligny and D. Burke, *The circuitry of the human spinal cord: its role in motor control and movement disorders*. Cambridge university press, 2005.
[87] N. Mrachacz-Kersting, B. A. Lavoie, J. B. Andersen, and T. Sinkjaer, “Characterisation of the quadriceps stretch reflex during the transition from swing to stance phase of human walking,” *Exp Brain Res*, vol. 159, no. 1, pp. 108–122, Nov. 2004, doi: 10.1007/s00221-004-1941-y.
[88] S. R. Goldberg, S. Õunpuu, A. S. Arnold, J. R. Gage, and S. L. Delp, “Kinematic and kinetic factors that correlate with improved knee flexion following treatment for stiff-knee gait,” *Journal of Biomechanics*, vol. 39, no. 4, pp. 689–698, Jan. 2006, doi: 10.1016/j.jbiomech.2005.01.015.
[89] M. G. Bowden, A. L. Behrman, M. Woodbury, C. M. Gregory, C. A. Velozo, and S. A. Kautz, “Advancing Measurement of Locomotor Rehabilitation Outcomes to Optimize Interventions and Differentiate between Recovery versus Compensation,” *Journal of neurologic physical therapy : JNPT*, vol. 36, no. 1, p. 38, Mar. 2012, doi: 10.1097/NPT.0b013e3182472cf6.

[90] M. G. Bowden, C. K. Balasubramanian, R. R. Neptune, and S. A. Kautz, "Anterior-Posterior Ground Reaction Forces as a Measure of Paretic Leg Contribution in Hemiparetic Walking," *Stroke*, vol. 37, no. 3, pp. 872–876, Mar. 2006, doi: 10.1161/01.STR.0000204063.75779.8d.
[91] S. J. Piazza and S. L. Delp, "The influence of muscles on knee flexion during the swing phase of gait," *Journal of Biomechanics*, vol. 29, no. 6, pp. 723–733, Jun. 1996, doi: 10.1016/0021-9290(95)00144-1.
[92] R. Tibshirani, "Regression Shrinkage and Selection Via the Lasso," *Journal of the Royal Statistical Society: Series B (Methodological)*, vol. 58, no. 1, pp. 267–288, 1996, doi: 10.1111/j.2517-6161.1996.tb02080.x.
[93] A. Y. Ng, "Feature selection, L 1 vs. L 2 regularization, and rotational invariance," in *Proceedings of the twenty-first international conference on Machine learning*, 2004, p. 78.
[94] N. Meinshausen and B. Yu, "Lasso-type recovery of sparse representations for high-dimensional data," *The Annals of Statistics*, vol. 37, no. 1, pp. 246–270, Feb. 2009, doi: 10.1214/07-AOS582.
[95] J. Schelldorfer, L. Meier, and P. Bühlmann, "GLMMLasso: An Algorithm for High-Dimensional Generalized Linear Mixed Models Using ℓ1-Penalization," *Journal of Computational and Graphical Statistics*, vol. 23, no. 2, pp. 460–477, Apr. 2014, doi: 10.1080/10618600.2013.773239.
[96] A. Groll and G. Tutz, "Variable selection for generalized linear mixed models by L 1-penalized estimation," *Stat Comput*, vol. 24, no. 2, pp. 137–154, Mar. 2014, doi: 10.1007/s11222-012-9359-z.
[97] Y. A. Majeed, S. S. Awadalla, and J. L. Patton, "Regression techniques employing feature selection to predict clinical outcomes in stroke," *PLOS ONE*, vol. 13, no. 10, p. e0205639, Oct. 2018, doi: 10.1371/journal.pone.0205639.
[98] H. A. Chipman, E. I. George, and R. E. McCulloch, "BART: Bayesian additive regression trees," *The Annals of Applied Statistics*, vol. 4, no. 1, pp. 266–298, Mar. 2010, doi: 10.1214/09-AOAS285.
[99] L. Hu, C. Gu, M. Lopez, J. Ji, and J. Wisnivesky, "Estimation of causal effects of multiple treatments in observational studies with a binary outcome," *Stat Methods Med Res*, vol. 29, no. 11, pp. 3218–3234, Nov. 2020, doi: 10.1177/0962280220921909.
[100] J. L. Hill, "Bayesian Nonparametric Modeling for Causal Inference," *Journal of Computational and Graphical Statistics*, vol. 20, no. 1, pp. 217–240, Jan. 2011, doi: 10.1198/jcgs.2010.08162.
[101] A. Kapelner and J. Bleich, "bartMachine: Machine learning with Bayesian additive regression trees," *arXiv preprint arXiv:1312.2171*, 2013.
[102] T. Hastie and R. Tibshirani, "Bayesian backfitting (with comments and a rejoinder by the authors," *Statistical Science*, vol. 15, no. 3, pp. 196–223, Aug. 2000, doi: 10.1214/ss/1009212815.
[103] R. McCulloch, R. Sparapani, R. Gramacy, C. Spanbauer, and M. Pratola, "BART: Bayesian additive regression trees," *R package version*, vol. 1, 2018.

[104] J. He, S. Yalov, and P. R. Hahn, “XBART: Accelerated Bayesian additive regression trees,” in *The 22nd International Conference on Artificial Intelligence and Statistics*, 2019, pp. 1130–1138.
[105] R. Sparapani, C. Spanbauer, and R. McCulloch, “Nonparametric Machine Learning and Efficient Computation with Bayesian Additive Regression Trees: The BART R Package,” *Journal of Statistical Software*, vol. 97, pp. 1–66, Jan. 2021, doi: 10.18637/jss.v097.i01.
[106] J. W. Lance, “The control of muscle tone, reflexes, and movement: Robert Wartenbeg Lecture,” *Neurology*, vol. 30, no. 12, pp. 1303–1303, 1980.
[107] P. B. C. Matthews, “The response of de-efferented muscle spindle receptors to stretching at different velocities,” *J Physiol*, vol. 168, no. 3, pp. 660–678, Oct. 1963.
[108] P. B. C. Matthews and R. B. Stein, “The sensitivity of muscle spindle afferents to small sinusoidal changes of length,” *The Journal of Physiology*, vol. 200, no. 3, pp. 723–743, 1969, doi: 10.1113/jphysiol.1969.sp008719.
[109] J. C. Houk, W. Z. Rymer, and P. E. Crago, “Dependence of dynamic response of spindle receptors on muscle length and velocity.,” *Journal of Neurophysiology*, vol. 46, no. 1, pp. 143–166, 1981.
[110] J. He, W. R. Norling, and Y. Wang, “A dynamic neuromuscular model for describing the pendulum test of spasticity,” *IEEE Transactions on Biomedical Engineering*, vol. 44, no. 3, pp. 175–184, Mar. 1997, doi: 10.1109/10.554764.
[111] P. Le Cavorzin, S. A. Poudens, F. Chagneau, G. Carrault, H. Allain, and P. Rochcongar, “A comprehensive model of spastic hypertonia derived from the pendulum test of the leg,” *Muscle & Nerve*, vol. 24, no. 12, pp. 1612–1621, 2001, doi: 10.1002/mus.1196.
[112] C. Pizzolato *et al.*, “CEINMS: A toolbox to investigate the influence of different neural control solutions on the prediction of muscle excitation and joint moments during dynamic motor tasks,” *Journal of Biomechanics*, vol. 48, no. 14, pp. 3929–3936, Nov. 2015, doi: 10.1016/j.jbiomech.2015.09.021.
[113] J. R. Franz, “A sound approach to improving exoskeletons and exosuits,” *Science Robotics*, Nov. 2021, doi: 10.1126/scirobotics.abm6369.
[114] R. W. Nuckols, S. Lee, K. Swaminathan, D. Orzel, R. D. Howe, and C. J. Walsh, “Individualization of exosuit assistance based on measured muscle dynamics during versatile walking,” *Science Robotics*, Nov. 2021, doi: 10.1126/scirobotics.abj1362.
[115] Z. Sheng, A. Iyer, Z. Sun, K. Kim, and N. Sharma, “A Hybrid Knee Exoskeleton Using Real-Time Ultrasound-Based Muscle Fatigue Assessment,” *IEEE/ASME Transactions on Mechatronics*, pp. 1–9, 2022, doi: 10.1109/TMECH.2022.3171086.
[116] S. Jezernik, G. Colombo, T. Keller, H. Frueh, and M. Morari, “Robotic Orthosis Lokomat: A Rehabilitation and Research Tool,” *Neuromodulation: Technology at the Neural Interface*, vol. 6, no. 2, pp. 108–115, 2003, doi: 10.1046/j.1525-1403.2003.03017.x.
[117] G. M. Bryan, P. W. Franks, S. C. Klein, R. J. Peuchen, and S. H. Collins, “A hip–knee–ankle exoskeleton emulator for studying gait assistance,” *The International*

Journal of Robotics Research, vol. 40, no. 4–5, pp. 722–746, Apr. 2021, doi: 10.1177/0278364920961452.
[118] Y. Ding *et al.*, "Biomechanical and Physiological Evaluation of Multi-Joint Assistance With Soft Exosuits," *IEEE Transactions on Neural Systems and Rehabilitation Engineering*, vol. 25, no. 2, pp. 119–130, Feb. 2017, doi: 10.1109/TNSRE.2016.2523250.
[119] P. Malcolm, S. Galle, W. Derave, and D. De Clercq, "Bi-articular Knee-Ankle-Foot Exoskeleton Produces Higher Metabolic Cost Reduction than Weight-Matched Mono-articular Exoskeleton," *Frontiers in Neuroscience*, vol. 12, 2018, Accessed: Jun. 16, 2022. [Online]. Available: https://www.frontiersin.org/article/10.3389/fnins.2018.00069
[120] G. Geenens, "Curse of dimensionality and related issues in nonparametric functional regression," *Statistics Surveys*, vol. 5, no. none, pp. 30–43, Jan. 2011, doi: 10.1214/09-SS049.
[121] M. de Rooij and W. Weeda, "Cross-Validation: A Method Every Psychologist Should Know," *Advances in Methods and Practices in Psychological Science*, vol. 3, no. 2, pp. 248–263, Jun. 2020, doi: 10.1177/2515245919898466.
[122] J. Ranstam and J. A. Cook, "LASSO regression," *British Journal of Surgery*, vol. 105, no. 10, p. 1348, Sep. 2018, doi: 10.1002/bjs.10895.
[123] H. Zou and T. Hastie, "Regularization and variable selection via the elastic net," *Journal of the Royal Statistical Society: Series B (Statistical Methodology)*, vol. 67, no. 2, pp. 301–320, 2005, doi: 10.1111/j.1467-9868.2005.00503.x.
[124] A. Natekin and A. Knoll, "Gradient boosting machines, a tutorial," *Frontiers in Neurorobotics*, vol. 7, 2013, Accessed: Jun. 15, 2022. [Online]. Available: https://www.frontiersin.org/article/10.3389/fnbot.2013.00021
[125] G. Biau and E. Scornet, "A random forest guided tour," *TEST*, vol. 25, no. 2, pp. 197–227, Jun. 2016, doi: 10.1007/s11749-016-0481-7.
[126] S. J. Olney and C. Richards, "Hemiparetic gait following stroke. Part I: Characteristics," *Gait & Posture*, vol. 4, no. 2, pp. 136–148, Apr. 1996, doi: 10.1016/0966-6362(96)01063-6.
[127] I. A. K. de Quervain, S. R. Simon, S. U. E. Leurgans, W. S. Pease, and D. McALLISTER, "Gait pattern in the early recovery period after stroke," *JBJS*, vol. 78, no. 10, pp. 1506–14, 1996.
[128] S. Mulroy, J. Gronley, W. Weiss, C. Newsam, and J. Perry, "Use of cluster analysis for gait pattern classification of patients in the early and late recovery phases following stroke," *Gait & Posture*, vol. 18, no. 1, pp. 114–125, Aug. 2003, doi: 10.1016/S0966-6362(02)00165-0.
[129] E. Knutsson and C. Richards, "Different types of disturbed motor control in gait of hemiparetic patients.," *Brain: a journal of neurology*, vol. 102, no. 2, pp. 405–430, 1979.
[130] S. Kinsella and K. Moran, "Gait pattern categorization of stroke participants with equinus deformity of the foot," *Gait & Posture*, vol. 27, no. 1, pp. 144–151, Jan. 2008, doi: 10.1016/j.gaitpost.2007.03.008.

[131] K. A. Shorter, A. Wu, and A. D. Kuo, “The high cost of swing leg circumduction during human walking,” *Gait & Posture*, vol. 54, pp. 265–270, May 2017, doi: 10.1016/j.gaitpost.2017.03.021.
[132] R. L. Waters and S. Mulroy, “The energy expenditure of normal and pathologic gait,” *Gait & Posture*, vol. 9, no. 3, pp. 207–231, Jul. 1999, doi: 10.1016/S0966-6362(99)00009-0.
[133] J. Abercrombie, “Clinical Lecture on Hemiplegia in Children,” *Br Med J*, vol. 1, no. 1381, pp. 1323–1325, Jun. 1887.
[134] A. S. Abramson, “Use and abuse of ambulation training in rehabilitation,” *Postgraduate medicine*, vol. 23, no. 2, pp. 178–185, 1958.
[135] J. Perry and J. M. Burnfield, “Gait analysis: normal and pathological function,” *Inc., Thorofare, NJ: Slack*, 1992.
[136] D. H. Sutherland, M. Santi, and M. F. Abel, “Treatment of stiff-knee gait in cerebral palsy: a comparison by gait analysis of distal rectus femoris transfer versus proximal rectus release,” *J Pediatr Orthop*, vol. 10, no. 4, pp. 433–441, Jul. 1990.
[137] D. C. Kerrigan, R. S. Roth, and P. O. Riley, “The modelling of adult spastic paretic stiff-legged gait swing period based on actual kinematic data,” *Gait & Posture*, vol. 7, no. 2, pp. 117–124, Mar. 1998, doi: 10.1016/S0966-6362(97)00040-4.
[138] D. H. Sutherland and J. R. Davids, “Common gait abnormalities of the knee in cerebral palsy,” *Clin Orthop Relat Res*, no. 288, pp. 139–147, Mar. 1993.
[139] J. McLaughlin *et al.*, “Selective dorsal rhizotomy: meta-analysis of three randomized controlled trials,” *Developmental Medicine and Child Neurology*, vol. 44, no. 1, pp. 17–25, Jan. 2002, doi: 10.1017/S0012162201001608.
[140] M. A. Eppinger, C. M. Berman, and C. A. Mazzola, “Selective dorsal rhizotomy for spastic diplegia secondary to stroke in an adult patient,” *Surg Neurol Int*, vol. 6, p. 111, Jun. 2015, doi: 10.4103/2152-7806.159382.
[141] J. V. G. Robertson, D. Pradon, D. Bensmail, C. Fermanian, B. Bussel, and N. Roche, “Relevance of botulinum toxin injection and nerve block of rectus femoris to kinematic and functional parameters of stiff knee gait in hemiplegic adults,” *Gait & Posture*, vol. 29, no. 1, pp. 108–112, Jan. 2009, doi: 10.1016/j.gaitpost.2008.07.005.
[142] G. G. Stoquart, C. Detrembleur, S. Palumbo, T. Deltombe, and T. M. Lejeune, “Effect of Botulinum Toxin Injection in the Rectus Femoris on Stiff-Knee Gait in People With Stroke: A Prospective Observational Study,” *Archives of Physical Medicine and Rehabilitation*, vol. 89, no. 1, pp. 56–61, Jan. 2008, doi: 10.1016/j.apmr.2007.08.131.
[143] N. Roche, R. Zory, A. Sauthier, C. Bonnyaud, D. Pradon, and D. Bensmail, “Effect of rehabilitation and botulinum toxin injection on gait in chronic stroke patients: a randomized controlled study,” *Journal of rehabilitation medicine*, vol. 47, no. 1, pp. 31–37, 2015.
[144] I. Campanini, A. Merlo, and B. Damiano, “A method to differentiate the causes of stiff-knee gait in stroke patients,” *Gait & Posture*, vol. 38, no. 2, pp. 165–169, Jun. 2013, doi: 10.1016/j.gaitpost.2013.05.003.

[145] D. Mazzoli *et al.*, "Electromyographic activity of the vastus intermedius muscle in patients with stiff-knee gait after stroke. A retrospective observational study," *Gait & Posture*, vol. 60, pp. 273–278, Feb. 2018, doi: 10.1016/j.gaitpost.2017.07.002.
[146] J. Boudarham, N. Roche, D. Pradon, E. Delouf, D. Bensmail, and R. Zory, "Effects of Quadriceps Muscle Fatigue on Stiff-Knee Gait in Patients with Hemiparesis," *PLOS ONE*, vol. 9, no. 4, p. e94138, Apr. 2014, doi: 10.1371/journal.pone.0094138.
[147] D. Thawrani, T. Haumont, C. Church, L. Holmes, K. W. Dabney, and F. Miller, "Rectus Femoris Transfer Improves Stiff Knee Gait in Children With Spastic Cerebral Palsy," *Clin Orthop Relat Res*, vol. 470, no. 5, pp. 1303–1311, May 2012, doi: 10.1007/s11999-011-2215-1.
[148] K. Fujita *et al.*, "Pedaling improves gait ability of hemiparetic patients with stiff-knee gait: fall prevention during gait," *Journal of Stroke and Cerebrovascular Diseases*, vol. 29, no. 9, p. 105035, Sep. 2020, doi: 10.1016/j.jstrokecerebrovasdis.2020.105035.
[149] J. A. Reinbolt, M. D. Fox, A. S. Arnold, S. Õunpuu, and S. L. Delp, "Importance of preswing rectus femoris activity in stiff-knee gait," *Journal of Biomechanics*, vol. 41, no. 11, pp. 2362–2369, Aug. 2008, doi: 10.1016/j.jbiomech.2008.05.030.
[150] A. Lewerenz, S. I. Wolf, T. Dreher, and B. K. Krautwurst, "Performance of stair negotiation in patients with cerebral palsy and stiff knee gait," *Gait & Posture*, vol. 71, pp. 14–19, Jun. 2019, doi: 10.1016/j.gaitpost.2019.04.005.
[151] S. R. Goldberg, S. Õunpuu, and S. L. Delp, "The importance of swing-phase initial conditions in stiff-knee gait," *Journal of Biomechanics*, vol. 36, no. 8, pp. 1111–1116, Aug. 2003, doi: 10.1016/S0021-9290(03)00106-4.
[152] I. Jonkers, C. Stewart, K. Desloovere, G. Molenaers, and A. Spaepen, "Musculo-tendon length and lengthening velocity of rectus femoris in stiff knee gait," *Gait & Posture*, vol. 23, no. 2, pp. 222–229, Feb. 2006, doi: 10.1016/j.gaitpost.2005.02.005.
[153] H. Böhm, M. Hösl, H. Schwameder, and L. Döderlein, "Stiff-knee gait in cerebral palsy: How do patients adapt to uneven ground?," *Gait & Posture*, vol. 39, no. 4, pp. 1028–1033, Apr. 2014, doi: 10.1016/j.gaitpost.2014.01.001.
[154] S. R. Goldberg, F. C. Anderson, M. G. Pandy, and S. L. Delp, "Muscles that influence knee flexion velocity in double support: implications for stiff-knee gait," *Journal of Biomechanics*, vol. 37, no. 8, pp. 1189–1196, Aug. 2004, doi: 10.1016/j.jbiomech.2003.12.005.
[155] M. D. Lewek, T. G. Hornby, Y. Y. Dhaher, and B. D. Schmit, "Prolonged Quadriceps Activity Following Imposed Hip Extension: A Neurophysiological Mechanism for Stiff-Knee Gait?," *Journal of Neurophysiology*, vol. 98, no. 6, pp. 3153–3162, Dec. 2007, doi: 10.1152/jn.00726.2007.
[156] D. L. Damiano, E. Laws, D. V. Carmines, and M. F. Abel, "Relationship of spasticity to knee angular velocity and motion during gait in cerebral palsy," *Gait & Posture*, vol. 23, no. 1, pp. 1–8, Jan. 2006, doi: 10.1016/j.gaitpost.2004.10.007.

[157] R. Gross, F. Leboeuf, J. B. Hardouin, B. Perrouin-Verbe, S. Brochard, and O. Rémy-Néris, "Does muscle coactivation influence joint excursions during gait in children with and without hemiplegic cerebral palsy? Relationship between muscle coactivation and joint kinematics," *Clinical Biomechanics*, vol. 30, no. 10, pp. 1088–1093, Dec. 2015, doi: 10.1016/j.clinbiomech.2015.09.001.
[158] A. Lamontagne, C. L. Richards, and F. Malouin, "Coactivation during gait as an adaptive behavior after stroke," *Journal of Electromyography and Kinesiology*, vol. 10, no. 6, pp. 407–415, Dec. 2000, doi: 10.1016/S1050-6411(00)00028-6.
[159] D. J. Clark, L. H. Ting, F. E. Zajac, R. R. Neptune, and S. A. Kautz, "Merging of Healthy Motor Modules Predicts Reduced Locomotor Performance and Muscle Coordination Complexity Post-Stroke," *Journal of Neurophysiology*, vol. 103, no. 2, pp. 844–857, Feb. 2010, doi: 10.1152/jn.00825.2009.
[160] F. C. Anderson, S. R. Goldberg, M. G. Pandy, and S. L. Delp, "Contributions of muscle forces and toe-off kinematics to peak knee flexion during the swing phase of normal gait: an induced position analysis," *Journal of Biomechanics*, vol. 37, no. 5, pp. 731–737, May 2004, doi: 10.1016/j.jbiomech.2003.09.018.
[161] S. Ounpuu, E. Muik, R. B. Davis, J. R. Gage, and P. A. DeLuca, "Rectus femoris surgery in children with cerebral palsy. Part I: The effect of rectus femoris transfer location on knee motion," *J Pediatr Orthop*, vol. 13, no. 3, pp. 325–330, May 1993, doi: 10.1097/01241398-199305000-00010.
[162] L. N. Awad, M. D. Lewek, T. M. Kesar, J. R. Franz, and M. G. Bowden, "These legs were made for propulsion: advancing the diagnosis and treatment of post-stroke propulsion deficits," *Journal of NeuroEngineering and Rehabilitation*, vol. 17, no. 1, p. 139, Oct. 2020, doi: 10.1186/s12984-020-00747-6.
[163] T. F. Winters, J. R. Gage, and R. Hicks, "Gait patterns in spastic hemiplegia in children and young adults," *J Bone Joint Surg Am*, vol. 69, no. 3, pp. 437–441, 1987.
[164] G. Leporace *et al.*, "Are there different gait profiles in patients with advanced knee osteoarthritis? A machine learning approach," *Clinical Biomechanics*, vol. 88, p. 105447, Aug. 2021, doi: 10.1016/j.clinbiomech.2021.105447.
[165] B. Toro, C. J. Nester, and P. C. Farren, "Cluster analysis for the extraction of sagittal gait patterns in children with cerebral palsy," *Gait & Posture*, vol. 25, no. 2, pp. 157–165, Feb. 2007, doi: 10.1016/j.gaitpost.2006.02.004.
[166] N. Roche, D. Pradon, J. Cosson, J. Robertson, C. Marchiori, and R. Zory, "Categorization of gait patterns in adults with cerebral palsy: A clustering approach," *Gait & Posture*, vol. 39, no. 1, pp. 235–240, Jan. 2014, doi: 10.1016/j.gaitpost.2013.07.110.
[167] L. Abbasi, Z. Rojhani-Shirazi, M. Razeghi, and H. Raeisi-Shahraki, "Kinematic cluster analysis of the crouch gait pattern in children with spastic diplegic cerebral palsy using sparse K-means method," *Clinical Biomechanics*, vol. 81, p. 105248, Jan. 2021, doi: 10.1016/j.clinbiomech.2020.105248.
[168] J. M. O'Byrne, A. Jenkinson, and T. M. O'Brien, "Quantitative Analysis and Classification of Gait Patterns in Cerebral Palsy Using a Three-Dimensional Motion

Analyzer," *J Child Neurol*, vol. 13, no. 3, pp. 101–108, Mar. 1998, doi: 10.1177/088307389801300302.
[169] E. Dolatabadi, A. Mansfield, K. K. Patterson, B. Taati, and A. Mihailidis, "Mixture-Model Clustering of Pathological Gait Patterns," *IEEE Journal of Biomedical and Health Informatics*, vol. 21, no. 5, pp. 1297–1305, Sep. 2017, doi: 10.1109/JBHI.2016.2633000.
[170] M. J. O'Malley, M. F. Abel, D. L. Damiano, and C. L. Vaughan, "Fuzzy clustering of children with cerebral palsy based on temporal-distance gait parameters," *IEEE Transactions on Rehabilitation Engineering*, vol. 5, no. 4, pp. 300–309, Dec. 1997, doi: 10.1109/86.650282.
[171] C. L. Vaughan and M. J. O'Malley, "A gait nomogram used with fuzzy clustering to monitor functional status of children and young adults with cerebral palsy," *Developmental Medicine & Child Neurology*, vol. 47, no. 6, pp. 377–383, 2005, doi: 10.1111/j.1469-8749.2005.tb01157.x.
[172] M. Manca, G. Ferraresi, M. Cosma, L. Cavazzuti, M. Morelli, and M. G. Benedetti, "Gait Patterns in Hemiplegic Patients with Equinus Foot Deformity," *BioMed Research International*, vol. 2014, p. e939316, Apr. 2014, doi: 10.1155/2014/939316.
[173] J.-J. J. Chen and R. Shiavi, "Temporal feature extraction and clustering analysis of electromyographic linear envelopes in gait studies," *IEEE Transactions on Biomedical Engineering*, vol. 37, no. 3, pp. 295–302, Mar. 1990, doi: 10.1109/10.52330.
[174] S. Straudi, M. Manca, E. Aiello, G. Ferraresi, S. Cavazza, and N. Basaglia, "Sagittal plane kinematic analysis of the six-minute walk test: a classification of hemiplegic gait," *Eur J Phys Rehabil Med*, vol. 45, no. 3, pp. 341–347, 2009.
[175] D. C. Kerrigan, E. P. Frates, S. Rogan, and P. O. Riley, "Hip Hiking and Circumduction: Quantitative Definitions," *American Journal of Physical Medicine & Rehabilitation*, vol. 79, no. 3, pp. 247–252, Jun. 2000.
[176] I. S. Dhillon, Y. Guan, and B. Kulis, "Kernel k-means: spectral clustering and normalized cuts," in *Proceedings of the tenth ACM SIGKDD international conference on Knowledge discovery and data mining*, New York, NY, USA, Aug. 2004, pp. 551–556. doi: 10.1145/1014052.1014118.
[177] M. Cuturi, "Fast global alignment kernels," in *Proceedings of the 28th international conference on machine learning (ICML-11)*, 2011, pp. 929–936.
[178] G. Hamerly and C. Elkan, "Learning the k in k-means," *Advances in neural information processing systems*, vol. 16, pp. 281–288, 2004.
[179] P. O. Riley and D. C. Kerrigan, "Kinetics of stiff-legged gait: induced acceleration analysis," *IEEE Transactions on Rehabilitation Engineering*, vol. 7, no. 4, pp. 420–426, Dec. 1999, doi: 10.1109/86.808945.
[180] A. K. Jain and R. C. Dubes, *Algorithms for clustering data*. Prentice-Hall, Inc., 1988.
[181] J. Wu, H. Xiong, and J. Chen, "Adapting the right measures for K-means clustering," in *Proceedings of the 15th ACM SIGKDD international conference on*

Knowledge discovery and data mining, New York, NY, USA, Jun. 2009, pp. 877–886. doi: 10.1145/1557019.1557115.
[182] D. Steinley, "Properties of the Hubert-Arable Adjusted Rand Index.," *Psychological methods*, vol. 9, no. 3, p. 386, 2004.
[183] N. X. Vinh, J. Epps, and J. Bailey, "Information theoretic measures for clusterings comparison: Variants, properties, normalization and correction for chance," *The Journal of Machine Learning Research*, vol. 11, pp. 2837–2854, 2010.
[184] A. Rosenberg and J. Hirschberg, "V-measure: A conditional entropy-based external cluster evaluation measure," in *Proceedings of the 2007 joint conference on empirical methods in natural language processing and computational natural language learning (EMNLP-CoNLL)*, 2007, pp. 410–420.
[185] V. A. Stanhope, B. A. Knarr, D. S. Reisman, and J. S. Higginson, "Frontal plane compensatory strategies associated with self-selected walking speed in individuals post-stroke," *Clinical Biomechanics*, vol. 29, no. 5, pp. 518–522, May 2014, doi: 10.1016/j.clinbiomech.2014.03.013.
[186] R. Tavenard *et al.*, "Tslearn, A Machine Learning Toolkit for Time Series Data.," *J. Mach. Learn. Res.*, vol. 21, no. 118, pp. 1–6, 2020.
[187] P. J. Rousseeuw, "Silhouettes: a graphical aid to the interpretation and validation of cluster analysis," *Journal of computational and applied mathematics*, vol. 20, pp. 53–65, 1987.
[188] T. M. Kodinariya and P. R. Makwana, "Review on determining number of Cluster in K-Means Clustering," *International Journal*, vol. 1, no. 6, pp. 90–95, 2013.
[189] W. D. Penny, K. J. Friston, J. T. Ashburner, S. J. Kiebel, and T. E. Nichols, *Statistical parametric mapping: the analysis of functional brain images*. Elsevier, 2011.
[190] T. C. Pataky, "One-dimensional statistical parametric mapping in Python," *Computer Methods in Biomechanics and Biomedical Engineering*, vol. 15, no. 3, pp. 295–301, Mar. 2012, doi: 10.1080/10255842.2010.527837.
[191] T. C. Pataky, "Generalized n-dimensional biomechanical field analysis using statistical parametric mapping," *Journal of Biomechanics*, vol. 43, no. 10, pp. 1976–1982, Jul. 2010, doi: 10.1016/j.jbiomech.2010.03.008.
[192] P. S. Roberts, S. Krishnan, S. P. Burns, D. Ouellette, and M. R. Pappadis, "Inconsistent Classification of Mild Stroke and Implications on Health Services Delivery," *Archives of Physical Medicine and Rehabilitation*, vol. 101, no. 7, pp. 1243–1259, Jul. 2020, doi: 10.1016/j.apmr.2019.12.013.
[193] S. A. Kettlety, J. M. Finley, D. S. Reisman, N. Schweighofer, and K. A. Leech, "Speed-dependent biomechanical changes vary across individual gait metrics post-stroke relative to neurotypical adults," *bioRxiv*, 2022.
[194] K. Kaczmarczyk, A. Wit, M. Krawczyk, and J. Zaborski, "Gait classification in post-stroke patients using artificial neural networks," *Gait & Posture*, vol. 30, no. 2, pp. 207–210, Aug. 2009, doi: 10.1016/j.gaitpost.2009.04.010.
[195] K. Kaczmarczyk, A. Wit, M. Krawczyk, J. Zaborski, and J. Pi\lsudski, "Artificial neural networks (ANN) applied for gait classification and physiotherapy monitoring

in post stroke patients," *Artificial neural networks—methodological advances and biomedical applications*, 2011.
[196] R. Shiavi, H. J. Bugle, and T. Limbird, "Electromyographic gait assessment, Part 2: Preliminary assessment of hemiparetic synergy patterns.," *Journal of Rehabilitation Research and Development*, vol. 24, no. 2, pp. 24–30, 1987.
[197] J. F. Alingh, B. E. Groen, J. F. Kamphuis, A. C. H. Geurts, and V. Weerdesteyn, "Task-specific training for improving propulsion symmetry and gait speed in people in the chronic phase after stroke: a proof-of-concept study," *J NeuroEngineering Rehabil*, vol. 18, no. 1, p. 69, Apr. 2021, doi: 10.1186/s12984-021-00858-8.
[198] L. N. Awad, D. S. Reisman, T. M. Kesar, and S. A. Binder-Macleod, "Targeting Paretic Propulsion to Improve Poststroke Walking Function: A Preliminary Study," *Archives of Physical Medicine and Rehabilitation*, vol. 95, no. 5, pp. 840–848, May 2014, doi: 10.1016/j.apmr.2013.12.012.
[199] L. N. Awad *et al.*, "Reducing circumduction and hip hiking during hemiparetic walking through targeted assistance of the paretic limb using a soft wearable robot," *Am J Phys Med Rehabil*, vol. 96, no. 10 Suppl 1, pp. S157–S164, Oct. 2017, doi: 10.1097/PHM.0000000000000800.
[200] L. N. Awad, A. Esquenazi, G. E. Francisco, K. J. Nolan, and A. Jayaraman, "The ReWalk ReStore™ soft robotic exosuit: a multi-site clinical trial of the safety, reliability, and feasibility of exosuit-augmented post-stroke gait rehabilitation," *J NeuroEngineering Rehabil*, vol. 17, no. 1, p. 80, Jun. 2020, doi: 10.1186/s12984-020-00702-5.
[201] K. Penke, K. Scott, Y. Sinskey, and M. D. Lewek, "Propulsive Forces Applied to the Body's Center of Mass Affect Metabolic Energetics Poststroke," *Archives of Physical Medicine and Rehabilitation*, vol. 100, no. 6, pp. 1068–1075, Jun. 2019, doi: 10.1016/j.apmr.2018.10.010.
[202] K. Genthe, C. Schenck, S. Eicholtz, L. Zajac-Cox, S. Wolf, and T. M. Kesar, "Effects of real-time gait biofeedback on paretic propulsion and gait biomechanics in individuals post-stroke," *Topics in Stroke Rehabilitation*, vol. 25, no. 3, pp. 186–193, Apr. 2018, doi: 10.1080/10749357.2018.1436384.
[203] Z. A. Wright, W. Z. Rymer, and M. W. Slutzky, "Reducing Abnormal Muscle Coactivation After Stroke Using a Myoelectric-Computer Interface: A Pilot Study," *Neurorehabil Neural Repair*, vol. 28, no. 5, pp. 443–451, Jun. 2014, doi: 10.1177/1545968313517751.
[204] E. M. Mugler *et al.*, "Myoelectric Computer Interface Training for Reducing Co-Activation and Enhancing Arm Movement in Chronic Stroke Survivors: A Randomized Trial," *Neurorehabil Neural Repair*, vol. 33, no. 4, pp. 284–295, Apr. 2019, doi: 10.1177/1545968319834903.
[205] R. Kitatani *et al.*, "Ankle muscle coactivation during gait is decreased immediately after anterior weight shift practice in adults after stroke," *Gait & Posture*, vol. 45, pp. 35–40, Mar. 2016, doi: 10.1016/j.gaitpost.2016.01.006.
[206] E. Chang, N. Ghosh, D. Yanni, S. Lee, D. Alexandru, and T. Mozaffar, "A Review of Spasticity Treatments: Pharmacological and Interventional Approaches,"

Crit Rev Phys Rehabil Med, vol. 25, no. 1–2, pp. 11–22, 2013, doi: 10.1615/CritRevPhysRehabilMed.2013007945.

[207] C. M. Kim and J. J. Eng, "Magnitude and pattern of 3D kinematic and kinetic gait profiles in persons with stroke: relationship to walking speed," *Gait & Posture*, vol. 20, no. 2, pp. 140–146, Oct. 2004, doi: 10.1016/j.gaitpost.2003.07.002.

[208] T. H. Cruz, M. D. Lewek, and Y. Y. Dhaher, "Biomechanical impairments and gait adaptations post-stroke: Multi-factorial associations," *Journal of Biomechanics*, vol. 42, no. 11, pp. 1673–1677, Aug. 2009, doi: 10.1016/j.jbiomech.2009.04.015.

[209] F. Matsuda *et al.*, "Analysis of strategies used by hemiplegic stroke patients to achieve toe clearance," *Japanese Journal of Comprehensive Rehabilitation Science*, vol. 7, pp. 111–118, 2016.

[210] J. F. Lehmann, S. M. Condon, and R. Price, "Gait abnormalities in hemiplegia: their correction by ankle-foot orthoses.," *Archives of Physical Medicine and Rehabilitation*, vol. 68, no. 11, pp. 763–771, 1987.

[211] S. K. Banala, S. H. Kim, S. K. Agrawal, and J. P. Scholz, "Robot Assisted Gait Training With Active Leg Exoskeleton (ALEX)," *IEEE Transactions on Neural Systems and Rehabilitation Engineering*, vol. 17, no. 1, pp. 2–8, Feb. 2009, doi: 10.1109/TNSRE.2008.2008280.

[212] A. Duschau-Wicke, A. Caprez, and R. Riener, "Patient-cooperative control increases active participation of individuals with SCI during robot-aided gait training," *Journal of NeuroEngineering and Rehabilitation*, vol. 7, no. 1, p. 43, Sep. 2010, doi: 10.1186/1743-0003-7-43.